

Lebensdauer lagenweisen Kristallwachstums

Lifetime of Layer-Wise Crystal Growth

D I S S E R T A T I O N

zur Erlangung des akademischen Grades

doctor rerum naturalium

(dr. rer. nat.)

im Fach Physik

eingereicht an der

Fakultät für Naturwissenschaften, Institut für Physik

Gerhard-Mercator-Universität Duisburg

von

Herrn Lothar Brendel

geboren am 10.02.1969 in Oberhausen

Rektor der Gerhard-Mercator-Universität Duisburg:

Prof. Dr.-Ing. I. Wolff

Dekan der Fakultät für Naturwissenschaften, Institut für

Physik:

Prof. Dr. K. Usadel

Gutachter:

1. Prof. Dr. D.E. Wolf

2. Prof. Dr. P. Entel

eingereicht am:

30. März 2001

Tag der mündlichen Prüfung:

27. Mai 2001

Abstract

The lifetime of layer-by-layer growth of crystal surfaces, mainly in the context of growth conditions found in molecular beam epitaxy (MBE), is the central issue of this thesis. These conditions imply a driven system far from equilibrium which relaxes due to surface diffusion. Since the means to address the questions arising in this context are primarily computer simulations, the introduction covers, besides the analytical modeling of growth processes, details of the simulation technique and pitfalls to avoid.

At first, the ceasing of layer-by-layer growth due to fluctuations in the particle supply is considered. A theory for the according lifetime is presented and confirmed for the one-dimensional surface. Special care is taken for the two-dimensional case where deviations from previous results are found, explained, and used to revise the assumptions on which the theory is based. In particular the applicability of the – commonly accepted – *conserved KPZ* continuum equation and the premise of a single morphologically relevant length scale are affected.

The practically more relevant scenario of layer-by-layer growth's breakdown caused by barriers to interlayer transport (which give rise to the *Villain instability*) is studied. Data obtained from computer simulations is compared to the predictions of a linear stability analysis and is used to foretell the effect of counteracting variations of energy barriers. The latter enables to decide in which cases a strained surface is either hindering or advantageous for layer-by-layer growth.

A mean field model describing surface growth, which lacked up to now a systematic treatment, is investigated. For the basic version, the asymptotic behavior is derived exactly and – tuning the sole control parameter – a transition from *Poisson-like* growth to persistent layer-by-layer growth is found together with a non-trivial powerlaw behavior right at the transition point. Finally the extensibility of the model to include a finite lifetime of layer-wise growth is examined.

The damping of oscillations of certain surface-sensitive quantities is the manifestation of the surface's roughening which terminates the layer-by-layer growth. A scenario alternative to the roughening is suggested. It leads as well to damping of oscillations and consists of a *step bunch* which dissolves

during growth and “floods” an adjacent terrace. Growth simulations of this process are compared to a deterministic model and to experimental results.

Finally several toy models for surface growth, subjected to *noise reduction* are considered. The latter technique makes possible layer-by-layer growth also in these models and the dependence of its lifetime on the degree of the noise reduction is studied. The main focus is on the behavior’s relation to continuum equations and the corresponding universality classes, which are commonly used to classify the different models.

Remark: The sections 3.3 and 3.4 as well as appendix D appeared already in the publication (Kallabis et al., 1997) as the outcome of a collaboration with Dr. Harald Kallabis. Therefore, they essentially coincide with sections 4.1 to 4.5 and appendix A of his thesis (Kallabis, 1997).

Keywords:

crystal growth, molecular beam epitaxy, layer-by-layer growth, shot noise

Zusammenfassung

Die Lebensdauer des lagenweisen Wachstums von Kristalloberflächen, insbesondere unter Bedingungen, wie sie bei der Molekularstrahlepitaxie (englisch: molecular beam epitaxy = MBE) zu finden sind, ist das zentrale Thema dieser Arbeit. Diese Wachstumsbedingungen kennzeichnen ein getriebenes System fern vom Gleichgewicht, welches letzterem durch Oberflächendiffusion zustrebt. Da die auftretenden Fragen im Wesentlichen mit Hilfe von Computersimulationen behandelt werden, beinhaltet die Einführung, neben einer analytischen Beschreibung von Wachstumsprozessen, Details der Simulationsmethode und dabei zu vermeidende Fehlerquellen.

Zuerst wird das Verschwinden des lagenweisen Wachstums bedingt durch Fluktuationen in der Teilchenzufuhr untersucht. Eine Theorie der entsprechenden Lebensdauer wird vorgestellt und für den eindimensionalen Fall bestätigt. Besonderes Augenmerk wird auf den zweidimensionalen Fall gerichtet, bei dem Abweichungen von früheren Resultaten gefunden und erklärt werden und welche zur Neubewertung einer der Theorie zu Grunde liegenden Annahme führt. Insbesondere die Anwendbarkeit der – gemeinhin akzeptierten – *erhaltenden KPZ*-Kontinuumsgleichung und der Voraussetzung einer einzigen für die Morphologie relevanten Längenskala sind hiervon betroffen.

Die praxisrelevantere Situation des Verschwindens des lagenweisen Wachstums durch den Interlagentransport behindernde Barrieren (die die Ursache für die *Villain-Instabilität* sind) wird anschließend untersucht. Simulationsergebnisse werden mit den Aussagen einer linearen Stabilitätsanalyse verglichen und erlauben den Effekt von gegensätzlichen Energiebarrierenänderungen vorherzusagen. Damit kann entschieden werden in welchen Fällen eine verzerrte Oberfläche vor- bzw. nachteilhaft für lagenweises Wachstum ist.

Ein existierendes mean field Modell zur Beschreibung von Oberflächenwachstum, welches bisher nicht systematisch untersucht wurde, wird behandelt. Für die Grundversion wird das asymptotische Verhalten exakt berechnet und ein Übergang, in Abhängigkeit vom einzigen Kontrollparameter, von *Poisson-artigem* Wachstum zu anhaltendem Lagenwachstum gefunden mit einem nichttrivialen Potenzgesetz genau am Übergangspunkt.

Ergänzend wird die Erweiterungsfähigkeit des Modells in Bezug auf ein Lagenwachstum endlicher Dauer untersucht.

Das Verschwinden des Lagenwachstums durch die Aufrauung der Oberfläche zeigt sich in der Oszillationsdämpfung gewisser oberflächensensitiver Messgrößen. Ein weiteres Szenario, welches ebenfalls zu dieser Dämpfung führt, wird vorgeschlagen. Es handelt sich dabei um ein sich während des Wachstums auflösendes Stufenbündel, welches sich auf eine benachbarte Terrasse „ergießt“. Wachstumssimulationen dieses Vorgangs werden mit einem deterministischen Modell und Experimenten verglichen.

Abschließend wird auf einige stark vereinfachte Wachstumsmodelle (sog. *toy models*) eine Fluktuationsschwächung angewandt. Diese Technik ermöglicht ein Lagenwachstum auch für diese Modelle, und dessen Lebensdauer in Abhängigkeit der Stärke der Fluktuationsschwächung wird untersucht. Dabei wird besonderes Augenmerk auf die Verbindung zu Kontinuumsversionen und den zugehörigen Universalitätsklassen gerichtet.

Anmerkung: Die Abschnitte 3.3 und 3.4 sowie der Anhang D sind bereits in der Publikation (Kallabis et al., 1997) als Ergebnis einer Zusammenarbeit mit Dr. Harald Kallabis erschienen. Aus diesem Grund stimmen sie im Wesentlichen mit den Abschnitten 4.1 bis 4.5 und Anhang A seiner Dissertation (Kallabis, 1997) überein.

Schlagwörter:

Kristallwachstum, Molekularstrahlepitaxie, lagenweises Wachstum, Schrotrauschen

Acknowledgements

First of all, I wish to express my gratitude to my supervisor Prof. Dr. D.E. Wolf for making my work on the subject of this thesis possible, for supporting me in any way needed and for his enduring willingness to discuss results and further steps.

Furthermore I want to thank Prof. Dr. J. Krug for many discussions which have always been particularly illuminating and stimulating.

I thank Prof. Dr. P. Grassberger for being a very accommodating head of institute during my last year in Jülich.

A huge amount of thanks goes to Harald Kallabis for being the perfect coworker, officemate and companion during all our common time.

I am indebted to Prof. Dr. M. Plischke for providing independent data that helped me to decide which simulation code was to be debugged.

I am appreciative to Alexander Schindler for our fruitful collaboration, reaching beyond physics to the occasionally arduous task of providing system administration to the “comphys”-group in Duisburg.

I also feel obliged for Helga Bongartz’ and Martina Kamps’ extensive help in administrative and computational issues during my whole stay in Jülich.

I thank Pavel Šmilauer for lots of discussions and for providing always a valuable link between the theoretical and experimental field of surface growth.

I thank Sabine Dippel for always sharing helpful information; to her and to Farhang Radjai, Tim Scheffler, and Stefan Luding I am also grateful for fruitful collaboration and illuminating discussions in the field of granular matter.

For careful proofreading of various parts of this work I am grateful to Harald Kallabis, Dirk Kadau, Frank Westerhoff, and Michael von den Driesch.

The names of all the remaining people who enriched my life during my

thesis, in Jülich and elsewhere, scientifically as well as socially, would produce a list beyond the scope of these acknowledgements. To mention just a few, there are (suppressing titles) Gerard Barkema, Ugo Bastolla, George Batrouni, Boris Chesca, Jason Gallas, Erwin Gerstner, Haye Hinrichs, Imre Jánosi, Antal Károlyi, Dimitri Ktitarev, Roberta Lantier, Sang Bub Lee, Susanna Manrubia, Barbara Montanari, Márton Sasvári, Heiko Rieger, Michael Schroeder, Stefan Schwarzer, Jacques Villain, and Ulrich Wenschuh, to whom – as well as to all the non-mentioned – I want to express my thanks and best wishes.

Finally I thank my family and all my friends in my home-town who showed constant interest, believe, support, and patience during the long time of finishing this work.

Contents

1	Introduction	1
1.1	Motivation	2
1.2	Outline of the thesis	3
1.3	Notations	4
2	Molecular Beam Epitaxy	6
2.1	The method	7
2.2	Central parameters	8
2.3	The idealized model	10
2.3.1	Ingredients	10
2.3.2	Fundamental length scales	12
2.3.3	Boundary conditions	14
2.4	Quantities of interest	14
2.4.1	Average height	14
2.4.2	Surface width	15
2.4.3	Kinematic intensity	15
2.4.4	Step density	16
2.4.5	Height-height correlation function	18
2.4.6	Adatom density	20
2.5	Simulation technique	20
2.5.1	Diffusion	20
2.5.2	Deposition	21
2.5.3	Kinetic Monte Carlo in general	22
2.5.4	Coarse grained model	25
2.6	Analytical modeling	27
2.6.1	Deposition	27
2.6.2	Relaxation	36
2.6.3	Physical origins	41

3	Kinetic roughening	47
3.1	From submonolayer to scaling	48
3.1.1	Layer-by-layer growth's end	48
3.1.2	Importance of shot noise	48
3.1.3	Layer coherence	50
3.2	Submonolayer considerations	51
3.2.1	The exponent γ	51
3.2.2	Measured length scales	54
3.3	A theory for the damping time	57
3.3.1	The scaling regime	58
3.3.2	Connection with submonolayer physics	60
3.3.3	The adatom current reconsidered	61
3.3.4	Competing mechanisms	63
3.4	Numerical Results in one dimension	65
3.5	Numerical results in two dimensions	68
3.6	Appropriateness of cKPZ revised	69
3.7	Summary	75
3.7.1	Experimental relevance	75
4	Unstable growth	76
4.1	Schwoebel barriers	77
4.2	Uphill current	79
4.3	Stability	83
4.4	Simulations in one dimension	83
4.5	Simulations in two dimensions	86
4.6	Discussion	87
4.6.1	Implications on energy barrier variations	87
4.6.2	Experimental access of the damping time	90
5	Cohen's Model	91
5.1	Constant coefficients	93
5.1.1	Poisson Growth: $\alpha = 0$	94
5.1.2	Anticipated numerical results	95
5.1.3	Continuum approach	96
5.1.4	The case $\alpha = 1/2$	98
5.1.5	The case $\alpha < 1/2$	101
5.1.6	The case $\alpha > 1/2$	103
5.1.7	Summary	108

5.2	Step functions	108
6	Debunching	111
6.1	Inverted behavior	112
6.2	An idealized step bunch	112
6.2.1	Deterministic modeling	114
6.2.2	Numerical results in one dimension	116
6.2.3	Numerical results in two dimensions	118
6.3	Discussion	119
7	Toy Models	121
7.1	Common features	122
7.1.1	Coarse graining and noise reduction	122
7.2	Simulated models	123
7.2.1	Eden growth	123
7.2.2	Models related to MBE	125
7.3	Analytical results	129
7.3.1	Dimensional arguments	131
7.3.2	Scaling	134
7.3.3	Surface current in the EW model	136
7.4	Discussion	136
7.4.1	Description by continuum equations	136
7.4.2	Microscopic considerations	138
8	Conclusion	140
A	Natural units	157
B	Order instead of haphazard	160
B.1	Kicking balls	161
B.2	Three regimes	163
C	Conserved dynamics	165
D	Crossover times	167
E	Airy Functions	170

List of Figures

2.1	The basic model for MBE	11
2.2	A typical configuration after 0.2 mono-layers	13
2.3	The step density in two dimensions	18
2.4	On the interpretation of G in the submonolayer regime	19
2.5	Poisson distribution compared to a random walk	29
2.6	Unsatisfied bonds for a one-dimensional surface region	45
3.1	Oscillations of the surface width in $d = 1$	49
3.2	Temporal development of the surface width with and without shot noise	49
3.3	Suppression of the damping by means of a small system size	50
3.4	The step density after the deposition of 20 mono-layers in one dimension	55
3.5	The diffusion length in two dimensions	55
3.6	The rescaled adatom density during the first mono-layer de- position in $d = 1$	56
3.7	The rescaled adatom density during the first mono-layer de- position in $d = 2$	57
3.8	The temporally averaged adatom density in $d = 2$	58
3.9	The theoretical picture of the quasi-stationary adatom density as a function of the tilt	62
3.10	Curves from fig. 3.1, with time scaled by $(D/F)^{1/3}$	65
3.11	Coverage at which the surface width reaches a given value in $d = 1$	66
3.12	Maxima of the kinematic intensity	66
3.13	$L^* = \tilde{l}$ as a function of D/F	67
3.15	Surface width of fig. 3.14 with time rescaled by $(D/F)^{4\gamma}$	68
3.14	Oscillations of w^2 testifying layer-by-layer growth in $d = 2$	69
3.16	Damping time as function of D/F in $d = 2$	70

3.17	Temporally averaged adatom density on a weakly tilted surface	71
3.18	Temporal growth of w^2 in two dimensions according to the power law $t^{2\beta}$	73
3.19	The slope from fig. 3.17 plotted vs. D/F	74
4.1	The energy landscape seen by an adatom on a terrace	78
4.2	Adatom density profile for the case of an energy barrier at the downward step	80
4.3	The situation of island nucleation on a large terrace	82
4.4	The damping time in the presence of Schwoebel barriers	84
4.5	The influence of the Ehrlich-Schwoebel on the damping time	85
4.6	The inverse slope as read off from fig. 4.5 versus the theoretical Schwoebel length	85
4.7	The damping time for a two dimensional system in the presence of Schwoebel barriers	86
4.8	The damping time for the two-dimensional surface, rescaled by a suitable power of the Schwoebel-length	87
4.9	The influence of strain on the diffusion and Schwoebel barrier	89
5.1	Interlayer transport in Cohen's model	92
5.2	Temporal development of the surface width for values below $\alpha = 1/2$	95
5.3	Numerical confirmation of $w^2 \propto t^{2/3}$ for $\alpha = 1/2$	101
5.4	Data collapse showing the transient superimposed on the Poisson-like growth for $\alpha < 1/2$	103
5.5	The solution to the transcendental equation (5.24)	105
5.6	Scaling plot confirming the divergence of the stationary oscillation's minimum	106
5.7	The linearly vanishing of the stationary oscillation's amplitude for $\alpha \rightarrow 1/2$	107
5.8	The saturation value $w_\infty^2 \propto \theta_{\text{crit}}^{-2}$ reached within a time $\propto \theta_{\text{crit}}^{-3}$	110
6.1	Debunching of a macro step	113
6.2	A nucleation event in the deterministic model	114
6.3	The time evolution of the bunch width in the deterministic model	115
6.4	Temporal evolution of the step bunch's width in $d = 1$	116

6.5	The step bunch after the deposition of 160 mono-layers, averaged over 200 simulation runs	117
6.6	The width of the bunch in $d = 2$, rescaled by $l_0 \propto (D/F)^{1/4}$	118
6.7	Surface configuration with the bunch at the right boundary after the deposition of 400 mono-layers	119
7.1	Oscillations of the surface width w^2 for the Eden model /version A	123
7.2	Data collapse with four different noise reduction parameters showing the damping time of the Eden model/version A	124
7.3	A linear rescaling showing that the damping exponent for version A is not simply $\mu = 1$	125
7.4	Data collapse with four different noise reduction parameters showing the damping time of the Eden model/version B	126
7.5	Data collapse with three different noise reduction parameters showing the damping time of the EW model	127
7.6	Data collapse with three different noise reduction parameters showing the damping time of the WV model	127
7.7	Data collapse with three different noise reduction parameters showing the damping time of the “1+”-model of Das Sarma and Tamborena	128
7.8	The most important situations, showing the differences in the rules for the WV, “1+”, and EW model	130
7.9	The measured λ in the case of the Eden model	133
7.10	The dependence of the surface current on the noise reduction parameter m for three different global tilts in the EW model.	137
7.11	Surface currents for the EW model	137
B.1	Kicking the rightmost ball	161
B.2	Temporal development of rightmost ball	164
E.1	The Airy function $\text{Ai}(y)$	172

List of Tables

7.1	The corrections to the exponent μ for the Eden models	125
7.2	The exponents e_λ and e_ν for the Eden models	134

Chapter 1

Introduction

1.1 Motivation

Crystals — what is so special about them? What are their properties responsible for the particular fascination and mystical inspiration since the early days of mankind? Probably an important peculiarity is the crystals' rôle as a major exception from a phenomenon, experienced for a long time, but only recently put in a memorable statement by B. Mandelbrot (Mandelbrot, 1983): “Clouds are not spheres, mountains are not cones, coastlines are not circles, and bark is not smooth, nor does lightning travel in a straight line.” That means, almost everything in nature is ramified and irregular, making the advent of an adequate mathematical description a thing of the 20th century. Crystals – or at least the apparent ones – are different, though: They are one of the very few things fitting into the world of Euclidean geometry and Platonic bodies without being man-made.

In fact, the internal symmetry (first of all the periodicity) and its close relation to mathematical group theory made the physical description of condensed matter in crystalline form tractable in the first place and opened the wide field of solid state physics (Ashcroft et al., 1976) (much less can be done for non-crystalline – *amorphous* – materials). This gain of knowledge lead to an increasing interest in growing crystals with well defined properties industrially, especially in the field of micro-electronic devices.

Regarding the extremely high order, it is obvious that identical constituents (atom/molecules in the simplest cases, *unit cells* in general) are essential for being arranged in crystalline form, tough this condition is not a sufficient one; just like (equal-sized) marbles in a box do not organize in crystal order all by themselves. Even when starting to array the marbles by hand, some form of global synchronization is required when more than one hand is at work. Otherwise the different regions will not fit when starting to touch; the corresponding material is termed *polycrystalline*, i.e. consisting of tiny crystalline regions, separated by *grain boundaries*.

A particular approach to achieve this synchronization is to grow the crystal layer-wise, such that the previous layer serves as a raster for positioning the atoms/molecules of the new layer. If this can be done successfully, i.e. the crystal structure is persistently inherited from the substrate, we speak of *epitaxial growth*. Consequently, a technique exploiting this mechanism is called *epitaxy*, where the distinction between *homo-* and *heteroepitaxy* is made, depending on whether substrate and grown material are the same or different, respectively.

One special procedure, where the arriving particles are provided by a beam, is the method of *molecular beam epitaxy* (MBE). This technique, which we shall introduce to more detail in the next chapter, is experimentally very well developed, and countless effects emerging in very specific situations and configurations are theoretically understood as well. On the other hand, there are some fundamental problems unanswered yet; this thesis will focus on the following: Even if the crystal structure is reproduced correctly, the picture of the existence of always one perfectly flat layer acting as a frame for the newcomers is a highly idealized one. Instead, growth of a new layer will start before the current one is completed. Now the question is: What are relevant mechanisms leading to this behavior and how do the growth conditions influence quantitatively the lifetime of layer-by-layer growth, i.e. the time up to which a well defined begin/completion of layers can be observed. Compared to what is possible in MBE nowadays, it resembles to a certain extent the situation of being able to construct airplanes while not knowing how to compute the trajectory of a falling stone.

1.2 Outline of the thesis

The thesis is organized as follows.

Chapter 2 is an introduction to a certain class of growth processes. Apart from a description of the principles of MBE and its idealizations towards a model appropriate for a feasible computer simulation, it covers details of the simulation technique and quantities extractable from the growing crystal surface. Moreover, it describes the analytical modeling by means of stochastic processes and Langevin equations, particularly taking into account the lattice constant.

Chapter 3 focuses on layer-by-layer growth being solely disturbed by the fluctuations in the particle beam which causes the surface's *kinetic roughening*. A theory for its lifetime is presented and compared to numerical results. The common assumptions on which this theory is founded is critically revised for the important scenario of a two dimensional surface. In particular, the applicability of the so called *conserved KPZ equation* is addressed.

A mechanism being more relevant than kinetic roughening in experimental situations is examined in chapter 4: Energy barriers to interlayer transport cause the breakdown of layer-by-layer growth due to the emergence of the *Villain instability*. Numerical simulations are compared to a prediction

based on a linear stability analysis and are furthermore used to foretell the effect of counteracting variations of energy barriers.

In chapter 5, the capabilities of a specific mean field model to describe layer-wise growth are investigated. For the first time, asymptotic behavior and transients are calculated and confirmed numerically. The extension to layer-by-layer growth of finite lifetime is discussed.

Chapter 6 deals with a completely different scenario than the previous ones: Layer-by-layer growth does not cease by an initially flat surface becoming rough but due to a terrace of finite size getting “flooded” by a dissolving large step. One- and two-dimensional simulations are compared to a deterministic model as well as to experimental findings.

The domain of MBE is left to a certain extent in chapter 7, where various growth models, which originally do not possess a tunable parameter, are treated. The method of *noise reduction* introduces such a parameter and makes layer-by-layer growth possible also there; the dependence of its lifetime on the degree of noise reduction is studied.

Finally, chapter 8 completes the thesis with summarizing and discussing the main findings of the thesis and the issues which have to be clarified yet.

1.3 Notations

We shall close this chapter with the clarification of some possibly unfamiliar or non-standard notations that we will encounter during this thesis.

- $a \propto b$ means plainly “ a varies linearly with b ”.
- $a \sim b$ denotes “ a is equal to b up to some fixed dimensionless number”. In contrast to “ \propto ” it prohibits the proportionality factor to depend on other variables or to introduce physical dimensions.
- $a \gtrsim b$ means “ a is larger but not much larger than b ”, i.e. the difference is small compared to the two values.
- $[x]$ is the floor function, it yields the largest integer not greater than x .
- $\Theta(x)$ denotes the Heaviside step function, being zero for negative arguments and unity for positive ones.
- $\partial_t f$ is the partial derivative of f with respect to t ; higher derivatives are e.g. $\partial_x^2 f$.
- $[x]$ stands for the physical dimension of the quantity x . E.g. if x is a velocity, then $[x] = \text{LT}^{-1}$, where L and T denote the dimensions of length and time, respectively.
- (hkl) are miller indices specifying a certain crystal plane. Since we will not use them for our considerations, the reader may refer to a textbook like e.g. (Ashcroft et al., 1976) for their precise meaning.

Chapter 2

Molecular Beam Epitaxy

2.1 The method

Molecular beam epitaxy (MBE), a technique whose roots date back more than 30 years (Arthur, 1968; Cho and Arthur, 1975), can be regarded as research's most prominent method for growing thin crystal films in a well controlled way (Herman and Sitter, 1989; Tsao, 1993); this applies to metals as well as to semiconductors. Under ultra-high vacuum (UHV) conditions, a beam of molecules or atoms – driven by an effusion cell which thermally evaporates the material to be deposited – is directed onto a crystal substrate of well defined temperature. On one hand, the UHV due to its high demands is a major reason for the less significant rôle of MBE in industry, on the other hand it possesses two advantages important to research: First, it makes possible very clean surfaces and hence avoids the necessity to deal with complicated chemical reactions, leaving the characteristics of the growth behavior solely to the properties of the materials under investigation. Second, it allows for the application of certain *in-situ* and *in-vivo*^a measurement techniques, which enable the study of fundamental properties of the processes taking place on the crystal. Moreover, the *in-vivo* techniques together with the beam's adjustable intensity can be used to control the growth procedure down to atomic scale. These techniques are mainly *reflection high-energy electron diffraction* (RHEED) for reciprocal space (cf. e.g. (Braun, 1996)) and scanning tunneling microscopy (STM) for real space (Voigtlander and Zinner, 1993).

Due to the well prepared conditions, the growing crystal exhibits only very few defects and the lattice structure prescribed by the substrate is kept (unless there is a significant mismatch in the lattice constant when doing hetero-epitaxy), which is the meaning of *epitaxy/epitaxial* at all. Nevertheless there is a variety of possible developments of the surface, which are categorized into three different growth modes:

1. The *Frank-Van der Merwe* mode is also known as layer-by-layer growth, where a new layer essentially starts growing only after the previous one is completed. The resulting surface structures are two-dimensional.
2. In *Volmer-Weber* mode, three dimensional mounds develop on the surface, individual layers are no longer well defined.

^a*in-situ*: no transport of the specimen necessary, *in-vivo*: during growth

3. The *Stranski-Krastanov* mode is actually a transient form: A few layers grow in Frank-Van der Merwe fashion, afterwards Volmer-Weber mode takes over.

In chapter 3 we will see how the lifetime of layer-by-layer growth is limited by the shot noise of the particle impingement. The transition time contained in the Stranski-Krastanov mode in turn is investigated in chapter 4 for certain growth conditions.

At this point another growth mode important to MBE should be mentioned: If during preparation the crystal is not cut at an angle corresponding to a high symmetry plane, but rather in its vicinity, we speak consequently of a *vicinal surface*. Due to the discreteness, this means a surface consisting of terraces which exhibit the high symmetry, separated by steps at some distance ℓ that increases as the miscut gets smaller. If ℓ is not too large (we shall discuss the precise meaning in section 3.3.3), growth will simply take place by the adatoms' incorporation at the steps. This is called *step flow* mode, even if an actual "flow" of the steps only occurs if there is a preference towards either the upward or the downward step (cf. chapter 4).

A related technique which gained popularity rather recently is *pulsed laser deposition* (PLD) (Chrisey and Hubler, 1994). Here, instead of providing a beam with an essentially constant flux, one uses laser pulses to ablate a certain amount from a reservoir consisting of the desired material's solid phase. With each pulse, the vaporized material is deposited onto the surface. By means of this technique, layerwise growth could be achieved where MBE failed (e.g. (Jenniches et al., 1999; Ohresser et al., 1999)). This topic is addressed from a theoretical point of view in (Hinnemann, 2000).

2.2 Central parameters

Growth under MBE conditions has two central parameters: The flux F quantifies the number of particles deposited per unit time into a unit area, while the diffusion constant D characterizes the Brownian motion of a free atom (called *adatom*) on the surface according to

$$\langle (\vec{x}(t) - \vec{x}(t_0))^2 \rangle = (t - t_0)D, \quad (2.1)$$

where $\langle \cdot \rangle$ denotes the average over many atoms (all subjected to the same conditions, of course). Treating the diffusion hops in terms of Arrhenius

dynamics (Zangwill, 1988), the diffusion constant is governed by a Boltzmann factor involving the energy barrier E_D to overcome and the substrate temperature T :

$$D = \nu a^2 \exp\left(-\frac{E_D}{k_B T}\right) \quad (2.2)$$

The attempt frequency ν is of the order of the material's Debye frequency which is typically around 10^{13} s^{-1} . The lattice constant a enters the play as the distance of a hop. Given that, we can construct two time scales from D and F . Since $F a^d$ is the number of particles deposited per unit time onto a lattice site, the time needed to deposit material for one mono-layer is

$$t_{\text{ML}} = \frac{1}{F a^d}.$$

On the other hand, the time associated with a diffusion step is

$$\tau = \frac{a^2}{D}, \quad (2.3)$$

and it is already expected intuitively that for $t_{\text{ML}} \gg \tau$ smooth growth is favored, since the adatoms have sufficient time to find a highly coordinated site before being “buried” by the freshly deposited atoms. Indeed we shall find the ratio

$$\frac{t_{\text{ML}}}{\tau} = \frac{D}{F} a^{-d-2} \quad (2.4)$$

as the only control parameter in a basic MBE model (cf. next section).

Experimentalists often prefer to use the growth velocity $a_{\perp}/t_{\text{ML}} - a_{\perp}$ being the lattice constant normal to the substrate – instead of the flux F , and they can control D only via the temperature. With respect to this, a more suitable form of eq. (2.4) would be

$$\ln\left(\frac{D}{F} a^{-d-2}\right) = \ln(\nu t_{\text{ML}}) - \frac{E_D}{k_B T},$$

and inserting typical values like one deposited mono-layer per minute, $E_D = 0.5 \text{ eV}$ and $T = 400 \text{ K}$, we end up with

$$\frac{D}{F} a^{-d-2} \approx 3 \cdot 10^8$$

In fact, the range covered by usual experiments is about 10^6 to 10^{10} .

Quite often (especially within plots), we will omit the factor a^{-d-2} when specifying the ratio (2.4), which means we are using natural units (cf. appendix A), where

$$a = a_{\perp} = t_{\text{ML}} = 1.$$

The same applies when we are expressing time in deposited mono-layers without explicitly mentioning it.

2.3 The idealized model

2.3.1 Ingredients

For our investigations, we consider the most basic model for molecular beam (homo-)epitaxy, which consists of the following basic processes (cf. fig. 2.1 on the following page):

- Particles out of a beam with flux F impinge on a d -dimensional surface^b.
- As *adatoms* they perform a random walk on the surface, characterized by a diffusion constant D .
- The random walk ends upon encountering a lateral bond, then the adatom is irreversibly incorporated into a perfect (hyper-)cubic lattice.
- When crossing a step edge during the random walk, the atom “falls” as deep as possible, avoiding the creation of holes and overhangs (*SOS* = solid-on-solid condition).

That means, we are excluding features which are present in reality like:

1. dissociation of lateral bonds, leading to the decay of dimers (i.e. island seeds), detachment of atoms from islands and diffusion along the island rims
2. desorption of adatoms back into the vacuum

^bIn the present work, only the relevant cases $d = 1$ and $d = 2$ are covered by numerical simulations.

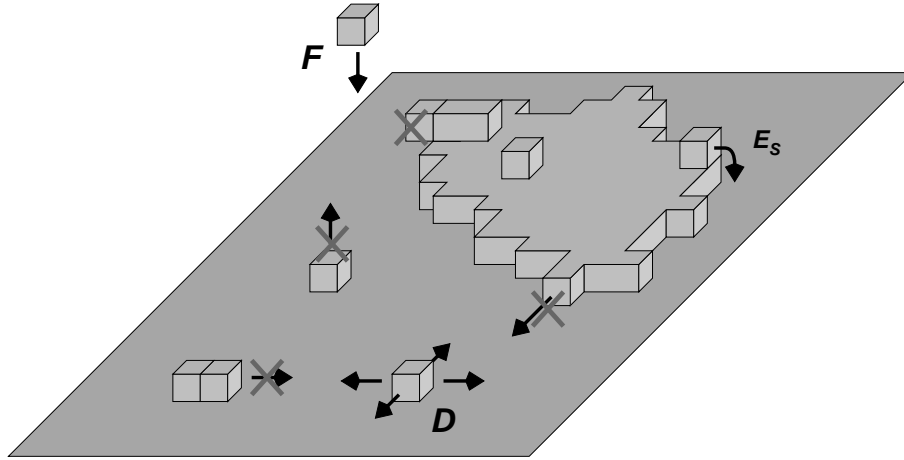


Figure 2.1: The basic model for MBE: On a simple cubic lattice, atoms without a lateral bond (termed *adatoms*) perform random walks with diffusion constant D until they encounter a site with at least one lateral bond. New adatoms are provided by deposition, quantified by F atoms per unit area and unit time. Neither holes nor overhangs are allowed. The additional energy barrier E_s involved in a downward hop is already an extension which we postpone until chapter 4.

3. a realistic underlying lattice (face centered cubic, body centered cubic, hexagonal... (Ashcroft et al., 1976))
4. deviations from a perfect lattice in form of defects, dislocations, strain and surface reconstruction (for semiconductors (Braun, 1996))

The justification to neglect 1.) and 2.) is the limit of low temperatures, where the Boltzmann factor in the Arrhenius rates for the corresponding processes is negligible compared to that in eq. (2.2). This implies a vanishing adatom concentration in equilibrium (cf. (Pimpinelli and Villain, 1999)) as well. On the other hand, decay of smaller islands is captured in an extension of the model, where $i^* + 1$ atoms in a cluster are necessary to form a stable, immobile island. This is called the *critical nucleus size*. We will use results with $i^* > 1$ only in one dimension (cf. section 3.4), though.

Concerning feature 3.), of course on a high symmetry surface of a simple cubic lattice, structures with symmetries different from experimental experiences will be found (since no relevant material possesses a simple cubic lattice, the only representative known is the rather exotic Polonium). But

since we are interested in rather general properties like typical island size and distance instead of precise island shapes, this is no significant drawback.

Much more interesting is the influence of the features 4.) on the results presented here (mainly the ones in chapter 3 and 4). These have to be regarded as future extensions, but some qualitative predictions can already be found in (Schindler, 1999).

2.3.2 Fundamental length scales

Since D and F are the central physical parameters (a possible finite system size disregarded for the moment), we can apply a dimensional analysis to reveal fundamental scales of length and time, as follows:

The only way the dimensions

$$[D] = \text{L}^2\text{T}^{-1} \quad , \quad [F] = \text{L}^{-d}\text{T}^{-1}$$

can be combined to yield length and time is

$$l_0 = \left(\frac{D}{F}\right)^{\frac{1}{2+d}} \quad , \quad t_0 = (D^d F^2)^{-\frac{1}{2+d}} \quad , \quad (2.5)$$

where the latter, when measured in mono-layers reads

$$\theta_0 \equiv \frac{t_0}{t_{\text{ML}}} = a^d \left(\frac{D}{F}\right)^{-\frac{d}{2+d}} = \left(\frac{a}{l_0}\right)^d$$

Note that l_0 is the only length scale constructible from D and F without involving the lattice constant. Moreover, it has a graphical meaning: It satisfies

$$D \frac{1}{F l_0^d} = l_0^2 \quad ,$$

which means that during the time needed for an atom to be deposited into an area of linear extent l_0 , just this area is being explored by a diffusing adatom. This has a consequence for systems smaller than l_0 : After the nucleation of an island, an adatom has enough time to visit the whole system before the next one is deposited. Hence, it will encounter the island almost for sure, which will therefore stay the only one in the system.

However, l_0 is not the only appearing length scale, it is not even the dominant one: In molecular beam epitaxy, the communication between different

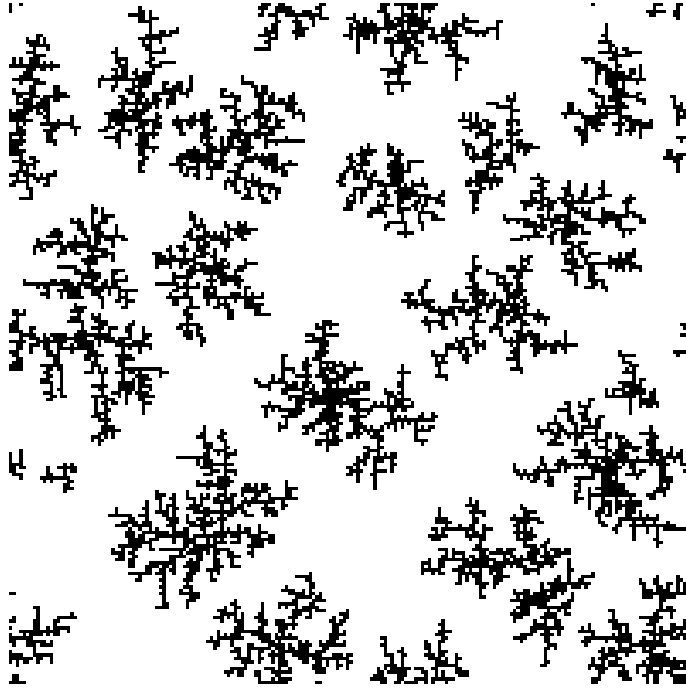


Figure 2.2: A typical configuration after growing 0.2 mono-layers at $D/F = 10^8$. Islands are shown in black.

regions of the substrate via diffusion of adatoms together with the process of island nucleation gives rise to the development of spatial correlations. These correlations manifest themselves through the characteristic distance l_D of nucleation events. We stress the term *characteristic*, since it is not merely an average distance. Instead, once an island is nucleated and starts to grow, it is surrounded by an adatom depletion zone, inhibiting further nucleations in its vicinity. This self-organization results in a more or less regular tessellation of the surface with a typical cell diameter of just l_D . This is shown in fig. 2.2, which also displays the tendency of the islands to become fractal due to the absence of edge diffusion. The dependence of l_D on D/F as well as other aspects of the submonolayer regime will be discussed in section 3.2.1.

2.3.3 Boundary conditions

If not stated otherwise, we will employ periodic boundary conditions (p.b.c.) in the lateral directions, i.e. when moving along \vec{e}_i , the unit vector in direction i , there is a wraparound after L_i , the system size in the corresponding direction:

$$h(\vec{x} + L_i\vec{e}_i) = h(\vec{x}),$$

Where necessary, they are extended to the more general *skewed boundary conditions*^c which allow for a global tilt H_i/L_i along direction i by setting

$$h(\vec{x} + L_i\vec{e}_i) = h(\vec{x}) + H_i,$$

however only one of the H_i will be non-zero in a typical situation.

Though we allow for different sizes L_i in each direction i , we will use L^d as an abbreviation for the total “area” $\prod_i L_i$.

2.4 Quantities of interest

As explained in the last section, we rely on the validity of the solid-on-solid (SOS) condition, i.e. we are able to describe the surface configuration by a single valued function $h(\vec{x})$, \vec{x} referring to a point in the d -dimensional reference plane. In terms of natural units, it maybe $h \in \mathbb{R}$ or $h \in \mathbb{Z}$ as well as $\vec{x} \in \mathbb{R}^d$ or $\vec{x} \in \mathbb{Z}^d$, depending on the choice of either continuum or discrete description, respectively. From the four possible combinations, the purely discrete case translates directly into the simple cubic lattice.

In the following, we discuss the most important quantities that can be obtained from the surface configuration.

2.4.1 Average height

The most trivial quantity is the average height, defined as

$$\bar{h} \equiv \frac{1}{A} \int h(\vec{x}) dA$$

^cSometimes they are called *helical* b.c. but that term is also used for a version of the periodic b.c. which gives up full exactness for the benefit of higher efficiency in computer simulations.

for the continuum case and correspondingly

$$\bar{h} \equiv \frac{1}{A} \sum_i h(\vec{x}_i)$$

for the discrete version. In this latter case, A , the measure of the substrate, is just the number of lattice sites in the reference plane. In the following, the over-bar will always denote such a spatial averaging of appropriate kind. In the case of more than one spatial variable being available for averaging, we will mention the correct one explicitly.

2.4.2 Surface width

This is the central quantity in this work, used to define the end of layer-by-layer growth. Though the definition

$$w^2 \equiv \overline{(h(\vec{x}) - \bar{h})^2} = \overline{h^2(\vec{x})} - \bar{h}^2$$

is in fact about the *squared* surface width, we will call w^2 as well as $w = \sqrt{w^2}$ surface width, and use the former most of the time.

In the ideal case of perfect layer-by-layer growth, a new layer only starts if the preceding one is completely filled, i.e. there are never more than two exposed layers. Therefore the width oscillates as $w^2(\theta) = \theta(1 - \theta)$ where θ is the coverage of the top layer (Kertész and Wolf, 1988).

In reality, the layers do not grow one after another but small islands can emerge on big islands, before their coalescence is completed. After some time there are many exposed layers and one cannot distinguish between integer and half-integer times: The oscillations are damped out as and the main purpose of this work is to present a theory for the dependence of the damping time on the growth conditions.

2.4.3 Kinematic intensity

This quantity can only be defined in the case of a discrete height variable, namely by

$$I \equiv \left(\overline{h(\vec{x}) \bmod 2} - \overline{(h(\vec{x}) + 1) \bmod 2} \right)^2, \quad (2.6)$$

that is the squared difference between the densities of even and odd surface positions (here h is measured in natural units to make the modulo operation

possible). The image behind this quantity is that of destructive interference: The surface is regarded as a diffraction grating, being perfectly reflective for a certain kind of waves. Observing it under a specific angle such that adjacent layers give rise to destructive interference (termed *off-Bragg* condition), one gets full intensity for a flat surface and zero intensity after perfectly growing another half mono-layer, resulting in oscillations during growth.

An experimental method being very close to this picture is *reflection high-energy electron diffraction* (RHEED), where the means of probing the surface are electrons with energies around 20 keV in a beam adjusted almost parallel to the surface. This grazing incidence makes RHEED a particularly surface sensitive method, and even though the electrons' scattering involves more complicated processes than captured in our picture (for a review cf. (Braun, 1996)), it was in fact RHEED that allowed for observing layer-by-layer growth in-situ already in 1980 (Harris et al., 1981) due to its characteristic oscillations.

In contrast, during step flow mode (cf. section 2.1), all layers receive an equal amount of material (apart from fluctuations) and I remains essentially constant.

2.4.4 Step density

Measuring width w^2 and kinematic intensity I provides information only about the distribution of the mass amongst the height levels, they are not influenced by the actual morphology. A complementary quantity is the step density, defined for the purely discrete case^d as

$$\rho_{\text{st}} \equiv \sum_{i=1}^d (1 - \delta_{h(\vec{x}), \vec{x} + \vec{e}_i}).$$

Obviously, the contribution of an island to ρ_{st} is due to its perimeter. In the one-dimensional case, the perimeter degenerates into just two points, which has the advantage of being constant in time and hence allowing for the direct extraction of the island density. The disadvantage is the equal weight assigned to all islands, i.e. many small defects can blur the “signal” of the regular islands, making the step density a rather noisy quantity in one dimension.

^dA generalization to $\vec{x} \in \mathbb{R}^d$ is possible.

For a higher dimensionality, the situation is somewhat different. In the idealized picture of a vanishing duration of the nucleation phase and a negligible amount of nucleations after this phase, the deposited material may be equally distributed among the islands. This coherent growth yields for the number of atoms in one island

$$n = \frac{Ft}{\rho_{\text{is}}},$$

where ρ_{is} is the density of islands (being constant since the end of the nucleation phase). For a (large) compact island, its number of perimeter sites U is related to its contained sites n by

$$U = c_d n^{(d-1)/d},$$

with a shape dependent factor c_d . Therefore, the step density is related to island density and time via

$$\rho_{\text{st}} = \frac{c_d \rho_{\text{is}}^{1/d}}{a^{d-1}} \left(\frac{t}{t_{\text{ML}}} \right)^{(d-1)/d}, \quad (2.7)$$

allowing again for an estimation of the island density.

Even if eq. (2.7) is not particularly useful without early time corrections due to the finite duration of the nucleation phase, its information content differs significantly from the case of fractal islands. Since in the latter case an adatom typically accretes at a thin island's arm (cf. fig. 2.2 on page 13) and it provides in turn a site for another attachment, atoms in an island have on average approximately two neighbors. Hence, the step density is expected to be roughly twice the coverage, which is confirmed in fig. 2.3 on the next page which also shows a right curvature of the graph even before coalescence at $t \approx 0.5$. This is due to the fact that the accretion process is not exactly like *diffusion limited aggregation* (DLA) (Witten and Sander, 1983), where approaching adatoms are efficiently captured by the outer regions of the island; in our case, adatoms can be deposited in the inner parts and increasingly fill the ramified structures.

An approach to access the step density experimentally is once again RHEED, but instead of adjusting for the off-Bragg condition, adjacent layers now lead to constructive interference (by choosing the proper observation angle). According to the considerations leading to the kinematic intensity

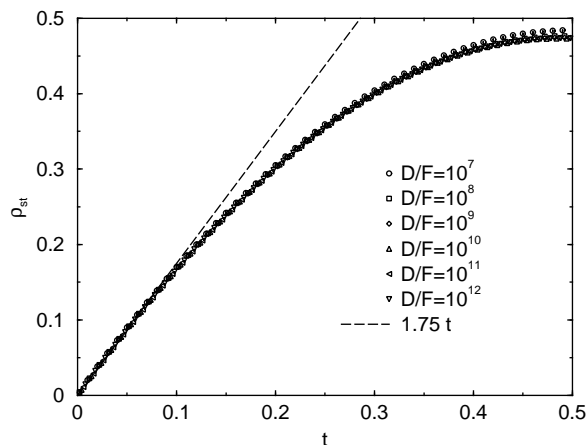


Figure 2.3: The step density in two dimensions for $D/F = 10^7 \dots 10^{12}$ without any rescaling at all. The slope for early times indicates an average lateral coordination number of approximately 2.25 for incorporated atoms, independent of D/F .

(2.6), this would lead to a reflected intensity independent of the height configuration. Now the assumption is that each step contributes to the incoherent scattering, i.e. the reflected intensity is bated proportionally to the step density.

2.4.5 Height-height correlation function

A quantity combining lateral and height information is the *height-height correlation function* (sometimes called likewise *height-difference correlation function*). Its definition

$$G(\vec{r}) = \overline{(h(\vec{x} + \vec{r}) - h(\vec{x}))^2}, \quad (2.8)$$

where the spatial averaging is performed with respect to \vec{x} , precludes open boundary conditions. It possesses the generic symmetry

$$G(-\vec{r}) = G(\vec{r}), \quad (2.9)$$

since we can substitute $\vec{x} \rightarrow \vec{x} + \vec{r}$ in eq. (2.8) which leaves the result unchanged, since every value of \vec{x} occurs during averaging.

In the case of periodic boundary conditions, $G(\vec{r})$ possesses the additional symmetry

$$G(\vec{r}) = G(\vec{r} - L_i \vec{e}_i),$$

which, due to eq. (2.9), has the two equivalent formulations

$$\begin{aligned} G(\vec{r}) &= G(L_i \vec{e}_i - \vec{r}) \\ G(L_i/2 \vec{e}_i - \vec{r}) &= G(L_i/2 \vec{e}_i + \vec{r}) \end{aligned}$$

If we average $G(\vec{r})$ once more with respect to \vec{r} , we get

$$\begin{aligned} \overline{G(\vec{r})} &= \overline{h^2(\vec{x} + \vec{r})} - \overline{h(\vec{x} + \vec{r})} \overline{h(\vec{x})} + \overline{h^2(\vec{x})} \\ &= \overline{h^2} - \overline{h} \overline{h} + \overline{h^2} \\ &= 2w^2, \end{aligned} \tag{2.10}$$

showing that indeed $G(\vec{r})$ contains more information than the width.

A typical use of $G(\vec{r})$ is the evaluation of so called *scaling properties* of a surface (cf. section 2.6.2), though it provides useful information already in the submonolayer regime. Let's consider the case of one-dimensional islands ($h = 1$ in natural units) with characteristic distance ℓ and average size s . Since the squared value in eq. (2.8) is either one or zero, $G(r)$ denotes just the density of pairs of lattice sites (a distance r apart) which have different height. Thus, for small r the contribution to this density will come from two intervals of length r at each island (cf. fig. 2.4a), i.e. with an island density

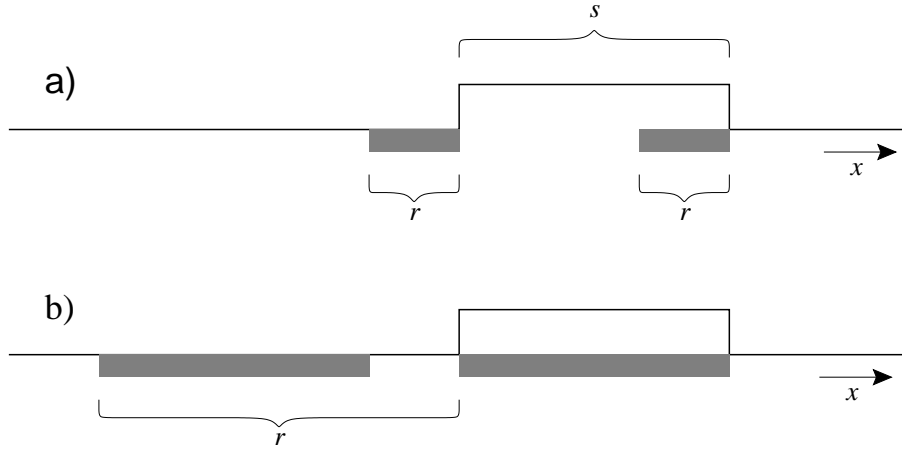


Figure 2.4: On the interpretation of $G(\vec{r})$ in the submonolayer regime (here for $d = 1$). Only the gray regions contribute to the averaging in eq. (2.8). They are of length r for $r \leq s$ (a), but do not grow further for $r \geq s$ (b).

of $1/\ell$ the linear behavior

$$G(r) = \frac{2}{\ell}r$$

contains the islands distance in its slope. This goes on until r reaches the island size s , then $G(r)$ dose not increase anymore (cf. fig. 2.4 on the page beforeb), which allows for the extraction of s .

2.4.6 Adatom density

This quantity is obtained trivially. Atoms without lateral bonds are counted and division by L^d yields the density. It will play a key rôle in section 3.6.

2.5 Simulation technique

2.5.1 Diffusion

The simulations discussed in this thesis are based on the model for MBE, as described in section 2.3, and therefore only need to include deposition, diffusion and accretion of adatoms. Diffusive motion on a d -dimensional simple (hyper-)cubic lattice is a very uncomplex task: In each time step, the adatom is moved to one of its $2d$ nearest neighbor sites with equal probability. To relate this step to a physical time, we consider the diffusion equation

$$\partial_t \rho = \nabla \cdot D \nabla \rho, \quad (2.11)$$

where a word about the diffusion constant D is in order: In principle, this is a phenomenological constant describing the relaxation speed of concentration gradients and has to be distinguished from the *tracer diffusion constant* in eq. (2.1) which relates time and displacement of a marked particle. For non-interacting particles these two parameters coincide, though (Pimpinelli and Villain, 1999), and the discretized version of eq. (2.11), i.e.

$$\begin{aligned} \rho(\vec{x}, t + \Delta t) &= \left(1 - 2d \frac{\Delta t D}{a^2}\right) \rho(\vec{x}, t) \\ &+ \frac{\Delta t D}{a^2} \sum_{i=1}^d (\rho(\vec{x} + a\vec{e}_i, t) + \rho(\vec{x} - a\vec{e}_i, t)), \end{aligned}$$

corresponds to the appropriate master equation (Gardiner, 1985) with $\rho(\vec{x}, t)$ interpreted as the probability for the adatom being at site \vec{x} . We read off the probability for a hop to a given nearest neighbor during time Δt being $\Delta t D/a^2$. Consequently the probability not to hop at all is $1 - 2d\Delta t D/a^2$, which yields the most economic choice for the time step, namely

$$\Delta t = \frac{a^2}{2dD}. \quad (2.12)$$

This means a hop is performed within every time step Δt ; choosing it smaller and smaller consumes more computer time only for the benefit of simulating more and more accurately the stochasticity of the waiting time according to its probability density (cf. section 2.6.1)

$$p(t) = \frac{2dD}{a^2} \exp\left(-\frac{2dDt}{a^2}\right).$$

If desired, this exactness can be achieved more efficiently by drawing the elapsed time associated with a hop from just this distribution instead of using its mean every time.

The time step (2.12) corresponds to *one* diffusing adatom, if there are N of them in the system, they perform independent random walks and the rate associated with the event of any of them hopping in any of the $2d$ directions is just

$$\nu_N = N \frac{2dD}{a^2}.$$

2.5.2 Deposition

There is yet another process competing with these N walkers, namely the arrival of a new particle out of the vapor. Since F denotes the number of deposited particles per unit time and unit area, the total deposition rate into the whole system is $\nu_{\text{dep}} = FL^d$. Therefore, the probability for a deposition is

$$p_{\text{dep}} = \frac{\nu_{\text{dep}}}{\nu_N + \nu_{\text{dep}}} = \left(\frac{2Nd}{L^d} \frac{D}{Fa^{d+2}} + 1 \right)^{-1},$$

showing also on this computational level, that only the *ratio* of D and F enters the description. If deposition is the selected process, one of the L^d is chosen with uniform probability.

A consequence of the deposition being a stochastic process as well, are the fluctuations of the amount of material added after time t . Only on average (or for an infinite system, as we will see later), it will be t/t_{ML} mono-layers. But since the morphology of the surface depends on the exact amount, we are *not* interested in including these fluctuations. Therefore, in the simulations, we will measure time always in deposited mono-layers.

2.5.3 Kinetic Monte Carlo in general

The procedure of selecting and performing concurrent events can be extended to any number of independent processes occurring in a system, each taking place with a rate ν_k . Then, the total rate, in a way expressing the activity of the system, reads

$$\nu_{\text{tot}} = \sum_i \nu_i, \quad (2.13)$$

and the probability for a specific process k to take place in the timestep $1/\nu_{\text{tot}}$ is distributed according to

$$p_k = \frac{\nu_k}{\nu_{\text{tot}}}. \quad (2.14)$$

Of course, concerning the time step, the same consideration as for the single hop (2.12) applies: In principal, instead of assigning a time $1/\nu_{\text{tot}}$ to each performed event, a value should be drawn from an exponential distribution

$$p(t) = \nu_{\text{tot}} \exp(-t\nu_{\text{tot}}),$$

but unless one is interested in something like correlation times on these small time scales, summing up its mean for every event is sufficient to obtain the total time elapsed.

The equations (2.13) and (2.14) form the basis of the *kinetic Monte Carlo* method (KMC) (Bortz et al., 1975):

1. determine all possible events (also called *transitions*) together with their rates
2. select one of them according to eq. (2.14)
3. perform the corresponding change in the system

4. advance the time by $1/\nu_{\text{tot}}$ according to eq. (2.13)
5. proceed at step 1.

Efficient update

When extending the model from the simple binary state of an atom (either free or irreversibly incorporated) to features like e.g. step edge barriers (cf. chapter 4), the energy barrier for a hop will depend on the local configuration and consequently its computation will get rather involved. To allow for sufficiently complex rules without giving up efficiency, the following scheme is of help: We assume the energy barrier for a certain hop to depend only on h_i , the height variables of the neighbors, relative to h , the height of the atom under consideration. If we furthermore restrict the influence to the three fundamental cases

1. $h - 1 < h_i$, that is a lateral bond to this neighbor
2. $h - 1 = h_i$, that is hopping without height change in direction i
3. $h - 1 > h_i$, that is hopping down in direction i ,

then we need two bits to code the information. Since the number of possible states representable by two bits is $2^2 = 4$, we can distinguish even four different cases (e.g. to refine the resolution of situation (1)). With this, we have to deal with 4^n relevant types of configurations, where n is the number of neighbors taken into account. Even including next nearest neighbors in two dimensions, the resulting number $4^8 = 65536$ is not tremendous and permits the usage of a lookup table. That means, coding the height difference information in a word of $2n$ bits (which can be done very efficiently), the resulting number provides an index to a data structure which contains information about the atom's possible hops and the corresponding rates. The method of assigning each neighbor two bits allows furthermore for a particularly aimed manipulation of this index number: The atom under consideration "is informed" about a height change of one specific neighbor, then only the corresponding two bits in the index number have to be updated to yield the new state of the atom.

Finding the transition

Knowing all the possible processes and their rates, one of them has to be selected as specified by eq. (2.14). This is done by ordering the processes

with respect to their label k , drawing a random number R from a uniform distribution over $[0 \dots 1)$, and then seeking the process k^* which fulfills

$$\sum_{k=0}^{k^*-1} p_k \leq R < \sum_{k=0}^{k^*} p_k. \quad (2.15)$$

Grouping events helps to speed up this search: Generally, there will be many processes with the same rate in the system^e. Hence, for each such rate ν_j shared by N_j events, we collect these into a group j with rate $N_j\nu_j$. If such a group is picked in the way described above (where $p_j = N_j\nu_j/\nu_{\text{tot}}$), one of its members is selected with uniform probability. The latter selection can be done in a random access manner unlike the sequential way (2.15), whose efficiency, however, can be increased as well by sorting the groups j according to descending p_j .

Finding the location

Once the decision about the process to take place is made, the corresponding atom in the lattice has to be found (unless the deposition process was selected). Storing this position in the group members makes this task trivial and fast to accomplish while consuming only a moderate amount of computer memory; therefore this approach was used for all the simulations presented here. If this storage has to be avoided, one can abandon the actual group members and keep track only of the numbers N_j , but then it is necessary to seek an appropriate site explicitly each time a certain group was picked (Clarke et al., 1991).

For the two-dimensional simulations in (Kallabis, 1997) this latter procedure was used, and selecting a corresponding site *randomly* was done as sketched in the following: Let the lattice sites be labeled in some order by the numbers $\{1, \dots, L^d\}$ and let

$$S : \{1, \dots, L^d\} \rightarrow \{1, \dots, L^d\}$$

be a randomized, bijective mapping. With this, we can traverse the lattice in a random fashion by counting i from 1 up to L^d and inspecting $S(i)$

^eActually, if this is not the case, the simple procedure is hardly feasible and more sophisticated methods like e.g. hierarchical schemes (Maksym, 1988; Blue et al., 1995) have to be employed.

until it refers to a lattice site which fits the event chosen beforehand. To avoid taking always the same “random” way $S(1), S(2), \dots$, the mapping S must be shuffled each time. This is done by drawing another i' randomly from $\{1, \dots, L^d\}$ and swapping $S(i) \leftrightarrow S(i')$, where i is still the index of the matching $S(i)$. While this algorithm seems to produce a quite random selection at first sight, it actually does the opposite, especially in the case of our simple model: $S(i)$ either refers to an adatom or to an immobile one. That means, we intend to use S to find an adatom *at random*; instead we move the same adatom most of the times while the others are “frozen”. The reason for this failure is explained in appendix B. In the affected simulation program used in (Kallabis, 1997), this unfortunate effect was mitigated to some extent by a hierarchic scheme, introduced to speed up the search for an appropriate site (Clarke et al., 1991) (actually it was the scheme originally proposed to accelerate the *event selection* (Maksym, 1988; Blue et al., 1995)). Nevertheless, the impact of this error on the surface’s evolution is rather drastic, the roughening proceeds significantly faster as we will see later (cf. fig. 3.16 on page 70). To which extent further results, published by others having used the same simulation program as the author of (Kallabis, 1997), are affected, has to be clarified yet.

Fortunately, it needs only a minor modification to cure the code: Instead of beginning always with $i = 1$ when traversing S , the starting point is chosen with uniform probability from $\{1, \dots, L^d\}$. To justify the term “cure” and the certainty about a “correct code” – particularly with regard to the findings in chapter 3 – it must be pointed out, that after applying this fix, the obtained results agreed with the outcome of three distinct programs (two written independently by the author, the other by (Plischke, 1999)).

2.5.4 Coarse grained model

Since the explicit simulation of the adatoms’ motion is rather time consuming, a treatment on a coarse grained level can be of help (Wolf, 1995): Instead of resolving down to the atomic level, the lattice is laterally subdivided into cells of linear size Δx , called *coarse graining length*. For each cell, the information about its height h and n , its number of contained atoms, is monitored. Either $n \leq i^*$, i.e. the cell contains n mobile adatoms or $n > i^*$ which corresponds to an island of “mass” n . This island may extend to neighboring cells, which has no influence on the dynamics, though. Reaching $n = (\Delta x/a)^d$ means a filled cell, resulting in resetting $n = 0$ and increasing

h by a_{\perp} . Within this scheme, an adatom is moved from cell to cell, the associated time step is therefore

$$\tau_{\text{CG}} = \frac{\Delta x^2}{D}$$

rather than eq. (2.3), which means a computational speedup of $(\Delta x/a)^2$.

Of course, the constraint $\Delta x \ll l_D$ must be fulfilled, lest losing information about individual islands. But there are other subtleties to be taken into account: It is assumed that an adatom entering a cell where $n > i^*$ is immediately (or rather within time τ_{CG}) incorporated at the step “hidden” in the cell. The reasoning that it has a number of $(\Delta x/a)^2$ micro-hops (not being resolved) to explore the cell and reach the step is valid only if there are no hindering energy barriers (cf. chapter 4)^f In the same way it is assumed that $i^* + 1$ adatoms in the cell meet to form a nucleus during time τ_{CG} . This is justified for $i^* = 1$ and plausible also for larger values in $d = 1$, but a quantitative description in form of the nucleation probability $p_{\text{nuc}}(\Delta x, i^*, d)$ remains to be derived. Especially the case $i^* > 1$ is desirable, since the detection of nucleations by evaluating cluster-sizes and comparing to i^* can be dropped in the coarse grained model.

We will use the coarse graining model only for $d = 1$ and $i^* \in \{1, 2, 3\}$ in section 3.4.

^fAnd even then only for $d \leq 2$.

2.6 Analytical modeling

2.6.1 Deposition

Poisson process

Since the particles in the beam are regarded as uncorrelated, so are their arrival times and the Poisson nature of their impingement on the surface can be seen quite easily: If we choose as unit of time the layer completion time t_{ML} and focus on one lattice site, then a small δt is just equal to the probability for one arrival during this time (provided it is short enough to neglect multiple events). If we divide the observation time into N intervals, i.e. $t = N \delta t$, we need h arrivals^g with probability δt and $N - h$ intervals without an event (probability $1 - \delta t$) to find h particles after the time t . Together with a combinatorial factor denoting the number of possibilities for the definite times of the h events, we get

$$p(h, t) = \binom{N}{h} \left(\frac{t}{N}\right)^h \left(1 - \frac{t}{N}\right)^{N-h},$$

which in the limit $N \rightarrow \infty$ becomes

$$p(h, t) = \frac{t^h}{h!} \exp(-t), \quad (2.16)$$

i.e. the Poisson distribution with its moments^h

$$\langle h^k \rangle = \exp(-t) \left(t \frac{d}{dt}\right)^k \exp(t)$$

The property important to us is the identity

$$\langle h^2 \rangle - \langle h \rangle^2 = t,$$

or, if we revert to dimensionful quantities

$$\langle h^2 \rangle - \langle h \rangle^2 = a_{\perp}^2 F a^d t, \quad (2.17)$$

which shows that inevitably the strength of the deposition noise is proportional to the deposition rate itself.

^gWe use h to count arrivals, already in mind stacking up particles of unit height.

^hThey are known as *Bell polynomials*(Bell, 1934).

For later comparisons, we also need to know two-time correlations of the stochastic variable $h(t)$, and hence we have to evaluate $\langle h(t)h(t') \rangle$. Therefore we rewrite eq. (2.16) as a conditional probability for general initial values:

$$p(h, t; h', t') = \Theta(h - h') \frac{(t - t')^{h-h'}}{(h - h')!} \exp(t - t')$$

(Here $t \geq t'$ is assumed and the expression 0^0 for $t = t', h = h'$ shall evaluate to unity as well as $\Theta(0)$.)

Given that, the correlation function becomes

$$\begin{aligned} \langle h(t)h(t') \rangle &= \sum_{h=0}^{\infty} \sum_{h'=0}^{\infty} h h' p(h, t; h', t') p(h', t'; 0, 0) \\ &= t t' + t' \end{aligned}$$

or more general

$$\langle h(t)h(t') \rangle - \langle h(t) \rangle \langle h(t') \rangle = \min\{t, t'\}. \quad (2.18)$$

For the sake of convenience though, the process of particle deposition may be modeled by something more symmetrical: Onto a random walk with its probability distribution (Gardiner, 1985)

$$p_{\text{RW}}(h, t) = \exp(-t) I_h(t), \quad (2.19)$$

where $I_h(x)$ is the modified Bessel function of the first kind and order h , a uniform motion with velocity unity (or rather a_{\perp}/t_{ML} when expressed dimensionfully) is superimposed. That is, we consider $p_{\text{RW}}(h - t, t)$ which deviates from the distribution (2.16) only for early times (the reason is the latter's constraint $h \geq 0$ due to the absence of particle removal). For later times, they become essentially identical (cf. fig. 2.5 on the next page).

Continuous formulation

Since the tools of calculus are of great help in most mathematical circumstances, one is always set on expressing a problem in a continuum form. In statistics this can be done quite elegantly by the use of *Langevin equations* (the name traces back to his early work on Brownian motion (Langevin, 1908)).

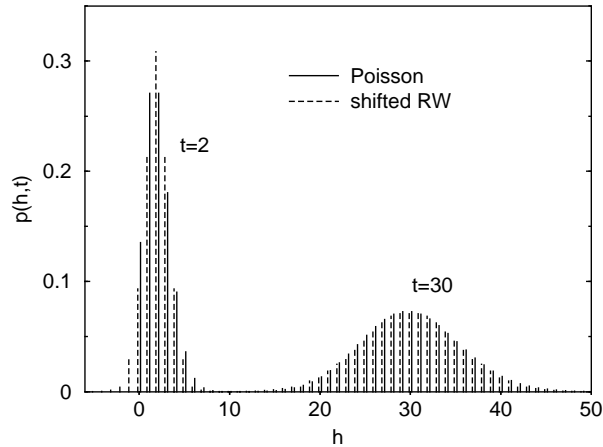


Figure 2.5: Poisson distribution compared to a (uniformly shifted) random walk. The constraint $h \geq 0$ for the former plays a significant rôle only for early times. Later, both take on the characteristic Gaussian shape.

A Langevin equation is a stochastic differential equation (SDE), i.e. a differential equation (ordinary or partial) which contains a stochastic quantity – the noise – turning the solution into a stochastic function as well. Despite their quite involved mathematical subtleties (cf. (Gardiner, 1985)), Langevin equations usually provide a rather direct and intuitive description of the physical system under consideration. For the purpose of deposition only, the simplest form is sufficient, reading

$$\partial_t h(t) = \eta(t), \quad (2.20)$$

where h is our height-function in time, and η is the noise. The trivially obtained solution

$$h(t) = h(t_0) + \int_{t_0}^t \eta(s) ds$$

is of limited use unless the statistic properties of the noise are given. It is common to choose

$$\langle \eta \rangle = 0,$$

since any nonzero value would merely describe a uniform motion, just as an additional constant in eq. (2.20) would do. Such a constant drift ct always vanishes in the *comoving frame*, i.e. under the transformation $h \rightarrow h - ct$.

To put it the other way round, we can interpret the absence of these terms as being in this comoving frame already.

To further specify the properties of the noise, one states its “correlator”, that is its covariance for two times of observation. The usual choice is *white noise*, where there are no correlations between η at two distinct points in time:

$$\langle \eta(t)\eta(t') \rangle = C \delta(t - t') \quad (2.21)$$

The prefactor C enters linearly in the correlation of $h(t)$ as

$$\begin{aligned} \langle h(t)h(t') \rangle &= \left\langle \int_0^t \eta(s) ds \int_0^{t'} \eta(s') ds' \right\rangle \\ &= \int_0^t \int_0^{t'} \langle \eta(s)\eta(s') \rangle ds' ds \\ &= C \min\{t, t'\}, \end{aligned} \quad (2.22)$$

from which we get the variance

$$\langle h^2(t) \rangle = C t, \quad (2.23)$$

which means simple diffusive behavior. Hence, a comparison to eq. (2.17) yields $C = a_{\perp}^2 F a^d$ and the comoving frame’s velocity of $a_{\perp} F a^d$.

Moreover, formula (2.22) evinces the correct two time correlation prescribed by eq. (2.18). It holds true even for arbitrarily small times, though eq. (2.20) actually corresponds to the shifted random walk (2.19) rather than the original Poisson process (2.16).

As can be concluded from eq. (2.22), in general it would be essentially the “area under the correlator”, i.e. the integral

$$\int_{-\infty}^{\infty} \langle \eta(t)\eta(0) \rangle dt$$

that determines the impact of the noise. Obviously, that is the reason to need a Dirac delta as an infinitely narrow correlator, which in turn implies the quite unrealistic feature of an infinite variance of η . This is another expression of the fact that there is no exact white noise in reality. In this respect, eq. (2.21) just means we are dealing with a noise whose correlation time is much smaller than any other time scale of interest, and the usage of eq. (2.21) instead of the real correlator is merely a matter of mathematical convenience (cf. also (Gardiner, 1985)).

The lattice constant a

After having discussed the situation of *one* lattice site, we now introduce the lateral dimension into the Langevin equation (restricted to $d = 1$ first, but the generalization to higher dimensions is most straight forward). For that, we write

$$\partial_t h(x, t) = \eta(x, t) ,$$

where the noise correlator

$$\langle \eta(x, t) \eta(x', t') \rangle = C(x - x') \delta(t - t')$$

now contains a spatial function as well. The time integration can be taken over from equations (2.22) and (2.23):

$$\langle h(x, t) h(x', t) \rangle = t C(x - x') \tag{2.24}$$

At this stage, there is nothing wrong in introducing the lateral lattice constant a into the correlator. If we restrict x to denote always the center of a lattice site, we can express it as

$$C(x - x') = C(0) \Theta(a/2 - |x - x'|) , \tag{2.25}$$

where again the amplitude can be determined by comparison to eq. (2.17):

$$\begin{aligned} \langle h^2(x, t) \rangle &= t C(0) \stackrel{!}{=} t a_{\perp}^2 F a^d \\ \Rightarrow C(0) &= a_{\perp}^2 F a^d = \frac{a_{\perp}^2}{t_{\text{ML}}} \end{aligned} \tag{2.26}$$

To be able to perform operations like spatial derivatives on the surface $h(x, t)$ (as below in section 2.6.2), it has to be sufficiently smooth. Clearly, taking the limit $a \rightarrow 0$ is of no use here; instead, a coarse graining procedureⁱ over a certain length a' is necessary:

$$H(x) = \frac{1}{a'} \int_x^{x+a'} h(x') dx' \tag{2.27}$$

To ensure $H(x)$ really being sufficiently differentiable, this simple averaging, i.e. folding with a box-function, is not suitable. For that, a smoother

ⁱThis is not to be confused with the coarse grained model of section 2.5.4.

kernel has to be employed like e.g. $\sin(x)/x$ which is used implicitly when, after a Fourier transformation, the operations are performed in reciprocal space with a short-wavelength cutoff. Nevertheless the procedure (2.27) serves well to elucidate the interplay of the length scales a and a' . The variance of the smoothed function $H(x)$ is readily available from eq. (2.24):

$$\begin{aligned}
 \langle H^2(x) \rangle &= \frac{1}{a'^2} \int_x^{x+a'} \int_x^{x+a'} \langle h(x')h(x'') \rangle dx' dx'' \\
 &= \frac{t}{a'^2} \int_x^{x+a'} \int_x^{x+a'} C(x' - x'') dx' dx'' \\
 &= a_{\perp}^2 \frac{t}{t_{\text{ML}}} \min \left\{ \frac{a}{a'} \left(1 - \frac{a}{4a'} \right), 1 \right\}
 \end{aligned} \tag{2.28}$$

The most natural choice would be to set the coarse graining length to half the lattice constant and hence by obtaining $\min\{\dots, 1\} = 1$ to retain the result (2.26). The common practice is different, though: Upon multiplying the Heaviside function in eq. (2.25) by a'/a , we get the same result when taking the limit $a \rightarrow 0$. In fact, this means replacing the correlator of finite width by a delta function:

$$C(x - x') \rightarrow \frac{a_{\perp}^2}{t_{\text{ML}}} a' \delta(x - x') \tag{2.29}$$

This is a very convenient method for the more complex evolution equations, since the delta function simplifies the evaluation of the occurring integrals. In fact, almost all Langevin equations with spatially uncorrelated noise are written in this way, and only in a few cases it is mentioned not to “take the δ -function literally” (e.g. (Nattermann and Tang, 1992; Rost and Spohn, 1994; Rost and Krug, 1997b)).

To recapitulate: The inherently finite correlation length a is removed (i.e. shrunken to zero), which has no influence on the *coarse grained* quantity as long as the noise’s amplitude is increased to compensate the smoothing effect of the coarse graining.

On the other hand, we notice that in the prefactor of the delta function in eq. (2.29)

$$\mathcal{F} \equiv \frac{a_{\perp}^2}{t_{\text{ML}}} a'^d = F a_{\perp}^2 a'^2, \tag{2.30}$$

called the *noise strength* (here generalized to d dimensions), bears an ingredient related to the former lattice constant, namely $1/t_{\text{ML}} = F a^d$. This

implies a diverging flux F for a vanishing a , which is obvious, since to cover a certain area within a fixed time using smaller and smaller particles, more and more of them are needed. Hence, to retain a meaningful flux, we have to substitute

$$\frac{1}{t_{\text{ML}}} = F a'^d, \quad (2.31)$$

by which the original lattice constant a has escaped the description completely and its rôle has been taken over by the coarse graining length a' . Even calling it “lattice constant” is justified somewhat in the sense that the coarse graining mimics instantaneous transport across a distance of order a' , just as if the resulting correlations were due to the deposition of particles with a finite size. With this justification, we will rename a' back to a later.

In the context of letting also a' vanish (one is always set on reducing the number of parameters), a few words about the handling of the quantities F , t_{ML} and \mathcal{F} are advisable here: If we rewrite the correlator in the usual way

$$\langle \eta(x, t) \eta(x', t') \rangle = \mathcal{F} \delta(x - x') \delta(t - t'),$$

we get from eq. (2.28)

$$\langle H^2(x) \rangle = \frac{\mathcal{F} t}{a'}, \quad (2.32)$$

whose putative divergence for $a' \rightarrow 0$ (which means nullifying the coarse graining procedure) seems to correspond to the undefined result

$$\langle h^2(x) \rangle = \mathcal{F} t \delta(0),$$

which follows from skipping the coarse graining entirely. But unlike the latter expression, eq. (2.32) tells us the cancellation $\mathcal{F} t / a' = a_{\perp}^2 t / t_{\text{ML}}$, which prevents any divergence.

On the other hand, one might like to push this even further by using equation (2.31) and arguing

$$\frac{a_{\perp}^2 t}{t_{\text{ML}}} = a_{\perp}^2 t F a' \xrightarrow{a' \rightarrow 0} 0.$$

Indeed, we already discussed above that a finite flux of zero-sized particles does not produce any coverage and that we have to rescale F accordingly in order to keep t_{ML} constant.

Hence, we learn that manipulating the lattice constant consistently is not always an obvious task. Naturally, it gets even more subtle in situations

beyond the simple random deposition. As a concluding example serves a Langevin equation containing an additional diffusion-like term, whose physical origin we shall discuss in section 2.6.2:

$$\partial_t h(x, t) = \nu \partial_x^2 h(x, t) + \eta(x, t) ,$$

where the noise keeps its correlator as

$$\langle \eta(x, t) \eta(x', t') \rangle = \mathcal{F} \delta^d(x - x') \delta(t - t') , \quad (2.33)$$

which is the standard notation for white noise.

Due to the linearity, this equation (as well as its cousins of higher order spatial derivatives) can be solved exactly (cf. (Krug, 1997)), yet already exhibits a non-trivial behavior. Above $d = 2$, it reaches a stationary state of finite width in the long time limit with

$$w_\infty^2 \equiv \langle h^2(x, t \rightarrow \infty) \rangle \sim \frac{\mathcal{F}}{\nu a^{d-2}}$$

for an infinite system size^j.

Again the divergence of w_∞^2 for $a \rightarrow 0$ lacks a physical motivation while its vanishing, when resolving

$$\frac{\mathcal{F}}{\nu a^{d-2}} = \frac{a_\perp^2}{\nu t_{\text{ML}}} a^2 ,$$

is in agreement with diffusive behavior where modes of shorter wavelength relax faster (actually as the wavelength's square).

While the above is true for a fixed parameter ν , in the context of discrete diffusion hops of step size a we may have

$$\nu = \frac{a^2}{\tau}$$

with some fixed, microscopic time τ , which leads us to

$$w_\infty^2 \sim a_\perp^2 \frac{\tau}{t_{\text{ML}}} ,$$

another most intuitive relation.

We conclude that the common practice of letting the lattice constant vanish while keeping the noise strength fixed, is often useful when examining the solution of a corresponding Langevin equation with respect to universal properties, but in the context of shot noise due to particle deposition it means an inconsistency which can lead to confusing interpretations.

^jFrom here on, we have renamed $a' \rightarrow a$.

Other sources of noise

Before turning to the deterministic part of the Langevin equation, other types of noise than deposition should be briefly considered. The adatoms' random walks are stochastic processes as well and this can indeed be described by a noise term η_c . This is done most suitably by writing it as the (negative) divergence of a stochastic surface current $\vec{j}(\vec{x}, t)$ possessing white noise properties according to

$$\langle j_m(\vec{x}, t) j_n(\vec{x}', t') \rangle = \mathcal{F}_c \delta_{m,n} \delta^d(\vec{x} - \vec{x}') \delta(t - t') \quad (2.34)$$

with (Tang and Nattermann, 1991)^k

$$\mathcal{F}_c \equiv 2D\Omega^2\rho, \quad (2.35)$$

where ρ is the adatom density and $\Omega = a^d a_\perp$ is the atomic volume. When considering the fluctuations averaged over the whole surface L^d , i.e.

$$\bar{\eta}_c(t) = -\frac{1}{L^d} \int_{L^d} \nabla \cdot \vec{j}(\vec{x}, t) d^d \vec{x},$$

we find it vanishing, provided periodic boundary conditions or a zero current at the border. In contrast, the corresponding $\bar{\eta}(t)$ resulting from the shot noise (2.33) is again white noise (2.21) with $C = (a/L)^d \mathcal{F}$. That means

$$\eta_c = -\nabla \cdot \vec{j} \quad (2.36)$$

preserves the system volume for every realization (not just on the average), hence the name *conserved noise*.

The same result without the detour via the current is obtained by assigning the correlator

$$\langle \eta_c(\vec{x}, t) \eta_c(\vec{x}', t') \rangle = -\mathcal{F}_c \nabla^2 \delta^d(\vec{x} - \vec{x}') \delta(t - t'), \quad (2.37)$$

a result easy to memorize by exchanging ∇ and $\langle \dots \rangle$ (which is merely a mnemonic, though).

The remaining source of further stochasticity is the process of island nucleation. This can be modeled by another noise term $\eta_{cc}(\vec{x}, t)$ with a correlator $\propto \nabla^4 \delta^d(\vec{x} - \vec{x}') \delta(t - t')$ which we shall not elaborate here (but cf. (Wolf, 1995; Somfai et al., 1996)). Later we will reveal that we need to focus only on the shot-noise anyway.

^k Ω^2 as a prefactor is absent in (Tang and Nattermann, 1991), since there it is the correlator of a *particle* current, cf. section 2.6.2.

2.6.2 Relaxation

After the treatment of the contributions producing disorder, the mechanisms that smooth the surface have to be taken into consideration. The most general extension to the Langevin equation (2.20) accounting for this reads

$$\partial_t h(\vec{x}, t) = \Phi[h(\vec{x}', t), \vec{x}] + \eta(\vec{x}, t), \quad (2.38)$$

where Φ is a functional of the current height configuration (with the additional parameter \vec{x}). Allowing only for local relaxation mechanisms and assuming translational invariance in the vertical direction, Φ reduces to a (possibly arbitrarily complex) combination of spatial derivatives of h . The class of permissible combinations is restricted in the presence of further symmetries like invariance under in-plane rotation or inversion. Nevertheless a great many terms are left and we will now discuss why there is only a finite number of growth equations to be considered.

Self-affine dynamical scaling

It is known that, unless the surface undergoes an instability (i.e. it develops modulations with a characteristic wavelength), the resulting height profile of equations like (2.38) exhibit *self affine dynamical scaling* (Family and Vicsek, 1985; Family and Vicsek, 1991). If this happens due to depositing particles, i.e. we are dealing with a driven system, we speak of *kinetic roughening* in contrast to the transition phenomenon of *thermal roughening* (cf. e.g. Pimpinelli and Villain, 1999).

Self affine scaling of an object means, that after rescaling all spatial directions with the proper factor, no change of the object can be observed. The special case where all directions share the same factor is called *self similarity*, an ubiquitous property in the context of fractals (Mandelbrot, 1983). Our object to deal with is the graph of the function $h(\vec{x})$, where – assuming isotropic physics – the scaling factor b is the same for all lateral directions. Note that $b > 1$ represents zooming out while $0 < b < 1$ means zooming in. Out of regular functions, only the homogeneous ones have this property, e.g. $h(x) = x^n$ in one dimension.

With *dynamical* scaling, time enters the play, and self affine dynamical scaling is said to apply if

$$h(b\vec{x}, b^z t) \triangleq b^\zeta h(\vec{x}, t) \quad (2.39)$$

holds true, i.e. if our current configuration $h(\vec{x}, t)$, scaled up by a factor b^ζ , matches a laterally zoomed out one (by factor b) at a later time $b^z t$. With noise involved, we cannot expect exact equality between these two configurations, they can only be equivalent in a statistical sense¹ (indicated by “ $\underline{\cong}$ ” instead of “ $=$ ”). The scaling characteristic is thus fully specified by the *dynamical exponent* z and the *roughness exponent* ζ , which are also said to define the *universality class* of the model that produces the configurations with the property (2.39).

A way to extract the exponents is to study the height difference correlation function $G(\vec{r}, t)$ (cf. section 2.4.5), which by virtue of the scaling property eq. (2.39) satisfies

$$G(r, t) = b^{-2\zeta} G(r, b^z t),$$

where with writing r rather than \vec{r} , we imply in-plane isotropy.

To keep the notation simple, we revert to natural units, i.e. r and t are dimensionless for the following considerations^m. Provided that, we can make the special choice $b = 1/r$ which reveals that G is actually a function of only one variable:

$$G(r, t) = r^{2\zeta} G(1, t/r^z) \equiv r^{2\zeta} \tilde{G}(t/r^z) \quad (2.40)$$

Some basic physical considerations help us to predict further features of the function $\tilde{G}(t/r^z)$: The self affine property is due to height correlations developing between distant locations $\vec{x} \leftrightarrow \vec{x}'$. But because of the communication being only local, it takes time to build up these correlations and for very large distances $G(r, t)$ should not change with r anymore. This implies $\tilde{G}(y)$ varying like $y^{2\zeta/z}$ for small arguments (and thus $G(r, t) \propto t^{2\zeta/z}$). On the other hand, shorter ranged correlations are set up early and do not change anymore, i.e. $G(r, t)$ is expected to be time independent for small r which in turn requires $\tilde{G}(y)$ approaching a constant for large arguments. The intermediate regime is fixed by $y \approx 1$ from which we infer the correlations spreading like $t^{1/z}$, or expressed as the *correlation length*

$$\xi \propto t^{1/z}. \quad (2.41)$$

Of course, in a system of finite size L the correlation length cannot exceed $L/2$ (assuming periodic boundary conditions); the system then has reached a

¹Such that they look the same for an observer, unless he has a photographic memory.

^mLater we will emphasize the cases where it is vital to take into account the actual units.

stationary state (in a statistical sense), where $G \propto r^{2\zeta}$ is valid up to $r = L/2$ which causes due to eq. (2.10) the corresponding power law for the width

$$w^2 \propto L^{2\zeta} .$$

On the other hand, if $\xi \ll L$, the averaging (2.10) is dominated by the part $r > \xi$ resulting in

$$w^2 \propto t^{2\beta} , \tag{2.42}$$

where $\beta \equiv \zeta/z$.

Writing it in a scaling form, first used in (Family and Vicsek, 1985), combines the two cases:

$$w^2(L, t) = L^{2\zeta} \tilde{w}^2\left(\frac{L}{t^{1/z}}\right) \tag{2.43}$$

with

$$\tilde{w}^2(y) \sim \begin{cases} \text{const} & \text{for } y \ll 1 \\ y^{-2\zeta} & \text{for } y \gg 1 \end{cases} \tag{2.44}$$

It summarizes how by investigating different sized systems in the steady state and the growing width w^2 in a large system the exponents ζ and ζ/z respectively can be measured. The scaling exponents actually have a graphical meaning: Such a self affine surface exhibits irregular bumps of all sizes up to a lateral length scale which is of the order of ξ , while the height scale of these largest bumps is given by w . That means their growth velocity in lateral and vertical direction is fixed by the exponents $1/z$ and β respectively, while ζ controls their change in aspect ratio with size. Therefore, a surface with negative ζ is called “smooth” (despite the fact that the system may take on a finite w^2 for $L \rightarrow \infty$, cf. (Kallabis, 1997)), while $\zeta > 0$ stands for “rough”. A value of zero usually makes logarithmic corrections appear and hence means $w^2 \propto \ln(\xi) \propto \ln(t)$. An exact $\zeta = 0$ is the case of e.g. sandpaper, its grains do not increase in size when taking larger and larger sheets, thus it is not “rough” in our sense.

The critical reader may cast doubt on the argument about the stationary correlations for $r < \xi$. Indeed, there are exceptions where $G(1, t)$ grows itself according to a power law in time which spoils the scaling properties (2.40) and (2.43). This behavior is called *anomalous scaling* (Amar et al., 1993;

Schroeder et al., 1993; Sarma et al., 1994; Sarma and Punyindu, 1997; Krug, 1997) and is mostly associated with a $\zeta \geq 1$ extracted from measurements according to eq. (2.43) which got to bear the name *super-roughness*. The statistical properties of such surfaces possess their own special features (Sarma and Punyindu, 1997; Lee and Doochul, 1997; Lopez et al., 1997; Pang and Tzeng, 2000a; Pang and Tzeng, 2000b) like e.g. multiscaling, which we shall not discuss further but close by noting that bumps with $\zeta > 1$ get steeper and steeper on large scales and therefore raise the problem of ruling out a well defined surface orientation and the solid on solid constraint.

Power counting

With this background about scaling exponents, we can apply a technique called *power counting* to sort out relevant terms for eq. (2.38) out of the pool of possible ones. Suppose, we start including all terms linear in h of even order (odd ones violate the in-plane $\vec{x} \rightarrow -\vec{x}$ -symmetry), that is

$$\partial_t h(\vec{x}, t) = - \sum_{k=1}^{\infty} (-\nu_{2k} \nabla^2)^k h(\vec{x}, t) + \eta(\vec{x}, t). \quad (2.45)$$

Now we replace $h(\vec{x}, t)$ by $b^{-\zeta} h(b\vec{x}, b^z t)$, yielding

$$\begin{aligned} \partial_{(b^z t)} h(b\vec{x}, b^z t) &= - \sum_{k=1}^{\infty} b^{2k-z} (-\nu_{2k} \nabla_b^2)^k h(b\vec{x}, b^z t) \\ &\quad + b^{\frac{2\zeta+d-z}{2}} \eta(b\vec{x}, b^z t), \end{aligned} \quad (2.46)$$

where ∇_b denotes the derivative with respect to the new spatial variable $b\vec{x}$ and we used the correlator (2.33) to express

$$b^{(d+z)/2} \eta(b\vec{x}, b^z t) = \eta(\vec{x}, t). \quad (2.47)$$

For we know that the above replacement should not have changed anything, all the powers of b in eq. (2.46) have to vanish (because then it is identical to eq. (2.45), just with renamed variables). Obviously this is impossible unless only one of the coefficients ν_{2k} is non-zero.

But let's – provided $\nu_2 \neq 0$ – insert the ansatz $z = 2$, $\zeta = (2 - d)/2$ into eq. (2.46). Then, the noise and the ν_2 -term loose their b -factor while all higher derivatives obtain with b^{2k-2} a *negative* power of b . That means, the

rescaled profile $b^{-\zeta}h(b\vec{x}, b^z t)$ does not solve exactly eq. (2.45) but a modified form, where all terms higher than $k = 1$ have a reduced influence. On larger and larger scales (growing b), their importance decreases more and more until only ν_2 is left; they are called *irrelevant* in the sense of scaling.

The reasoning above was putting the cart before the horse, of course. Actually, a solution to eq. (2.45) simply will *not* exhibit self affine scaling with $z = 2$, $\zeta = (2-d)/2$ on small scales, this will become true only asymptotically (large b) where it is indistinguishable from a solution to the equation with ν_2 alone.

In fact, such a gradual change in the scaling behavior is known as *cross-over* for which an illustrative example is the case $\nu_4 \gg \nu_2$ (in natural units) with all higher terms being zero. Here, with $z = 4$, $\zeta = (4-d)/2$ the (initially) dominant ν_4 -term stays unrescaled while the ν_2 -term increases with b^2 . When finally features of such size b have been developed that $b^2\nu_2 > \nu_4$, the behavior according to $z = 2$, $\zeta = (2-d)/2$ will take over. Still the ν_4 -term is operative on smaller scales, but when measuring e.g. w^2 , these are dominated by the large scale behavior.

Summarizing, if ν_{2k} is the first non-zero coefficient, then

$$\begin{aligned} z &= 2k \\ \zeta &= \frac{z-d}{2} \end{aligned}$$

are the (asymptotic) scaling exponents.

In the same way, we can handle now the different types of noise: Employing the correlator (2.37) instead of (2.33), the conserved noise turns out to rescale as

$$b^{(d+2+z)/2} \eta_c(b\vec{x}, b^z t) = \eta_c(\vec{x}, t),$$

which differs from eq. (2.47) only by an “enhanced dimensionality” $d \rightarrow d+2$. This leaves z untouched, only the roughness exponent drops to $\zeta = (z-d-2)/2$ already indicating that conserved noise is less capable of roughening the surface. This applies even more to the nucleations noise where the same calculation leads to $d \rightarrow d+4$ and hence $\zeta = (z-d-4)/2$. Moreover, by means of this analysis, we can conjecture that shot-noise is dominant on large scales in the case of all three types terms being present, the other two are irrelevant with $\zeta = (z-d)/2$.

Unfortunately, the convenient method of power counting is only reliable for linear equations (where more can be calculated than just their exponents, cf. (Krug, 1997; Kallabis, 1997)). With nonlinearities involved, the

coefficients in the equation may prove to depend on the scale b themselves, which has to be dealt with by performing not only a rescaling transformation but also a coarse graining step to eliminate short wavelength contributions after zooming out. This makes up a renormalization cycle which provides the basis of the *renormalization group* theory (RG) (Forster et al., 1977; Medina et al., 1989; Tang and Nattermann, 1991; Nattermann and Tang, 1992), a topic mathematically too involved to be discussed here any further.

2.6.3 Physical origins

Having discussed permissibility and relevance of contributions to the deterministic part, we come to the question the occurrence of which relaxation terms in the Langevin equation is physically to be expected or plausible. We restrict ourselves to the most prominent ones, though on the other hand one of them cannot possibly describe ideal MBE. The reason is that without evaporation and without holes and overhangs (see section 2.3), elapsed time and deposit volume (per unit area) can be identified. Hence, in the comoving frame of velocity ΩFt , the surface current \vec{j} – the only means for relaxation – is related to the change in height by a conservation law:

$$\partial_t h = -\nabla \cdot \vec{j} \quad (2.48)$$

In the presence of deposition we have to add shot noise, while the diffusion noise can be included in the current \vec{j} (cf. eq. (2.36)).

Relaxation dynamics of conservative type – most commonly called *conserved dynamics* – has an important implication on the scaling exponents, namely these are related to each other by

$$z = 2\zeta + d \quad (2.49)$$

in this case, as shown in appendix C (see also (Tang and Nattermann, 1991)).

Because the lattice constants reduce to unity when natural units are employed, confusion can emerge about the character of the current. The conservation law (2.48) clearly involves a *volume* current density while the more common definition is *particle* density times velocity, which we shall designate as J . Their different dimensions

$$[j] = \text{HLT}^{-1} \quad [J] = \text{L}^{d-1}\text{T}$$

reflect the obvious relation

$$j = a_{\perp} a^d J = \Omega J .$$

This has to be kept in mind when performing dimensional analyses.

The Edwards-Wilkinson equation

We encountered this equation

$$\partial_t h = \nu \nabla^2 h + \eta \tag{2.50}$$

already during the discussion of the lattice constant's rôle in section 2.6.1. Though it has the form of a noisy diffusion equation, the ν -term can be of various origin. For the case of equilibrium (i.e. $F = 0$ and the noise being of thermal nature), evaporation-condensation dynamics produces such a term (to leading order) where ν is the product of surface tension and interface mobility (Spohn, 1993; Krug, 1997).

But evaporation is negligible under MBE conditions (Villain, 1991), and the surface current being responsible for relaxation (cf. eq. (2.48)) reads

$$\vec{j} = -\nu \nabla h , \tag{2.51}$$

i.e. it is a current driven by height differences. This suggests gravity as the dominant force which is certainly not the case for atomistic growth processes.

In fact, Edwards and Wilkinson derived eq. (2.50) in the context of off-lattice sedimentation (Edwards and Wilkinson, 1982), and though it was shown later (Krug, 1989) that the absence of a lattice produces an additional relevant term (namely the *KPZ-nonlinearity* as introduced below), the scaling exponents

$$z = 2 \quad , \quad \zeta = \frac{2-d}{2}$$

are said to define the Edwards-Wilkinson (EW) universality class. Its most prominent representative amongst lattice models is the one suggested by Family (Family, 1986) where after a particle is deposited at a randomly chosen site, it can perform a relaxation step to minimize its height. To do so, it can hop to one of its nearest neighbor sites. We will meet this model again in chapter 7.

Even though we just now ruled out the EW-term for MBE conditions in equilibrium, it can appear upon turning on deposition. One origin is an

asymmetry in the adatoms' accretion concerning upward/downward-steps, as we will discuss to more detail in chapter 4. Other processes are the knockout mechanism (Evans, 1991; Vvedensky et al., 1993) and downward-funneling (Evans, 1991).

The Kardar-Parisi-Zhang equation

Perhaps the most famous equation in the field of moving interfaces is the Kardar-Parisi-Zhang (KPZ) equation (Kardar et al., 1986), distinct from the EW-equation through the presence of another term, the *KPZ-nonlinearity*:

$$\partial_t h = \nu \nabla^2 h + \lambda (\nabla h)^2 + \eta \quad (2.52)$$

The nonlinearity stems from a purely geometrical consideration in the first place: If growth takes always place normal to the local surface orientation, then already the trivial case of an interface growing with a constant, isotropic velocity v_0 , which reads in the projected form as

$$\partial_t h = v_0 \sqrt{1 + (\nabla h)^2}, \quad (2.53)$$

yields $v_0/2(\nabla h)^2$ as leading order term of a gradient expansion. This will not change for a non-trivial, anisotropic local growth velocity (e.g. induced by deposition $F \neq 0$), unless it cancels the square root in eq. (2.53) exactly. We note that eq. (2.52) cannot be brought into the form (2.48), and hence it is no candidate for the description of conserved dynamics like present in MBE.

There are two reasons for the most outstanding attention payed to the KPZ equation (which is, when expressed in terms of $\vec{u} \equiv -\lambda \nabla h$, also known as *noisy Burgers equation*): First, it can be considered as *the* generic growth equation in the sense that, with respect to its two terms, all further ones are irrelevant in the sense of scaling (Krug, 1997; Pimpinelli and Villain, 1999). That means, since generally the absence of its terms in other equations is only an approximation (like in MBE the presence of desorption, holes and overhangs is not prohibited completely in reality), on large enough length and time scales – possibly not relevant for practical purposes anymore – the statistical properties of almost every growing interface should be governed by eq. (2.52) (Krug and Spohn, 1991). Exceptions are situations where the disorder is (besides the \vec{x} -dependence) not a function of time but of height, i.e. the case of *quenched disorder*.

The second reason is, that despite the enormous analytical and numerical effort spent on the KPZ equation (cf. (Meakin, 1993; Ala-Nissila et al., 1993)), up to now only a few of its properties are known exactly. A helpful symmetry in this context is its tilt invariance: If $h(\vec{x}, t)$ is a solution to eq. (2.52), then the same applies after the transformation

$$h(\vec{x}, t) \rightarrow h(\vec{x} - \lambda \vec{s}t, t) - \frac{\vec{s} \cdot \vec{x}}{2} + \frac{\lambda \vec{s}^2}{4}t, \quad (2.54)$$

albeit with a shifted noise $\eta(\vec{x} - \lambda \vec{s}t, t)$ (which makes no difference for white noise (2.33)). Because λ appears explicitly in this *global* transformation, it must be the same on all length scales; in the language of renormalization group theory, it is *not renormalized*. That means, when applying power counting to the KPZ equation, the factor $b^{z+\zeta-2}$ assigned to the nonlinearity has to remain unity in any case, yielding the scaling relation

$$z + \zeta = 2,$$

which leaves only one exponent to be determined. In one dimension (and only there), the stationary properties of an interface behaving according to eq. (2.52) coincide with the ones for the linear eq. (2.50) (Krug and Spohn, 1991), implying the same exponent $\zeta = 1/2$. This in turn yields $z_{\text{KPZ}} = 3/2$ for $d = 1$.

We shall not elaborate the partially elusive properties of the KPZ equation like a possible upper critical dimension (cf. (Moore et al., 1995; Lässig and Kinzelbach, 1997) vs. (Halpin-Healy and Zhang, 1995; Ala-Nissila, 1998)) or the *strong coupling regime* (Sun and Plischke, 1994; Frey and Tauber, 1994) but rather close with the note that the tilt-invariance can be used to measure the parameter λ explicitly. As can be read off the transformation (2.54), a tilt \vec{s} increases the average growth velocity by an amount $\lambda \vec{s}^2/4$. Hence, plotting this extra velocity vs. $\vec{s}^2/4$ reveals the strength of the nonlinearity.

Mullins' equation

The fourth order linear equation

$$\partial_t h = -K \nabla^4 h + \eta$$

is usually termed *Mullins' equation*, though in his original work (Mullins, 1963), he treated the deterministic version ($\eta = 0$). Nevertheless, the underlying idea of the surface current

$$\vec{j} = -K \nabla(-\nabla^2 h)$$

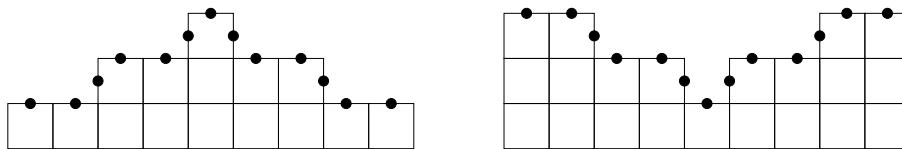


Figure 2.6: Unsatisfied bonds for a one-dimensional surface region of negative (left) and positive curvature (right): A difference in coordination number is effective only in the immediate vicinity of the central site, all other kinks appear pairwise.

being driven by gradients in the (negative) local curvature, still applies to situations involving noise (Wolf and Villain, 1990; Golubović and Bruinsma, 1991), keeping in mind that in equilibrium η must denote conserved noise.

Usually this Gibbs-Thomson-like favoring of larger curvature (sign taken into account) is explained in a simple broken-bond-type fashion (Pimpinelli and Villain, 1999), where local minima (maxima) offer a higher (lower) density of highly coordinated (Barabasi and Stanley, 1995). However, it should be pointed out that in one dimension, this approach is only of very limited applicability, as explained in fig. 2.6. While the origin of K as a product of adatom mobility and surface stiffness (Mullins, 1963; Krug et al., 1995) can be regarded as valid for situations slightly out of equilibrium, kinetic effects are expected to take over in driven systems (Villain, 1991).

The conserved KPZ equation

The equation

$$\partial_t h = -K \nabla^4 h - \lambda \nabla^2 (\nabla h)^2 + \eta \quad (2.55)$$

got its name from its formal resemblance with the KPZ equation (2.52). The crucial difference to the latter is the possibility to bring it into the form of conserved dynamics (2.48), with a surface current

$$\vec{j} = \nabla (K \nabla^2 h + \lambda (\nabla h)^2) . \quad (2.56)$$

which has been widely discussed (Sun et al., 1989; Villain, 1991; Wolf and Villain, 1990; Lai and Sarma, 1991; Tang and Nattermann, 1991) in the context of molecular beam epitaxy. We shall have a closer look at the non-linear term, driving a current according to differences in the squared surface tilt, to more extent in section 3.3.3.

As a counterpart to the tilt invariance (2.54) for the KPZ equation, there has been belief in an analogous symmetry for the cKPZ equation (Sun et al., 1989) for a long time (see (Halpin-Healy and Zhang, 1995; Barabasi and Stanley, 1995), though there has been doubt as well (Villain, 1991; Tang and Nattermann, 1991)). This symmetry would proof the non-renormalization of λ in the cKPZ equation, which in turn implies the scaling relation

$$\zeta + z = 4 ,$$

and together with the relation (2.49) for conserved dynamics it yields the scaling exponents

$$\zeta = \frac{4-d}{3} \quad , \quad z = \frac{8+d}{3} . \quad (2.57)$$

While being correct in a *first-order renormalization* treatment (Lai and Sarma, 1991), they obtain second-order corrections (Janssen, 1997); a result which rules out the validity of the symmetry proposed in (Sun et al., 1989). But since these corrections are tiny, the values (2.57) should be a good approximation for comparisons to numerical data.

Let's close this chapter by mentioning approaches to reintroduce the vertical lattice constant a_{\perp} back into the continuum equations by adding a potential with vertical period a_{\perp} . For the KPZ equation (2.52) this is interpreted directly as a pinning potential, while for the conserved KPZ equation (2.55) it is introduced as a local chemical potential of the adatoms. The resulting equations are called *driven sine-Gordon* (Rost and Spohn, 1994) and *conserved driven sine-Gordon* (Rost and Krug, 1997b) respectively. As can be concluded from the latter's name, it can be brought into the form (2.48).

Chapter 3

Kinetic roughening

3.1 From submonolayer to scaling

Based upon the ideal MBE model presented in section 2.3 and its extensions, numerous work has been done related to the statistical properties of the submonolayer regime (characteristic distances, island size distribution, island shapes, . . . , cf. (Tang, 1993; Amar et al., 1994; Bales and Chrzan, 1994; Schroeder and Wolf, 1995; Amar and Family, 1996b)) of which we will only need a minute fraction in the following section. A comparable extensive investigation was granted to the asymptotic regime, where dynamical scaling is expected to hold and possible adequate continuum equations can be discussed (for a summary cf. (Barabasi and Stanley, 1995)). Disproportionally less is known about the transition from the former to the latter. In 1994 it was observed in computer simulations of the one-dimensional situation (Brendel, 1994; Wolf, 1995) that the time \tilde{t} this transition takes depends algebraically on the growth parameter D/F :

$$\frac{\tilde{t}}{t_{\text{ML}}} \propto \left(\frac{D}{F}\right)^\delta \quad (3.1)$$

In this chapter we shall present a theory for this transition time as well as simulation data for $d = 1$ and $d = 2$. To motivate the basic concepts of the theory, let's anticipate three results of the simulation.

3.1.1 Layer-by-layer growth's end

As read off fig. 3.1 on the next page, the oscillations of the squared surface width $w^2(t)$ as a manifestation of layer-by-layer growth cease when w^2 reaches a value of order unity, independent of D/F^a . This is specific to the system state and not just inherent to the quantity w^2 ; one could e.g. imagine a morphological scenario of deep trenches separating plateaus on which layer-by-layer growth takes place locally. The result would be an oscillating $w^2(t)$ around an arbitrarily high value.

3.1.2 Importance of shot noise

Since it is obvious that in the case considered here fluctuations are responsible for the limited lifetime of layer-by-layer growth, first all three different sources

^aActually, the time needed for the development of a certain width w^2 will serve as the definition of the measured damping time \tilde{t} .

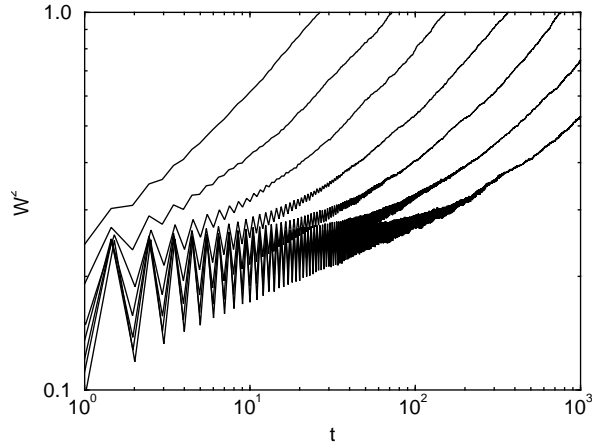


Figure 3.1: Oscillations of the (squared) surface width $w^2(t)$ in $d = 1$ for $D/F = 10^4 \dots 10^{10}$ (from left to right) and $i^* = 1$. Layer-by-layer growth ceases around $w^2 = 0.5$, independent of D/F .

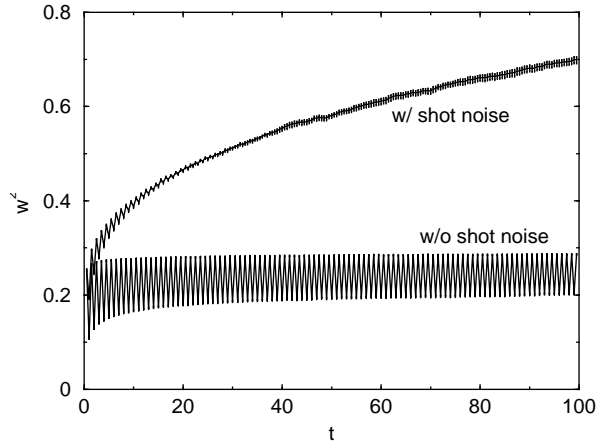


Figure 3.2: Temporal development of the surface width w^2 with and (almost) without shot noise for $D/F = 10^3$. Clearly it is the shot noise responsible for the damping. The manner to suppress it is described in the text.

of noise discussed at the end of section 2.6.1 come into play: shot noise, diffusion noise and nucleation noise. Though the first one was shown to dominate the other two on large length scales in section 2.6.2, it is not clear

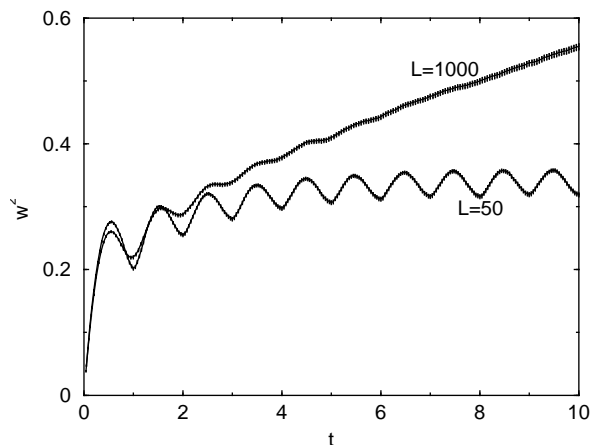


Figure 3.3: Suppression of the damping by means of a small system size for $D/F = 10^4$ in $d = 1$. This effect is employed systematically in section 3.4 to determine the layer coherence length \tilde{l} .

a priori that we deal with such scales in the case of damped layer-by-layer growth. However fig. 3.2 on the preceding page gives clear evidence that shot noise is necessary for damping, at least on time scales considered here.

The shot noise in the simulation in fig. 3.2 on the page before was overcome in the following way: Instead of picking the site for a deposition simply at random, it is ensured that during the deposition of one mono-layer each site is hit exactly once. The order of this deposition pattern is random though and changes after each mono-layer. Though this procedure does not eliminate shot noise on short time scales (compared to the mono-layer time t_{ML}), it has the advantage of not raising any questions about the physical interpretation (except for a possible experimental realization, of course). In chapter 7 we will get to know other means to suppress the noise. In (Sun et al., 1989), where yet another method was employed, an analytic treatment predicts roughness of merely logarithmic type in $d = 2$ ^b, which makes the apparent absence of any roughening at all in fig. 3.2 on the preceding page understandable.

3.1.3 Layer coherence

As to be expected, arbitrarily small systems do not get rough. Already a size of $L = 50$ is sufficient to cause a stationary state with persisting oscillations,

^bThis prediction could be confirmed also for the method utilized here.

which is shown in fig. 3.3 on the page before. This minimal length scale below which no roughness is developed, we shall call it *layer coherence length*, depends on D/F and will be another central ingredient of the forthcoming theory.

3.2 Submonolayer considerations

Before setting up the theory for the damping, we will have to review some properties of the submonolayer regime. The dependence of the characteristic island distance l_D on the growth conditions has already been well studied (Zinsmeister, 1968; Zinsmeister, 1969; Zinsmeister, 1971; Stoyanov and Kashchiev, 1981; Venables et al., 1984; Villain et al., 1992; Pimpinelli et al., 1992; Wolf, 1995; Jensen et al., 1997), but a brief theoretical derivation shall be outlined here for the simplest case of $i^* = 1$.

3.2.1 The exponent γ

After their nucleation, islands grow until they start to “touch” each other at a time when each one has obtained on average $(l_D/a)^{d'}$ atoms, i.e. around a coverage of $(l_D/a)^{d'-d}$. We distinguish between the dimensionality of the islands d' and the one of the substrate to include also fractal islands^c. During coalescence, the formation of island seeds has a vanishing probability. This means, there has been only one nucleation event in an area l_D^d during this time, from which we can infer for the nucleation rate within this area

$$\nu_{\text{nuc}} \sim \frac{(l_D/a)^{d-d'}}{t_{\text{ML}}} . \quad (3.2)$$

The island edges, which are a distance l_D apart, prescribe the boundary conditions for the adatoms' diffusion equation

$$\partial_t \rho = D \Delta \rho + F$$

and so the scale of the quasi-stationary adatom density ($\partial_t \rho \ll F$) can be concluded already from dimensional considerations (see also (Villain et al.,

^cThe case of compact islands ($d' \geq d$) shows that we have omitted a geometrical factor < 1 here. A more thorough treatment, especially in the context of fractal islands can also be found in (Bales and Chrzan, 1994).

1992)):

$$\rho \sim \frac{Fl_D^2}{D} \quad (3.3)$$

This density is one factor entering the collision rate of adatoms which equals – because of $i^* = 1$ – the nucleation rate. The other factor is the number of sites visited by an adatom during its lifetime τ , with

$$\tau \sim \frac{l_D^2}{D},$$

a relation following immediately from eq. (3.3) and the fact that new adatoms are supplied with the flux F . The number of hops performed during this time, namely

$$\tilde{N} = \frac{\tau D}{a^2} \sim \frac{l_D^2}{a^2} \quad (3.4)$$

is a valid measure for the visited sites only in substrate dimensions higher than two^d. For the two-dimensional case, the correction is only logarithmic (Henyey and Seshadri, 1982)

$$N_{d=2} \approx \frac{\tau D}{a^2 \ln(\tau D/a^2)} \sim \frac{l_D^2}{a^2 \ln(l_D^2/a^2)}$$

while for $d = 1$ the correct number is obviously significantly less, namely the square root of \tilde{N} :

$$N_{d=1} \sim \frac{l_D}{a}$$

If we neglect the logarithmic correction (as is usual practice, except e.g. (Tang, 1993)), both cases can be written simply as

$$N \sim (l_D/a)^d,$$

a notation valid only for $d = 1$ and $d = 2$.

Now, the product $N\rho a^d$ has the meaning of the probability for one specific adatom to encounter another one (before its lifetime expires by being

^dBelow $d = 3$, a random walker will revisit every site with probability one, actually it does so arbitrarily often for long times. This causes the ratio (no. distinct visited sites)/ \tilde{N} to vanish asymptotically.

3.2. SUBMONOLAYER CONSIDERATIONS

incorporated into an island). To obtain the nucleation rate we have to multiply it by $F l_D^d$, since this is the number of atoms deposited per unit time into the corresponding area l_D^d :

$$\nu_{\text{nuc}} \sim \frac{l_D^d}{a^d} \frac{F l_D^2}{D} a^d F l_D^d = \frac{F^2}{D} l_D^{2+2d}$$

Combining this with the property (3.2), we end up with

$$\left(\frac{l_D}{a}\right)^{2+d+d'} \sim \frac{D}{F a^{d+2}} \quad (3.5)$$

usually written as

$$l_D \propto (D/F)^\gamma, \quad (3.6)$$

where

$$\gamma = \frac{1}{2+d+d'}. \quad (3.7)$$

Since one-dimensional islands are necessarily compact, $\gamma_{d=1} = 1/4$ is fixed while in two dimensions the islands' fractality may increase the exponent from $1/6$ to approximately $1/5.72$ ^e, a tiny difference of less than 5%. Taking into account the logarithmic correction in $d = 2$, too, eq. (3.5) changes into

$$\left(\frac{l_D}{a}\right)^{1/\gamma} \frac{1}{2 \ln(l_D/a)} \sim \frac{D}{F a^{d+2}}, \quad (3.8)$$

or inverted

$$\frac{l_D}{a} \sim \left(\frac{D}{F a^{d+2}}\right)^\gamma \left| W_{-1}^\gamma \left(-\frac{F a^{d+2}}{2D\gamma c} \right) \right|$$

where c is the dimensionless proportionality constant from relation (3.8) and $W_{-1}(x)$ is a branch of the *Lambert W function* (Corless et al., 1996). It provides the correction factor which increases even more slowly than $\ln^\gamma(D/F)$.

It should be pointed out once more that eq. (3.7) only holds true in one and two dimensions. For $d \geq 3$, the number of visited sites is a fraction of \tilde{N} as given by eq. (3.4) and therefore eq. (3.7) changes into

$$\gamma_{d \geq 3} = \frac{1}{4+d'},$$

^e $d' = 1.72$ holds true for clusters grown by diffusion limited aggregation, cf. (Tang, 1993).

a result of mainly theoretical interest, of course.

The calculation of the exponent γ can be extended to larger critical nuclei i^* by employing rate equations for the density of adatoms, dimers, trimers, etc. This has been done as well as other extensions like e.g. adatom desorption and island diffusion (Stoyanov and Kashchiev, 1981; Venables et al., 1984; Villain, 1992; Villain et al., 1992; Bartelt and Evans, 1993; Wolf, 1995; Jensen et al., 1997; Pimpinelli and Villain, 1999). It is noteworthy that only recently the value of γ for the case $d = 1, i^* > 1$ was derived correctly (Kallabis et al., 1998) to yield

$$\gamma = \frac{i^*}{2i^* + 3}, \quad (3.9)$$

which does obviously *not* include $\gamma = 1/4$ for $i^* = 1$. The two-dimensional result (cf. e.g. (Wolf, 1995))

$$\gamma = \frac{i^*}{2(i^* + 1) + d'} \quad (3.10)$$

remains unchanged, though.

3.2.2 Measured length scales

The one-dimensional result $\gamma = 1/4$ for $i^* = 1$ has been confirmed by computer simulations very well (cf. (Pimpinelli et al., 1992; Wolf, 1995; Kallabis et al., 1998)). Here we verify that the length scale $(D/F)^{1/4}$ is not only visible in the submonolayer regime, which is a new result (see fig. 3.4 on the following page).

The fractality in $d = 2$, on the other hand, may well need a closer inspection. fig. 3.5 on the next page shows the diffusion length l_D measured as the reciprocal square root of the nucleation density (i.e. number of nucleations per unit area) in the first mono-layer. Though an overall power law dependence on D/F is essentially confirmed, the extraction of a precise value for the exponent turns out to be an arduous task. The effective value γ_{eff} , as can be seen in the figure's inset, increases from values even below $1/6$ (compact islands) to almost $1/5$ for the largest D/F . The latter deviation shrinks upon taking into account the logarithmic correction (3.8), which in turn makes the situation for small D/F even worse, where corrections to scaling due to lattice effects can be surmised.

3.2. SUBMONOLAYER CONSIDERATIONS

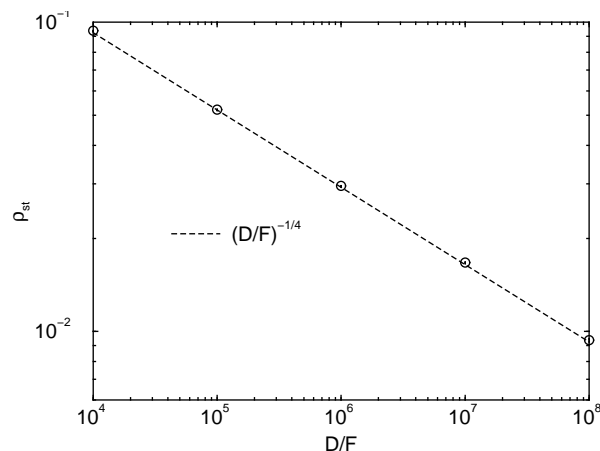


Figure 3.4: The step density after the deposition of 20 mono-layers in one dimension. Since there are two steps per island, it should satisfy $\rho_{st} \sim 1/l_D$ as it is clearly the case.

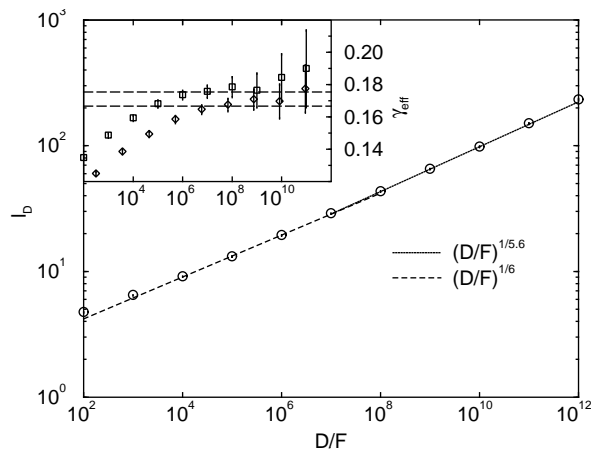


Figure 3.5: The diffusion length l_D in two dimensions measured as (no. nucleations/unit area) $^{-1/2}$. The inset shows the effective exponent γ_{eff} (squares), obtained as the consecutive slopes in the double-logarithmic plot. The diamonds demonstrate the effect of the logarithmic correction (3.8), which is applied by multiplying the abscissa values by $\ln(l_D^2)$ before evaluating the consecutive slopes. The horizontal lines in the inset finally denote the values $1/6$ and $1/5.7$.

3.2. SUBMONOLAYER CONSIDERATIONS

An indirect way to measure the exponent γ is the scaling of the adatom density. According to eq. (3.3) it should behave as

$$\rho_{\text{ad}} \propto \left(\frac{D}{F}\right)^{2\gamma-1}, \quad (3.11)$$

but due to the island growth, it is time dependent as well. This is visible in fig. 3.7 on the following page, where the ordinate was rescaled to obtain a data collapse for early times. The deviation of the corresponding γ_{eff} to lower values than $1/6$ is in agreement with the data for $D/F < 10^8$ in fig. 3.5 on the page before.

In contrast to its one-dimensional counterpart in fig. 3.6, the precise value for γ_{eff} in fig. 3.7 on the next page depends on the point in time (within the interval of quasi-stationarity being valid) where the densities are compared. The reason is, as can be seen in a more precise calculation like in (Tang, 1993), a logarithmic correction does not only appear as a constant in eq. (3.8) but also in a dynamic fashion as $\ln(D/F t)$. Nevertheless the data collapse is of fair quality; the strong discrepancy reported for the same quantity in (Kallabis, 1997) turned out to be erroneous, as confirmed by its author, it was caused by an inconsistency in the D/F -data.

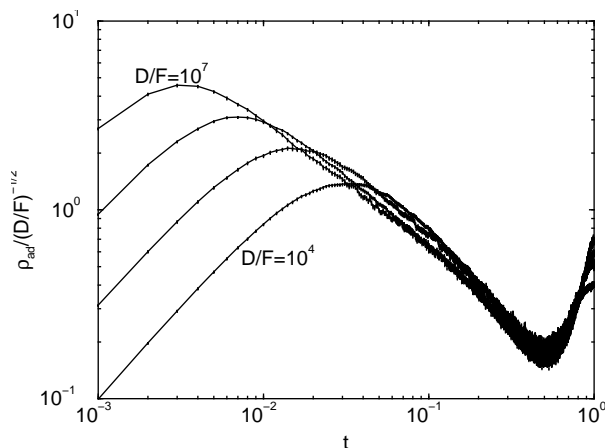


Figure 3.6: The adatom density during the first mono-layer deposition in the one-dimensional system, rescaled by the theoretical value $(D/F)^{-1/2}$ (cf. eq. (3.11)). As can be seen, the scaling is approximately valid (though with a moderate quality) from the onset of the aggregation dominated regime up to and even beyond coalescence.

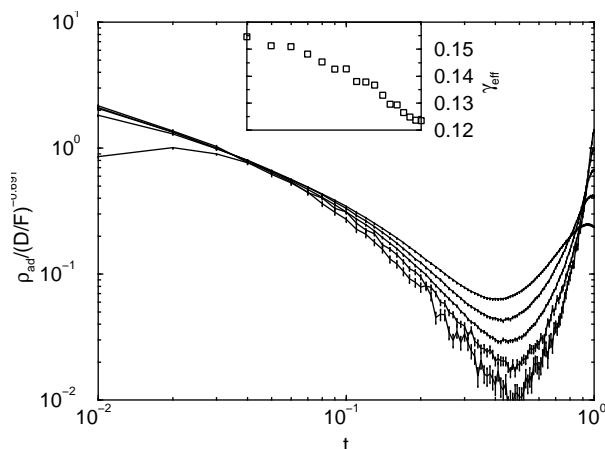


Figure 3.7: The adatom density during the first mono-layer deposition, rescaled by $(D/F)^{2\gamma-1}$ (cf. eq. (3.11)) with an effective exponent $\gamma_{\text{eff}} = 0.1545$ for $D/F = 10^3 \dots 10^7$ from top to bottom at $t = 0.5$. The inset (whose abscissa coincides with the main plot) shows the value of γ_{eff} for which the best collapse at that specific point in time is obtained.

If we revert to mean quantities and pose the question which length scale is “felt” by the adatom diffusion field on average, we retain an exponent γ_{eff} very close to the theoretical value. Fig. 3.8 on the following page shows the corresponding data, namely the adatom density averaged over the interval $t = 0.5 \dots 4.5$ for different D/F . The obtained exponent -0.65 implies $\gamma_{\text{eff}} = 0.175 = 1/5.714$ (cf. eq. (3.11)).

We now turn to the task of relating the diffusion length l_D , a quantity already present in the submonolayer regime, to the transient regime, where after a characteristic time \tilde{t} the concept of a well defined layer with features of a specific size on it is no longer applicable.

3.3 A theory for the damping time

The main subject of this chapter is the emergence of surface roughness responsible for the damping of the oscillations. The simulation results fig. 3.3 on page 50 show that layer-by-layer growth goes on forever if the linear size of the system is smaller than a layer coherence length \tilde{l} . Up to this length the layers grow coherently, for larger distances they get out of phase. Remarkably, \tilde{l} seems to be larger than the characteristic distance between islands

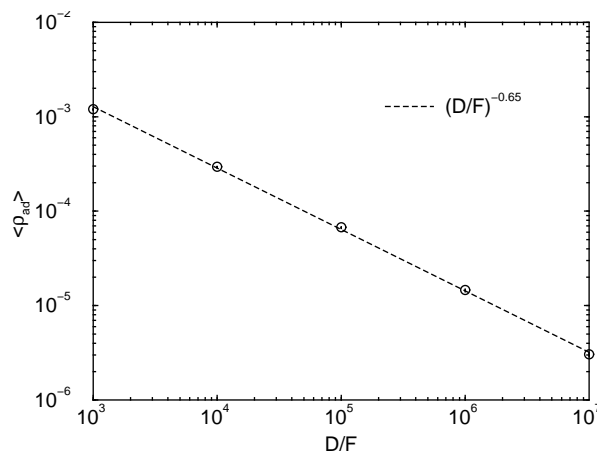


Figure 3.8: The adatom density, temporally averaged over $t = 0.5 \dots 4.5$, exhibits a power law dependence on D/F with an exponent -0.65 which coincides strikingly well with $\gamma = 1/5.72$.

l_D , since in fig. 3.3 on page 50 the size $L \approx 5l_D$ was enough to suppress the dephasing drastically. In other words, the surface becomes rough only on scales larger than \tilde{l} rather than the diffusion length l_D .

In order to study kinetic roughening one may average the film thickness over the distance \tilde{l} . Then one cannot resolve individual islands any more, but still sees the dephasing between layers. Phenomena on this scale can be described by continuum equations, which, as already discussed in section 2.6, provide the most transparent theoretical framework in which to discuss the smoothing mechanisms competing with the shot noise. The layer coherence length \tilde{l} as well as the damping time \tilde{t} play an important rôle for kinetic roughening as natural cutoffs of the continuum growth equation at small length and time scales. This idea will be worked out now.

3.3.1 The scaling regime

As introduced in section 3.1.1, the transition from layer-by-layer growth with its oscillations to kinetic roughening happens at time \tilde{t} , where after one expects that the surface shows self affine scaling as described in section 2.6.2:

$$w(t) \sim a_{\perp} \left(\frac{\xi(t)}{\tilde{l}} \right)^{\zeta} \quad \text{with} \quad \xi(t) \sim \tilde{l} \left(\frac{t}{\tilde{t}} \right)^{1/z}. \quad (3.12)$$

In concordance to chapter 2, w is the root mean square variation of the film thickness, a_{\perp} the thickness of one atomic layer, and ξ the correlation length up to which the surface roughness has fully developed until time t . In contrast to equations (2.41) and (2.42), this dimensional formulation incorporates the idea of $w(\tilde{t}) \approx 1$ and the correlations at \tilde{t} extending over the regions being in phase.

Moreover, \tilde{t} is the time at which a continuum description of kinetic roughening becomes appropriate. We know from section 2.6.2, that whenever desorption and the formation of defects in the growing film can be neglected the equation of motion must have the form

$$\partial_t h = -\nabla \cdot \vec{j} + \eta, \quad (3.13)$$

where h is measured as deviation of the film thickness from its average value and $\eta(x, t)$ denotes the shot noise with its standard correlator according to eq. (2.33).

In the conserved KPZ equation, as discussed in section 2.6.2, the adatom current has two terms, one driven by differences in the surface curvature and the second one by differences in the squared surface tilt, i.e.

$$\vec{j} = \nabla (K \nabla^2 h + \lambda (\nabla h)^2), \quad (3.14)$$

where we shall mainly focus on the coefficients in the following.

Now, eq. (3.12) shows that the only characteristic length, time and height entering the description of the rough surface (coarse grained on scale \tilde{l}) are \tilde{l} , \tilde{t} and a_{\perp} , respectively. Therefore the three parameters entering the cKPZ equation, namely K , λ and \mathcal{F} (the latter via the correlator (2.33) of η) must be functions of these three quantities. For example, λ has the dimension $\text{L}^4 \text{H}^{-1} \text{T}^{-1}$. This implies that it must be the product of a dimensionless factor and $\tilde{l}^4 / (a_{\perp} \tilde{t})$. Similarly one obtains

$$K \sim a_{\perp} \lambda \sim \frac{\tilde{l}^4}{\tilde{t}}. \quad (3.15)$$

As in all Langevin equation describing the evolution of the height, η has the dimension HT^{-1} . Taking the dimensions of the δ -functions in (2.33) (L^{-d} and T^{-1} , respectively) into account, one finds that \mathcal{F} is

$$\mathcal{F} \sim \frac{a_{\perp}^2 \tilde{l}^d}{\tilde{t}}. \quad (3.16)$$

3.3.2 Connection with submonolayer physics

In order to derive (3.1) from (3.15), (3.16) one has to know how K (or $a_{\perp}\lambda$) and \mathcal{F} depend on D and F . This question will be answered in the following.

The physics of kinetic roughening should be determined by the same microscopic processes that are also responsible for the phenomena in the submonolayer regime. There, the characteristic time is the layer completion time,

$$t_{\text{ML}} = \frac{1}{Fa^d},$$

and there are two characteristic lengths, the diffusion length l_D and the lateral lattice constant a . Therefore, it must be possible to express K , λ and \mathcal{F} in terms of l_D , a , t_{ML} and a_{\perp} .

The coefficients λ and K characterize the morphology dependence of the non-equilibrium adatom density, which drives the surface current (see section 3.3.3). The most important morphological feature is the typical distance between islands. Therefore it is natural to assume that K and $a_{\perp}\lambda$ are only functions of l_D and t_{ML} . The only dimensionally correct expressions are then (Politi and Villain, 1996)

$$K \sim a_{\perp}\lambda \sim \frac{l_D^4}{t_{\text{ML}}}. \quad (3.17)$$

By contrast, the shot noise cannot depend on surface diffusion and indeed, we know already from eq. (2.30) that \mathcal{F}/a_{\perp}^2 is only a function of a and t_{ML} :

$$\mathcal{F} = \frac{a_{\perp}^2 a^d}{t_{\text{ML}}} = F(a_{\perp} a^d)^2 \quad (3.18)$$

Comparing equations (3.17) and (3.18) to (3.15) and (3.16) one finds that

$$\frac{\tilde{l}^4}{\tilde{t}} \sim \frac{l_D^4}{t_{\text{ML}}} \quad \text{and} \quad \frac{\tilde{l}^d}{\tilde{t}} \sim \frac{a^d}{t_{\text{ML}}}.$$

This, finally, leads to the central result of this chapter,

$$\frac{\tilde{t}}{t_{\text{ML}}} \sim \left(\frac{l_D}{a}\right)^{4d/(4-d)} \quad \text{and} \quad \frac{\tilde{l}}{a} \sim \left(\frac{l_D}{a}\right)^{4/(4-d)}. \quad (3.19)$$

Note in particular that indeed the layer coherence length $\tilde{l} \gg l_D$.

With (3.6) the exponent δ defined in (3.1) is

$$\delta = \gamma \frac{4d}{4-d}, \quad (3.20)$$

provided the cKPZ equation is the appropriate continuum equation for the growth process.

At the upper critical dimensionality $d = d_c = 4$ the scales \tilde{l} and \tilde{t} should depend exponentially on l_D , while for $d > d_c$ the oscillations are expected to persist forever and the surface to remain smooth.

3.3.3 The adatom current reconsidered

In this section eq. (3.17) will be rederived without using dimensional arguments, i.e. we give a microscopic derivation of the nonlinear contribution to the adatom current (2.56) (see also (Krug, 1997)).

It was proposed by Villain (Villain, 1991) that in growth processes far from equilibrium, where local chemical potentials along the surface are ill defined, diffusion currents should be driven by gradients in the growth-induced, non-equilibrium adatom density ρ ,

$$\vec{j} = -D \Omega \nabla \rho. \quad (3.21)$$

We remind that the atomic volume Ω enters because (3.13) expresses volume rather than mass conservation (see also section 2.6.3).

As we argued for the derivation of the exponent γ , on a singular surface the balance between deposition and capture of adatoms at steps leads to a stationary adatom density $\rho = \rho_0$ given by eq. (3.3), i.e. it is of the order

$$\rho_0 \sim \frac{F}{D} l_D^2. \quad (3.22)$$

On a vicinal surface the adatom density is reduced due to the presence of additional steps; however this effect is felt only if the tilt^f $|\nabla h|$ reaches a_\perp/l_D , in which case eq. (3.22) is replaced by $\rho \sim (F/D)(a_\perp/|\nabla h|)^2$. For $|\nabla h| > a_\perp/l_D$ the steps produced by the tilt are the only sinks and step flow takes over. In terms of a coarse grained description of the surface this implies

^fTo prevent any misunderstandings, we point out that the tilt $|\nabla h|$ does not mean a rotation of the crystal axes.

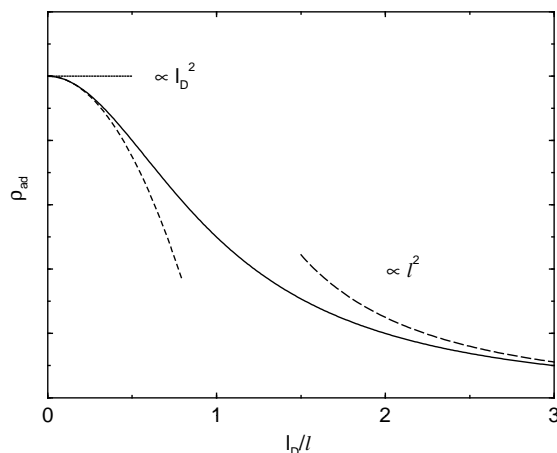


Figure 3.9: The theoretical picture of the quasi-stationary adatom density as a function of the tilt $|\nabla h| = a_{\perp}/\ell$. For small tilts $\ell \gg l_D \rho$ saturates to a value given by eq. (3.3) while for large slopes the step distance ℓ dominates. The short dashed parabola stresses the behavior around zero tilt.

that the local adatom density depends on the local miscut or surface tilt. A useful interpolation formula which connects the regimes $|\nabla h| \ll a_{\perp}/l_D$ and $|\nabla h| \gg a_{\perp}/l_D$ is (Politi and Villain, 1996)

$$\rho(\nabla h) = \frac{\rho_0}{1 + (l_D |\nabla h| / a_{\perp})^2} \quad (3.23)$$

$$\sim \frac{F}{D} l_D^2 - \frac{F}{D} l_D^4 \left(\frac{|\nabla h|}{a_{\perp}} \right)^2 + \text{h.o.t.}, \quad (3.24)$$

which is illustrated in fig. 3.9.

Inserting the leading quadratic term of this gradient expansion into (3.21), which is appropriate for describing long wavelength fluctuations around the singular orientation, we obtain

$$\vec{j} = \nabla \lambda (\nabla h)^2$$

with $\lambda \sim F a^d l_D^4 / a_{\perp}$, which agrees with the result (3.17) of the previous section.

3.3.4 Competing mechanisms

Whereas for the considered computer simulation model the theoretical arguments given in the preceding sections are perfectly appropriate, the question arises how relevant these results are in general experimental situations. It has been argued that generically one should expect non-equilibrium contributions to the surface current which are driven by a height difference (Villain, 1991; Wolf and Villain, 1990; Krug et al., 1993). To leading order in a gradient expansion one gets an adatom current of the Edwards-Wilkinson (EW) form:

$$\vec{j} = -\nu \nabla h \quad (3.25)$$

Tilt induced non-equilibrium surface currents originate from step edge barriers of Ehrlich-Schwoebel-type (Ehrlich and Hudda, 1966; Schwoebel and Shipsey, 1966) (cf. also chapter 4), as well as kick-out or diffusion exchange processes at step edges. Whereas the latter two lead to a downhill current stabilizing the surface ($\nu > 0$), the former generates an uphill current ($\nu < 0$) and consequently an instability which will be considered in the next chapter.

In the case of kick-out processes the coefficient ν cannot depend on the diffusion length, because they are caused by deposition events in the immediate vicinity of a downward step. The only dimensionally correct expression is therefore

$$\nu = \frac{a^2}{t_{\text{ML}}} = Fa^{d+2}. \quad (3.26)$$

The corresponding current is proportional to the local step density $|\nabla h|/a_{\perp}$ and the deposition rate F . As can be seen from the model's descriptions in section 2.5, such contributions are inherently absent in the simulations discussed here.

In general, the adatom current will contain the terms (3.14) as well as (3.25). The latter one dominates the surface roughness on large scales. Whether or not it influences the damping of the growth oscillations, however, depends on the crossover time $t_{\lambda\nu}$ from cKPZ- (λ -dominated) at early to EW- (ν -dominated) behavior at late times. If the oscillations are damped out before the crossover takes place, the λ -term determines the damping, hence the above result applies. Let \tilde{t}_{λ} and \tilde{t}_{ν} denote the damping times if only the λ - or the ν -term were present in the continuum equation of motion. Then (3.19) and (3.20) hold if

$$\tilde{t}_{\lambda} \leq t_{\lambda\nu}.$$

If, however, this is not the case, then \tilde{t}_λ is replaced by \tilde{t}_ν , as long as no further terms in the continuum description provide further time scales.

The crossover time $t_{\nu\lambda}$ is estimated in the following way: First we calculate the typical height fluctuation $h_\nu(t)$ after time t , if the λ -term would be absent. Similarly, $h_\lambda(t)$ is the fluctuation amplitude, if $\nu = 0$. Equating h_λ and h_ν then gives $t_{\lambda\nu}$. By dimensional analysis one gets (see appendix D)

$$\mathcal{F}t_{\lambda\nu} \sim \left(\frac{\lambda}{\mathcal{F}}\right)^{4/(d+2)} \left(\frac{\mathcal{F}}{\nu}\right)^{(d+8)/(d+2)} \sim a_\perp^2 a^d \left(\frac{l_D}{a}\right)^{16/(d+2)}, \quad (3.27)$$

where besides the definition of the mono-layer time equations (3.18) and (3.26) have been used to replace the parameters λ , \mathcal{F} and ν .

This has to be compared with (3.19), expressed in terms of \mathcal{F} as

$$\mathcal{F}\tilde{t}_\lambda \sim a_\perp^2 a^d \left(\frac{l_D}{a}\right)^{4d/(4-d)}. \quad (3.28)$$

For $d \leq 2$ the damping time \tilde{t}_λ is smaller or of equal order of magnitude as the crossover time $t_{\lambda\nu}$. This implies that kick-out processes at step edges, although leading to an EW-term in the growth equation and hence modifying the later roughness, do not change our results (3.19) for the layer coherence length and the damping time.

However, if for example the sticking probability at an up step would be much smaller than at a down step (e.g. due to a step decoration by surfactant atoms (Markov, 1994)), one would expect a downhill current depending on l_D rather than the lattice constant a , i.e. with

$$\nu \sim \frac{l_D^2}{t_{\text{ML}}}$$

instead of (3.26). In this case (3.27) is replaced by

$$\mathcal{F}t_{\lambda\nu} \sim a_\perp a^d \left(\frac{l_D}{a}\right)^{-2d/(2+d)},$$

which is never larger than $\mathcal{F}\tilde{t}_\lambda$. The damping time should then be given by (D.8)

$$\frac{\tilde{t}_\nu}{t_{\text{ML}}} \sim \left(\frac{l_D}{a}\right)^{2d/(2-d)}.$$

3.4 Numerical Results in one dimension

Simulations were carried out based on the minimal model described in chapter 2.3. The resulting (squared) surface width w^2 as a function of time for various D/F and $i^* = 1$ was already shown in fig. 3.1 on page 49 and revealed that for a given D/F , the oscillations in the surface width persist up to a coverage \tilde{t}/t_{ML} , which increases with D/F . Beyond \tilde{t}/t_{ML} , the crossover to kinetic roughening is observed, where w^2 approaches a power law $t^{2\beta}$ with the cKPZ prediction of $\beta = 1/3$ in one dimension (Villain, 1991; Lai and Sarma, 1991; Tang and Nattermann, 1991). Rescaling the time by $(D/F)^{1/3}$ in fig. 3.10 we find not only an excellent collapse of the crossover regions for all curves of fig. 3.1 on page 49 but also a convincing turning into the power law $t^{2\beta}$. This means that $\delta = 1/3$ within numerical accuracy, in agreement with (3.20) and $\gamma = 1/4$ (Pimpinelli et al., 1992).

The damping time was measured for higher values of i^* as well by determining the coverage \tilde{t}/t_{ML} , where $w = 0.71$, 0.57 or 0.65 for $i^* = 1, 2, 3$, respectively. Its dependence on l_D (the latter measured again as the reciprocal of the nucleation density in the first layer) shows fig. 3.11 on the following page, where it can be read off that $\tilde{t}/t_{\text{ML}} \propto l_D^{4/3}$, independent of the values $i^* = 1, 2, 3$, in agreement with the theoretical result (3.19). This ensures that the confirmation of the correct δ for $i^* = 1$ was not just by chance.

In order to check that the damping time and the layer coherence length are the appropriate scales also for other quantities showing oscillations during the

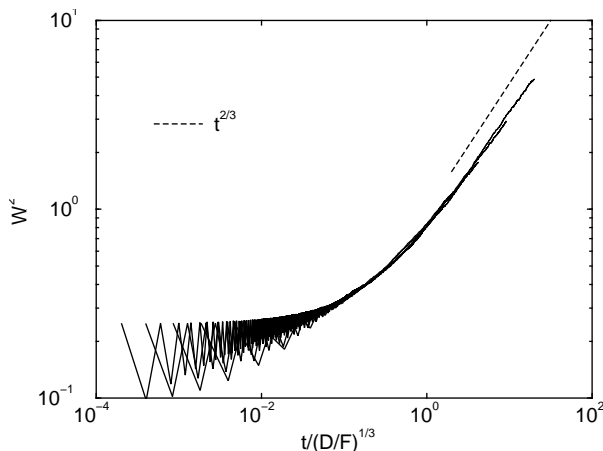


Figure 3.10: Curves from fig. 3.1 on page 49, with time scaled by $(D/F)^{1/3}$.

3.4. NUMERICAL RESULTS IN ONE DIMENSION

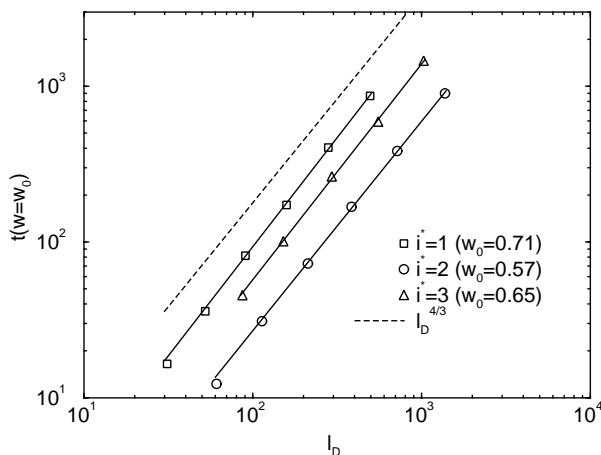


Figure 3.11: Coverage \tilde{t}/t_{ML} , at which the surface width reaches a given value, as a function of the diffusion length l_D for different values i^* . The straight lines are fits to the last four data points in each set of data. Their slopes are 1.39 ± 0.09 , 1.34 ± 0.09 and 1.38 ± 0.09 for $i^* = 1, 2, 3$, respectively.

layer-by-layer growth, we investigated the kinematic intensity I (cf. section 2.4.3) as well. fig. 3.12 shows I at integer times (i.e. its upper envelope), rescaled in the same way as in fig. 3.10 on the preceding page. Again, we find that the number of observable oscillations varies with the growth conditions as described by (3.19).

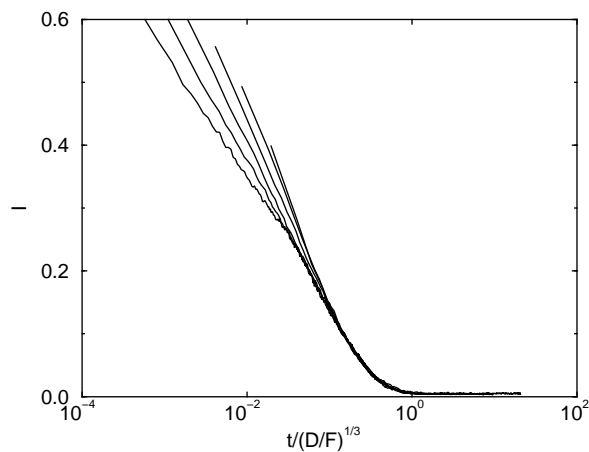


Figure 3.12: Maxima of the kinematic intensity for $D/F = 10^5 \dots 10^{10}$ (top to bottom), and $i^* = 1$. Time is rescaled by $(D/F)^{1/3}$.

3.4. NUMERICAL RESULTS IN ONE DIMENSION

Finally, a finite size analysis was carried out to measure the layer coherence length \tilde{l} explicitly, which was up to now a rather abstract quantity. As mentioned in the beginning (cf. section 3.1.3), the surface does not roughen when the system size L is smaller than \tilde{l} . Instead, the oscillations of the surface width w persist forever and after a transient time, their amplitude becomes stationary. We take the variance of the surface width $w(t)$ during the layer completion time t_{ML} ,

$$A(t)^2 = \langle w^2 \rangle_{[t, t+t_{\text{ML}}]} - \langle w \rangle_{[t, t+t_{\text{ML}}]}^2,$$

as a measure of the squared amplitude of the oscillations. $\langle \dots \rangle_{[t, t+t_{\text{ML}}]}$ means the time average over the interval $[t, t+t_{\text{ML}}]$. If this variance becomes equal to the ensemble fluctuations of w at fixed time, no oscillations can be observed. We find that $A(t)$ approaches a stationary value which decreases with increasing system size. For system sizes larger than a certain value L^* , $A(t)$ is equal to the statistical fluctuations of w itself. This means that in a system of size $L > L^*$ the oscillations can die out (or rather cannot be distinguished from noise anymore for long times). Therefore, L^* can be identified with \tilde{l} . According to (3.19) and (3.6) with $\gamma = 1/4$ in one dimension for $i^* = 1$ (Pimpinelli et al., 1992), one expects $\tilde{l} \sim (D/F)^{1/3}$. Indeed, the simulation results shown in fig. 3.13 are in excellent agreement with the theoretical prediction.

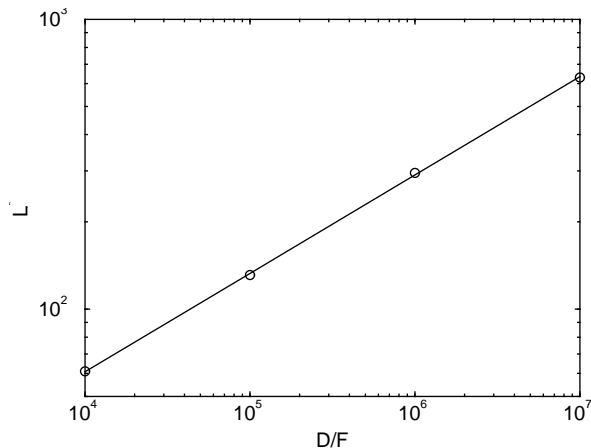


Figure 3.13: $L^* = \tilde{l}$ as a function of D/F . The fit has a slope of 0.339 ± 0.006 .

3.5 Numerical results in two dimensions

In $d = 2$, we observe qualitatively the same behavior as in one dimension, which is displayed by fig. 3.14 on the following page; the damping time increases with growing D/F and is reached when w^2 is of order unity (though for very low D/F the oscillations last somewhat “longer” on the ordinate than for higher values).

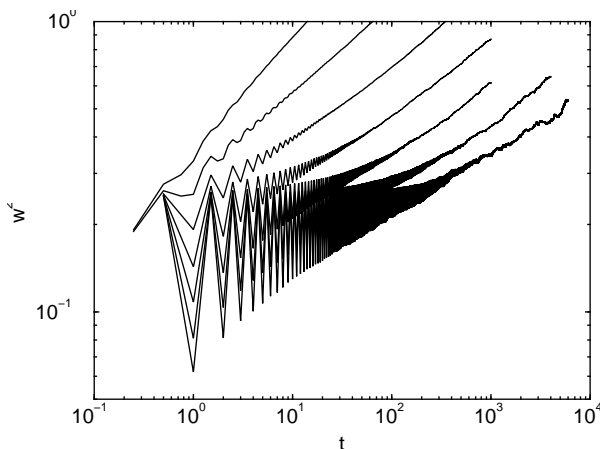


Figure 3.14: Oscillations of w^2 testifying layer-by-layer growth in $d = 2$ for $D/F = 10^2 \dots 10^5$ (left to right) and $i^* = 1$.

But upon rescaling time by $(D/F)^{4\gamma}$ (according to eq. (3.19) and with setting $\gamma = 1/5.7$), no data collapse can be obtained (see fig. 3.15 on the page before). Comparing the curves to the ones in fig. 3.14 makes clear that the exponent 4γ is too *small* though $\gamma = 1/5.7$ was already overestimated as known from fig. 3.5 on page 55. That means, taking into account the correct γ_{eff} or as well rescaling directly by l_D^4 using the measured l_D would make the situation even *worse*. In other words, the formulas (3.19) are not applicable in two dimensions. To extract the correct exponent (if a power law holds true at all), we determine \tilde{t} again by means of a fixed width, here $w^2(\tilde{t}) = 0.5$, and plot it versus D/F in fig. 3.16 on the following page. Though the curve bends downwards for higher D/F , it is out of question that it ever reaches an exponent $2/3$, instead the asymptotic value seems to be close to unity, a discrepancy we will discuss in the next section.

3.6 Appropriateness of cKPZ revised

When reconsidering the derivation of the equations (3.19), we see that with respect to the dimensional analysis we may cast doubt either on the usage of the shot noise strength \mathcal{F} or on the morphology relevant coefficient λ (or equivalently K). Because the former is known to be exact and its relevance is proven by the comparison done in fig. 3.2 on page 49 and since we have no real hint for the microscopic origin of the K -term, let's turn our attention once more to the tilt-dependent adatom density: The appearance of the cKPZ-nonlinearity $(\nabla h)^2$ was due to the non-vanishing second order term in the gradient expansion (3.24). Though the interpolation formula exhibits the correct asymptotic behavior (for small and large tilts), there is no physical necessity for a parabolic shape of $\rho(\nabla h)$ around $\nabla h = 0$. It is merely the lowest order analytical term of correct symmetry. That means, in principle, the leading term could be of fourth order as well or even of any power when employing $|\nabla h|$ (and thus giving up analyticity).

Fortunately, a numerical measurement of the adatom density can be done, providing a direct way to clarify the situation. To perform such an investigation, the temporally averaged adatom density on a weakly tilted surface (with skewed boundary conditions, cf. section 2.3.3) was monitored for different inclinations and different D/F ; the corresponding results are found

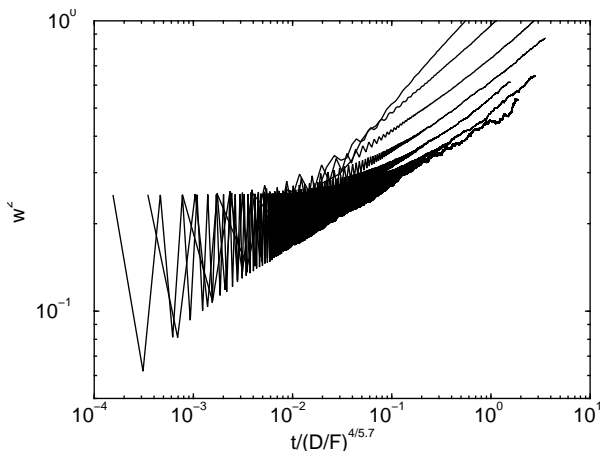


Figure 3.15: Squared surface width of fig. 3.14 on the following page with time rescaled by $(D/F)^{4\gamma}$ (cf. eq. (3.19)). No data collapse is obtained.

3.6. APPROPRIATENESS OF CKPZ REVISED

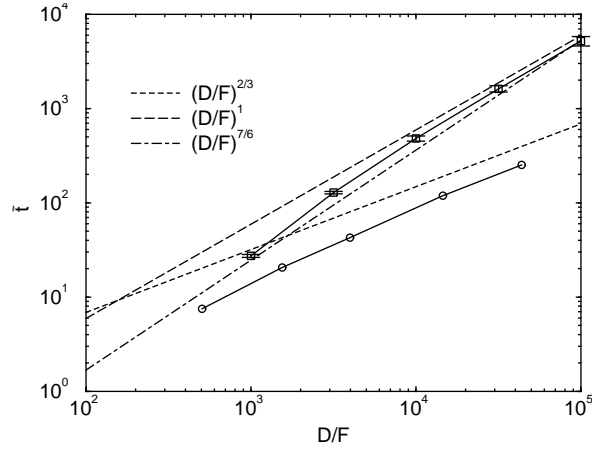


Figure 3.16: Damping time \tilde{t} (obtained via defining $w^2(\tilde{t}) = 0.5$) as function of D/F (squares). The small circles show the data from (Kallabis, 1997), erroneous (cf. section 2.5.3) though strikingly close to the theoretical prediction (3.20).

in fig. 3.17. Obviously there is *no parabolic* shape but a *cusp* with linear branches.

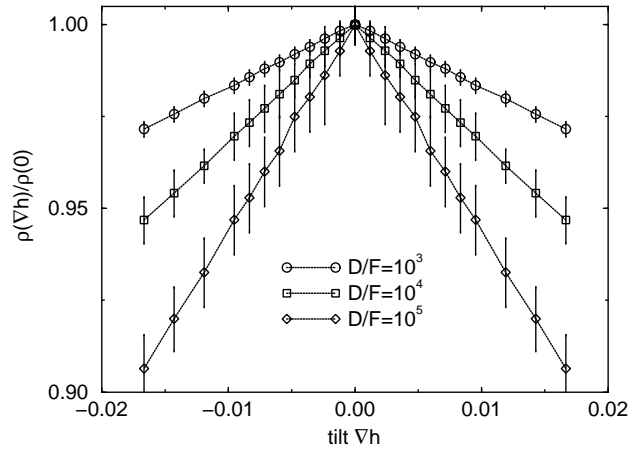


Figure 3.17: Adatom density on a weakly tilted 840×840 -surface for $D/F = 10^3 \dots 10^5$, temporally averaged over $t = 0.5 \dots 4.5$. Identical data is plotted for negative and positive tilts to emphasize the cusp, which is present down to tilts where undeniably $1/|\nabla h| \gg l_D$ holds true.

3.6. APPROPRIATENESS OF CKPZ REVISED

A few words about the temporal averaging are in order: Because the density of sinks for adatoms varies during the deposition of one mono-layer (islands nucleate, grow and coalesce, afterwards the interstice is filled to yield an almost flat surface again) also the adatom density oscillates, therefore the averaging. But since on a tilted surface some material is incorporated into the steps instead of participating in the layer-by-layer growth, the oscillations' frequency is a little bit larger than unity. Averaging over a fixed time interval would give this effect an influence on the desired quantity. However, since the interval boundaries 0.5 and 4.5 are located close to flat local minima, no significant differences compared to choosing the boundaries always right at the minima could be found. Neither was there a difference when using a different (integer) interval length.

Actually, a qualitative explanation for the presence of a cusp can be given: A first derivative being zero at $\nabla h = 0$ means that doubling a very low step density has a vanishing effect on the system because, provided $a_{\perp}/|\nabla h| \gg l_D$ still holds true, islands will always grow at a distance of order l_D away from the steps. Now the reasoning is, that the adatoms diffusion field cannot distinguish between sinks made from islands and sinks being terrace steps. But this is true only in one dimension, where island edges and tilt induced excess steps are both points on a line. For $d > 1$ however, adatoms are able to circumvent islands located close to steps; this allows the adatom density field indeed to react on every additional step "slipped in".

If we repeat the calculation in section 3.3 with the small-tilt approximation of eq. (3.23)

$$\rho(\nabla h) = \rho(0) \left(1 - \frac{(\nabla h)^2 l_D^2}{a_{\perp}^2} \right)$$

replaced by

$$\rho(\nabla h) = \rho(0) \left(1 - c_1 \frac{|\nabla h| l_D}{a_{\perp}} \right), \quad (3.29)$$

(where c_1 is some numerical constant) leading to a new

$$\frac{l_D^3}{a_{\perp} t_{\text{ML}}} \sim \chi' \sim \frac{\tilde{l}^3}{a_{\perp} \tilde{t}}, \quad (3.30)$$

the equations (3.19) change into

$$\frac{\tilde{t}}{t_{\text{ML}}} \sim \left(\frac{l_D}{a}\right)^{\frac{3d}{3-d}} \quad (3.31)$$

$$\text{and} \quad \frac{\tilde{l}}{a} \sim \left(\frac{l_D}{a}\right)^{\frac{3}{3-d}}. \quad (3.32)$$

In two dimensions this means $\tilde{t} \propto l_D^6$, which – because of $\gamma \approx 1/6$ – implies $\tilde{t} \propto D/F$, a result in agreement with the simulation data shown in fig. 3.16 on page 70.

Despite this coincidence and the direct numerical confirmation of a cusp in $\rho(|\nabla h|)$, the implications on the necessary modification of the continuum equation are not straight forward. Inserting eq. (3.29) plainly into eq. (3.21) yields

$$\partial_t h = \lambda' \nabla^2 |\nabla h| + \eta,$$

an equation mathematically ill defined at all local minima/maxima^g. Therefore, a regularization will have to be employed, taking into account the adatoms' movement towards sinks which are a distance of order l_D apart, a distance which is not resolved in the continuum picture.

Nevertheless, a kind of third order derivative seems to be on the right lines, for a dynamical exponent of $z = 3$ in the context of conserved dynamics implies via eq. (2.49) a roughness exponent $\zeta = 1/2$ in two dimensions, which in turn means $\beta = 1/6$. This value agrees much better with the numerically obtained $w^2(t)$ than the classical cKPZ value $\beta_{d=2} = 1/5$ (cf. equations (2.57)^h) as can be seen in fig. 3.18ⁱ. This leads to the conclusion that the cKPZ equation is *not* a valid continuum description of the ideal MBE model in two dimensions (at least for the time scales considered here).

The riddle of the damping time \tilde{t} in two dimensions could be regarded as solved, were it not for an inconsistency concerning the cusp branches. The slope in eq. (3.29) containing the length l_D cannot be confirmed by the simulations as displayed in fig. 3.19 on the following page. Instead of $(D/F)^\gamma$ a power close to $(D/F)^{1/4}$ is found which suggests eq. (3.29) to be changed

^gAllowing for δ -functions is no way out since the troublesome operator acts on them as well, producing their derivatives.

^hThough we must keep in mind, that these equations are not exact.

ⁱFurthermore, in (Rost and Krug, 1997b) a generalization of the exponent $4/(4-d)$ in equations (3.19) to $z/(z-d)$ was proposed, which coincides with eq. (3.32) for $z = 3$.

into

$$\rho(\nabla h) = \rho(0) \left(1 - c_1 \frac{|\nabla h| l_0}{a_\perp} \right), \quad (3.33)$$

l_0 being the length introduced in eq. (2.5).

Since $\rho(0)$ still contains l_D as known from fig. 3.8 on page 58, eq. (3.33) lets two length scales enter the coefficient λ which turns eq. (3.30) into

$$\frac{l_D^2 l_0}{a_\perp t_{\text{ML}}} \sim \lambda' \sim \frac{\tilde{l}^3}{a_\perp \tilde{t}}, \quad (3.34)$$

such that eq. (3.31) is replaced by

$$\frac{\tilde{t}}{t_{\text{ML}}} \sim \left(\frac{l_D^2 l_0}{a^3} \right)^{\frac{d}{3-d}} \quad (3.35)$$

$$\frac{\tilde{l}}{a} \sim \left(\frac{l_D^2 l_0}{a^3} \right)^{\frac{1}{3-d}}. \quad (3.36)$$

For $d = 2$ we get

$$\tilde{t} \propto l_D^4 l_0^2 \propto \left(\frac{D}{F} \right)^{4\gamma+1/2},$$

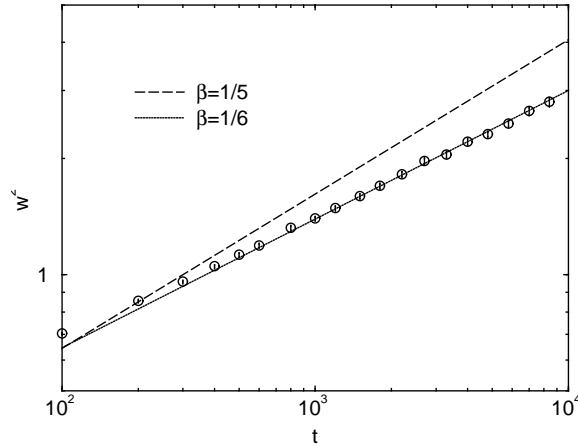


Figure 3.18: Temporal growth of w^2 in two dimensions according to the power law $t^{2\beta}$ for $D/F = 10^3$. The dashed line represents the classical cKPZ value (2.57) as opposed to an equation with conserved dynamics and $z = 3$ (dotted line). A fit to the numerical data (circles) yields $2\beta \approx 0.32$.

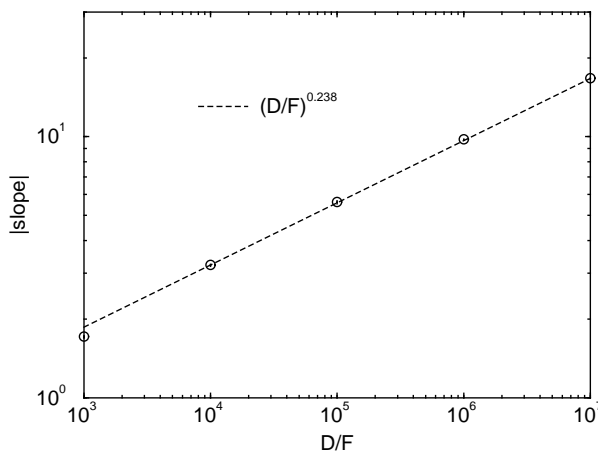


Figure 3.19: The (absolute value of the) slope from fig. 3.17 on page 71 plotted vs. D/F (plus additional data for $D/F = 10^6$ and 10^7). The dashed line represents a power law with exponent 0.238.

i.e. an exponent $\delta \approx 4/6 + 1/2 = 7/6$ which fits the simulation data in fig. 3.16 on page 70 to the same degree as $\delta = 1$. The larger error-bar for $D/F = 10^5$ makes a more conclusive judgement difficult.

3.7 Summary

The applicability of the theory to the one dimensional case can be viewed as confirmed, whereas in the real two-dimensional scenario the situation is more ambiguous. Concerning the appearance of the length scale l_0 , we are faced with a kind of dilemma: Though the exponent $\delta = 7/6$ fits the numerical data rather well, the fact that *both* length-scales – l_D and l_0 – are relevant for the adatoms diffusion field as proven in fig. 3.8 on page 58 and fig. 3.19 on the preceding page respectively, is burdensome. In general, it prohibits the extraction of powerlaws on the mere basis of dimensional analysis since in principle any function $f(l_D/l_0)$ could be involved. This would affect the comparisons done in section 3.3.4 as well. But since the numerical data does not contradict $\delta = 7/6$, we can speculate that the artificial length scale $(l_D^2 l_0)^{1/3}$ appearing in eq. (3.34) is the only relevant for this problem.

A much clearer, yet unexpected result for the two-dimensional case is the cusp in $\rho(\nabla h)$, which objects the cKPZ equation as the appropriate

continuum description for the ideal MBE model.

3.7.1 Experimental relevance

Regarding the experimental observability of layer-by-layer growth's ceasing due to kinetic roughening, we can conclude that with $\delta \gtrsim 1$ the time \tilde{t} will not be reached in situations with typical values for D/F , several ten thousand of mono-layers and more are just too many. In (Pimpinelli and Villain, 1999) this was already presumed, albeit on a quantitatively different basis.

Chapter 4

Unstable growth

4.1 Schwoebel barriers

In the previous chapter, we saw that for realistic values of D/F the mechanism of kinetic roughening only provides a very weak impact on layer-by-layer growth. In most experimental setups stronger effects will be present. Besides external influences like e.g. an inhomogeneity in the particle beam on a macroscopical scale (Kunkel et al., 1990; Wolf, 1997), these are growth instabilities due to various features not included in our ideal model for MBE, as already mentioned in section 2.3. Perhaps the most prominent is the Villain instability (Villain, 1991) caused by the so-called Ehrlich-Schwoebel barrier (Schwoebel and Shipsey, 1966; Schwoebel, 1968). This barrier consists of a higher activation energy for diffusion hops at downward steps (cf. fig. 4.1 on the next page):

$$E_{\text{step-edge}} = E_D + E_s \quad (4.1)$$

For ordinary hopping diffusion, the physical origin for this barrier lies in the temporary loss of coordination. In general, for the real, two dimensional case, it will depend on the orientation of the step, and the potential may be more complicated than a simple barrier as well (Kyuno and Ehrlich, 1997). Theoretical calculations of step edge barriers on first principles are rare (Stumpf and Scheffler, 1994; Zhang et al., 1995; Stumpf and Scheffler, 1996; Yu and Scheffler, 1997), but utilization of empirical potentials becomes more and more popular (Kodiyalam et al., 1996; Trushin et al., 1997; Maca et al., 2000). Furthermore, there are experimental approaches as the observation of individual atoms (Bromann et al., 1995; Fu et al., 1998; Kyuno and Ehrlich, 1998) or e.g. the evaluation of the onset of nucleations in the 2nd layer (Šmilauer and Harris, 1995).

In terms of Arrhenius dynamics we can speak of a reduced rate for a downward hop, where the reduction can be expressed by the probability to overcome the barrier, given that this movement would have taken place in the absence of the latter:

$$p_{\text{cross}} = \exp\left(-\frac{E_s}{k_B T}\right)$$

Accordingly $1 - p_{\text{cross}}$ is interpreted as a reflection probability. The case $p_{\text{cross}} = 0$ as the limit of an infinitely strong Schwoebel barrier will be treated in section 5.1, while the other extreme $p_{\text{cross}} = 1$ obviously corresponds to the case without any barrier, which we have dealt with in chapter 3.

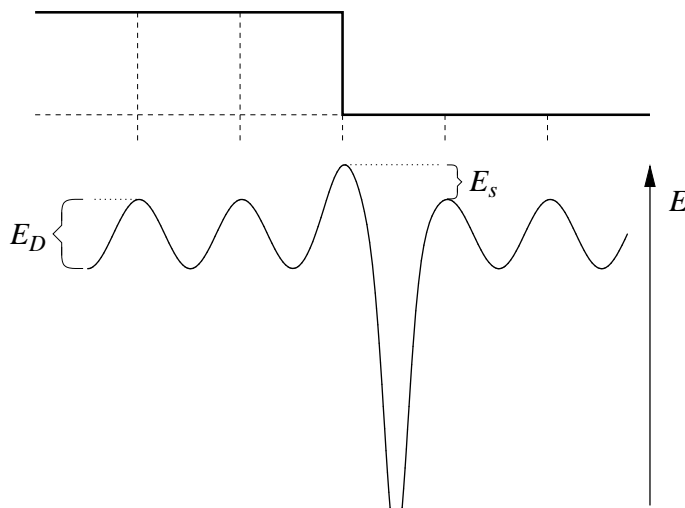


Figure 4.1: The energy landscape (schematically) seen by an adatom on a terrace. At the downward-step it encounters an additional barrier E_s .

A quantity equivalent to p_{cross} is a length (usually called *Schwoebel length*) defined as

$$\frac{l_s}{a} \equiv \frac{1}{p_{\text{cross}}} - 1 = \exp\left(\frac{E_s}{k_B T}\right) - 1, \quad (4.2)$$

whose graphical meaning we will consider below ^a.

As can be expected, and as we will analyze below, a reduced interlayer transport leads to an uphill current, which destabilizes the growth, since with bumps created by fluctuations, more and more material is transported upwards these small hills and finally mounds with a characteristic size emerge on the surface. This has been verified experimentally as well as numerically in numerous works (e.g. (Ernst et al., 1994; Nostrand et al., 1995; Johnson et al., 1994; Stroscio et al., 1995; Thürmer et al., 1995; Siegert and Plischke, 1994; Šmilauer and Vvedensky, 1995; Siegert and Plischke, 1996; Amar and Family, 1996a)). Special attention has been paid to the long time evolution of the shape and size of such mounds, the *coarsening process* (Stroscio et al., 1995; Amar and Family, 1996a; Politi and Villain, 1996; Politi, 1997; Rost and Krug, 1997a; Amar and Family, 1998; Politi, 1998; Siegert, 1998; Tang et al., 1998; Šmilauer et al., 1999), while we are – as in the previous chapter –

^aThe definition without -1 is found likewise in the literature

interested in the intermediate times, the onset of the instability in this case.

There are situations where the steps' rôles are exchanged in the sense that aggregation at the upper step is hindered while hopping down at the lower step happens unhindered. This can occur e.g. in the case of decorations due to surfactants (Markov, 1994; Kandel, 1997). Sometimes the expression “negative Schwoebel barrier” is found in the literature to denote this effect, but according to eq. (4.1) this is a misnomer. We should prefer “inverse Schwoebel barrier” or even better “inverse Schwoebel effect”.

4.2 Uphill current

The treatment of a one dimensional vicinal surface is rather straight forward and dates back to the work of Burton, Cabrera and Frank (Burton et al., 1951). In this continuum picture, step edges as perfect sinks (i.e. vanishing adatom density) are the boundary conditions for the diffusion equation of the adatom concentration

$$\partial_t \rho = D \partial_x^2 \rho + F .$$

Its solution in the quasi-static regime ($\partial_t \rho \ll F$) is a symmetric parabolic density profile

$$\rho(x) = \frac{F}{2D} x(\ell - x)$$

between two sinks a distance ℓ apart. Now, the Schwoebel barrier breaks this symmetry by making the sink at the downward step a non-perfect one, which in turn means that we have to prescribe the current right at this location. From earlier inspection of the diffusion mechanism (see section 2.2) we infer

$$|J| = \frac{D p_{\text{cross}}}{a} \rho \quad (4.3)$$

$$\text{i.e.} \quad \rho = a \exp\left(\frac{E_s}{k_B T}\right) |\nabla \rho| , \quad (4.4)$$

since $p_{\text{cross}} D/a^2$ is the average time needed to overcome the barrier and hence to travel the distance a .

But this relation has the following flaw: For a vanishing barrier, we do not return to the result for a perfect sink, since eq. (4.4) requires the density to vanish together with its gradient. The limit $a \rightarrow 0$ (which is actually apt

for a continuum description) is of no use here since it abolishes any finite barrier. The artifice to cure this, is to modify the exponential according to

$$\exp\left(\frac{E_s}{k_B T}\right) \rightarrow \exp\left(\frac{E_s}{k_B T}\right) - 1$$

which turns eq. (4.4) into

$$\rho = l_s |\nabla \rho|,$$

(with the Schwoebel length l_s defined in eq. (4.2)), and thus allows for a zero density together with a finite current.

The resulting quasi-static density profile (upward step at $x = 0$, downward step at $x = \ell$)

$$\rho(x) = \frac{F}{2D} x \left(\frac{\ell^2 + 2\ell l_s}{\ell + l_s} - x \right)$$

is shown in fig. 4.2 together with a graphical interpretation of the Schwoebel length: The linear extrapolation of the density across the downward step intersects the level $\rho = 0$ just after a distance l_s . (For a microscopic interpretation cf. (Kallabis, 1997).)

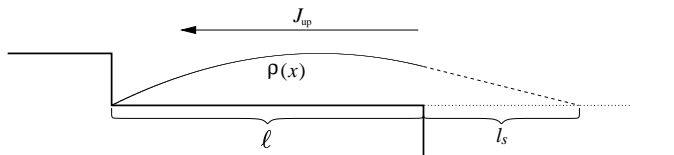


Figure 4.2: Adatom density profile for the case of an energy barrier at the downward step, its asymmetry leads to a net current uphill. The dotted line as linear extrapolation of the density illustrates the Schwoebel length l_s .

To ensure that the above modification is merely an introduction of a lattice correction to a continuum view, we can do a comparison to the discrete case where each incoming atom performs a random walk until it is incorporated at the downward-step (with barrier) or at the upward-step (without barrier). A detailed treatment of this random walk with boundary conditions yields the corresponding incorporation probabilities (Kallabis, 1997):

$$p_{\text{up}}(i) = \frac{i a + l_s}{\ell + l_s}$$

$$p_{\text{down}}(i) = 1 - p_{\text{up}}(i) = \frac{\ell - i a}{\ell + l_s}$$

The index i counts the starting position on the terrace where $i = 1$ and $i = \ell/a$ refer to the sites next to the down-step and right at the up-step, respectively.

By means of these probabilities, we can express the net uphill-current as averaged over one terrace via

$$\begin{aligned}
 J_{\text{net}} &= J_{\text{up}} - J_{\text{down}} \\
 &= F \sum_{i=1}^{\ell/a} (\ell - i a) p_{\text{up}}(i) - F \sum_{i=1}^{\ell/a} i a p_{\text{down}}(i) \\
 &= F \frac{\ell - a}{2} \frac{1}{1 + \ell/l_s}.
 \end{aligned} \tag{4.5}$$

If we compare this to the continuum expression

$$\bar{J} = -\frac{1}{\ell} \int_0^\ell (-D\nabla\rho) dx = F \frac{\ell}{2} \frac{l_s}{\ell + l_s},$$

it differs only by the correction $-a$, which reveals another lattice effect: An adatom deposited right at the upward step does not move and hence provides no contribution to the current.

From eq. (4.5) we can see how the Schwoebel length “controls” the current: If it is equal to the terrace size, the *average* current on the terrace is just the half of its maximal value which is obtained for $l_s \rightarrow \infty$.

Actually this latter case was the one discussed for its stabilizing effect on step flow (Schwoebel and Shipsey, 1966; Villain, 1991). The basic principle can be understood quite easily: For an uphill current essentially proportional to the terrace size ℓ , a wider terrace leads to a higher velocity of its upward step, which in turn tends to shrink the terrace size again. For the two dimensional case this only works well if the steps’ shape remains straight (i.e. effective translational symmetry parallel to the steps), a requirement which the *Bales-Zangwill instability* (Bales and Zangwill, 1990) counteracts. In the end, even the two dimensional, vicinal surface gets unstable and forms mounds (Rost et al., 1996).

The unphysical behavior of a finite current for a flat surface $J_{\text{net}}(\ell \rightarrow \infty) = Fl_s/2$ ^b in eq. (4.5) is due to foreclosing islands, i.e. the situation should change if ℓ becomes large enough for island nucleation to take place. In a

^bTo be more precise, there is even a discontinuity, since the sign of J_{net} is opposite to the tilt.

naive picture (Krug, 1997), this can be taken into account in the following way: In the presence of islands, not the whole terrace is involved in the current “production”, but only the part of size l_D closest to the downward-step (cf. fig. 4.3), which can be reflected in eq. (4.5) by replacing $\ell \rightarrow l_D$. Furthermore, since on the rest of the terrace there is no current, its average value is obtained by multiplying eq. (4.5) with the weight l_D/ℓ , resulting in

$$J_{\text{up}} = \frac{l_D}{\ell} F \frac{l_D - a}{2} \frac{l_s}{l_D + l_s} \quad (4.6)$$

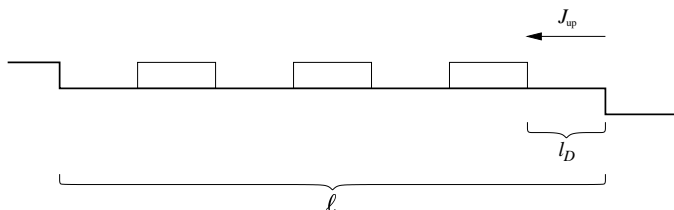


Figure 4.3: The situation of island nucleation on a large ($\ell \gg l_D$) terrace. Due to symmetry, the left part does not contribute to the current, only a fraction of order l_D/ℓ is involved. A typical situation will look much less regular, of course.

Since “up” means towards $+x$ for a positive tilt ($\nabla h = a_{\perp}/\ell$ in a coarse grained view) and towards $-x$ for a negative one, we can rewrite eq. (4.6) as

$$j \sim \frac{Fa}{2} \frac{l_D^2 l_s}{l_D + l_s} \nabla h,$$

where we have included the particle volume to get a volume current (cf. section 2.6.3) and have also used that $a \ll l_D$. By comparison with the current of Edwards-Wilkinson type (2.51), we identify the parameter ν of the destabilizing term as

$$\nu \sim -\frac{Fa}{2} \frac{l_D^2 l_s}{l_D + l_s}. \quad (4.7)$$

A more rigorous treatment of nucleation effects by means of an extended BCF theory (Myers-Beaghton and Vvedensky, 1991) confirms the limiting behavior of eq. (4.7) for $l_D \ll \ell$ and $l_D \gg \ell$ (Krug, 1997), making it a useful interpolation formula.

4.3 Stability

Having set up the destabilizing term, we consider the stabilizing one. In order to perform a linear stability analysis, we regard the next relevant term in the (linear) Langevin equation which is of fourth order, i.e. we inspect

$$\partial_t h = \nu \nabla^2 h - K \nabla^4 h. \quad (4.8)$$

In our limiting case of irreversible incorporation of adatoms, where there is no relaxation into equilibrium upon switching off the particle beam, the precise microscopic origin of the stabilizing term and thus the form of its prefactor K is still an open question (random nucleation is suggested in (Politi and Villain, 1996)), but on dimensional grounds

$$K \sim Fa l_D^4$$

should be expected. But even then, the presence of step edge barriers may alter this relation, which we express as

$$K = Fa l_D^4 k(l_s/l_D),$$

where the only known property of the scaling function $k(y)$ is that it becomes a constant for vanishing argument.

With this, eq. (4.8) could easily be solved, but already a dimensional analysis shows that there is only one possible characteristic time. Namely with

$$[\nu] = \text{L}^2\text{T}^{-1} \quad [K] = \text{L}^4\text{T}^{-1},$$

we get

$$\tau \sim \frac{K}{\nu^2} \sim \frac{1}{Fa} k(l_s/l_D) \left(\frac{l_D}{l_s} + 1 \right)^2 \quad (4.9)$$

as the time scale for the onset of the instability, which we can identify with the damping time t_d .

4.4 Simulations in one dimension

In the simulations, we measure the damping time in the same way as in sections 3.4 and 3.5. Here we choose it to be the time necessary to develop a surface width of $w^2 = 0.6$. The simulations were carried out for parameters $D/F = 10^3 \dots 10^{9.5}$ (i.e. $l_D \approx 5.6 \dots 237$) and $l_s = 4 \dots 99$. The resulting data, shown in fig. 4.4 on the following page, expose no power law for times below t_{ML} , only data points with $t_d > 4$ are exploitable for evaluation.

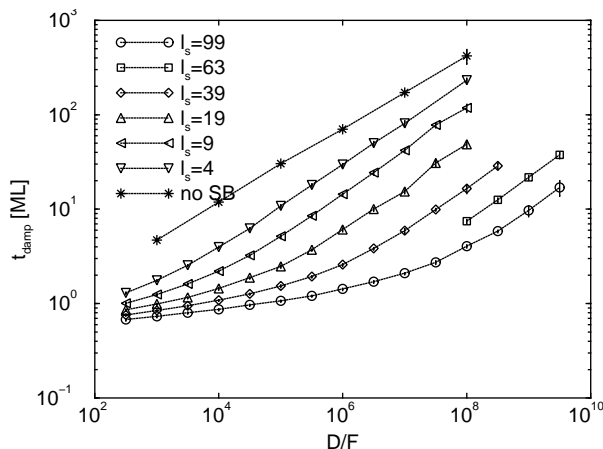


Figure 4.4: The damping time t_d (in units of t_{ML}), defined as the time for the system to reach $w^2 = 0.6$, in the presence of Schwoebel barriers. The substrate dimension is $d = 1$.

To test the validity of eq. (4.9), the data from the same source is plotted in a different way: The square root of t_d and the theoretical $l_D \propto (D/F)^{1/4}$ should be related linearly in the case of a constant function k in eq. (4.9). This is essentially confirmed by fig. 4.5 on the next page.

Clearly, the two graphs for weaker barriers show a negative curvature which becomes clear when we compare the damping due to the Villain instability to the case of kinetic roughening being responsible. That means we contrast

$$t_d \propto \left(\frac{l_D}{l_s}\right)^2 \quad \text{to} \quad \tilde{t} \propto l_D^{4/3}$$

Since t_d growth faster with l_D , the kinetic roughening takes over when $t_d > \tilde{t}$, i.e. the crossover time scales like

$$t_x \propto l_s^4. \quad (4.10)$$

The correspondence between the inverse of the slopes (dotted lines) in figure 4.5 and the Schwoebel length according to eq. (4.2) is displayed in fig. 4.6 on the following page. Apart from an offset of 4 lattice constants, the relation between the theoretical Schwoebel length l_s and the length extracted from the damping time t_d is linear with a proportionality constant of order one. Hence, the theory in this case can be regarded as confirmed.

4.4. SIMULATIONS IN ONE DIMENSION

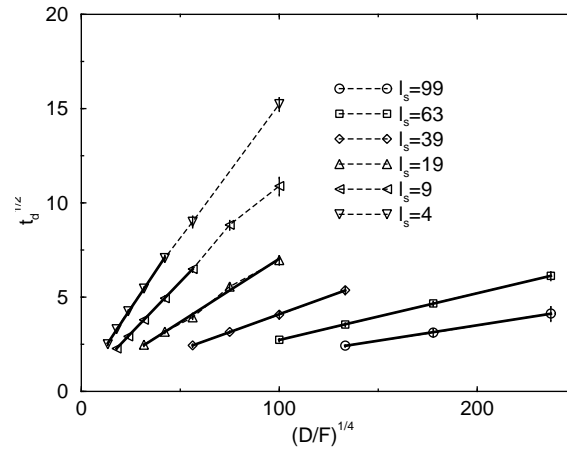


Figure 4.5: The influence of the Ehrlich-Schwoebel on the damping time t_d (plotted in units of t_{ML}) for $D/F = 10^4 \dots 10^7$. In agreement with eq. (4.9), the square root of the damping time is a linear function of l_D . The curvature for weak barriers ($l_s \leq 4$) can be assigned to a crossover effect (cf. text). Consequently only the first five data points were used to determine the slopes (solid lines).

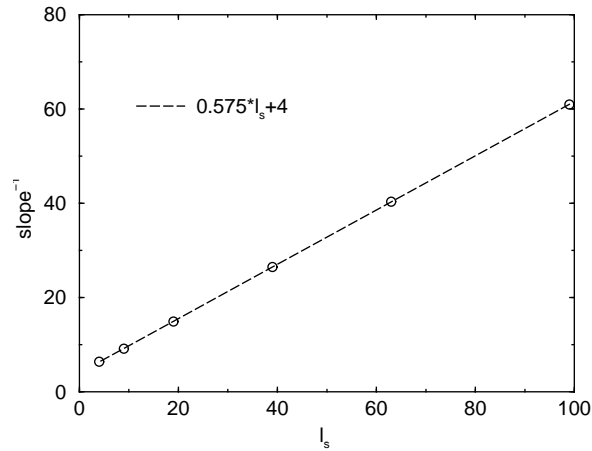


Figure 4.6: The inverse slope as read off from fig. 4.5 versus the theoretical Schwoebel length. The linear dependence is according to eq. (4.9) is verified, albeit with a variance in form of an offset.

4.5 Simulations in two dimensions

The case of a two dimensional substrate is revealed by the simulation data as a more complex scenario, for which the solution (4.9) cannot be simply adopted: Though there are the same qualitative dependencies (a damping time increasing with growing l_D and decreasing l_s), the power law's exponent 0.57 for high l_D is significantly larger than $2\gamma \approx 1/3$ as shown in fig. 4.7.

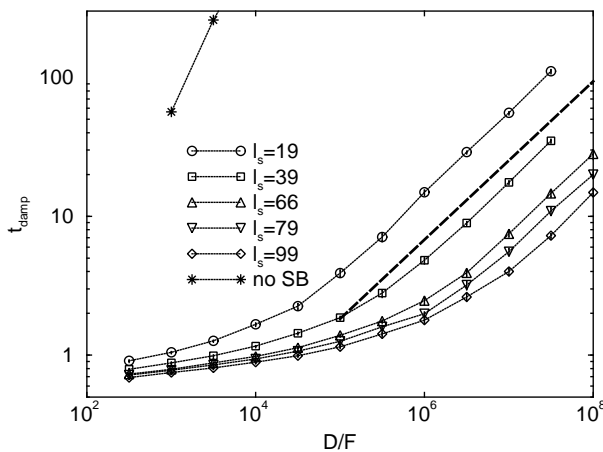


Figure 4.7: The damping time (measured in units of t_{ML}) for a two dimensional system in the presence of Schwoebel barriers. The dashed line depicts the power law $(D/F)^{0.57}$.

A more striking difference to the one-dimensional case however is the fact that the damping time does not solely depend on the *ratio* of l_D and l_s , but they enter in different powers. This can be read off from fig. 4.8 on the following page, where the damping time was rescaled by the factor $l_s^{-1.62}$ whereby – apart from early time deviations for large l_s – a collapse onto the power law $(D/F)^{0.57}$ could be obtained. In other words

$$\frac{t_d}{t_{ML} l_s^{-1.62}} \propto \left(\frac{D}{F}\right)^{0.57} \Leftrightarrow \frac{t_d}{t_{ML}} \propto \frac{l_D^{0.57/\gamma}}{l_s^{1.62}} \approx \left(\frac{l_D^2}{l_s}\right)^{1.62} \quad (4.11)$$

where we have used $1/\gamma \approx 5.7$.

However, due to our findings in chapter 3, we cannot categorically exclude the length l_0 from the considerations. That means, the result of fig. 4.8 would

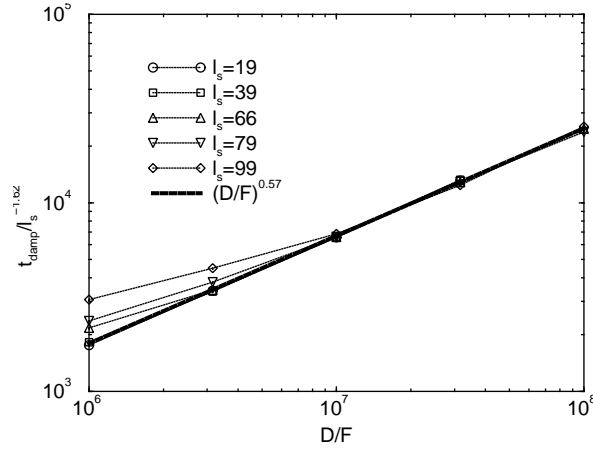


Figure 4.8: The damping time (in units of t_{ML}) for the two-dimensional surface, rescaled by a suitable power of l_s . The deviations for large Schwoebel lengths correspond to the “curved” region $t_d < 4$ in fig. 4.7 on the preceding page.

be compatible with the relation

$$\frac{t_d}{t_{\text{ML}}} \sim \left(\frac{l_0^{4/3}}{l_D^{1/3} l_s} \right)^{1.62} \quad (4.12)$$

as well (when setting $\gamma = 1/5.76$), which has even the advantage of being dimensionless. Nevertheless, we use solely l_D to express the D/F -dependence in the next section.

4.6 Discussion

4.6.1 Implications on energy barrier variations

Though the empirical law (4.11) differs strongly from the one dimensional case eq. (4.9), both findings give information about the relative importance of the length scales l_D and l_s . In practice, these two can be changed by varying the deposition rate F , the temperature T or the energy barriers E_D and E_s .

The influence in the first case is clear, for only l_D depends on F . Thus, lowering the flux will increase l_D according to eq. (3.6) and therefore prolong

the layer-by-layer growth, just as in the case without any interlayer barriers. The effect is even stronger for the temperature dependence: Raising the temperature will increase the diffusion constant D and consequently l_D as well, while it makes the Schwoebel length smaller according to eq. (4.2). The suppression of the surface roughening by this interplay is most plausible.

Yet there may occur situations where the changes in the length scales l_D and l_s counteract. We will discuss such a case, namely self diffusion on a strained Pt(100) surface. Here it was found in (Schindler, 1999) by employing semi-empirical lattice potentials to take into account the dependence of the energy barriers on the precise local configuration, that homogeneous strain lets the diffusion barriers raise while the Schwoebel barrier drops (or vice versa) in such a way that their sum is essentially invariant. This is true for ordinary hopping diffusion as well as for exchange diffusion, only the sign under compression/tension is different (cf. fig. 4.9 on the next page).

That means, if we have due to strain

$$E_D \rightarrow E_D - \Delta E \quad , \quad E_s \rightarrow E_s + \Delta E \quad ,$$

with the same ΔE , the length scales change like (cf. equations (2.2), (3.6) and (4.2))

$$\begin{aligned} l_D &\rightarrow c^\gamma l_D \\ l_s &\rightarrow c l_s \end{aligned}$$

with the same

$$c = \exp\left(\frac{\Delta E}{k_B T}\right) \quad ,$$

i.e. *both* increase (decrease) for a positive (negative) ΔE .

Now the quantitative prediction about the relative importance is called for: In the two dimensional case we get according to eq. (4.11)

$$\left(\frac{t_d}{t_{ML}}\right)^{1/1.62} \propto \frac{l_D^2}{l_s} \rightarrow c^{2\gamma-1} \frac{l_D^2}{l_s} \quad ,$$

and therefore, since $2\gamma_{d=2} \approx 1/3 < 1$, the influence of the Schwoebel length overcompensates the one of the diffusion length in the sense that a positive ΔE (i.e. an augmented Schwoebel barrier) *shortens* the damping time. This

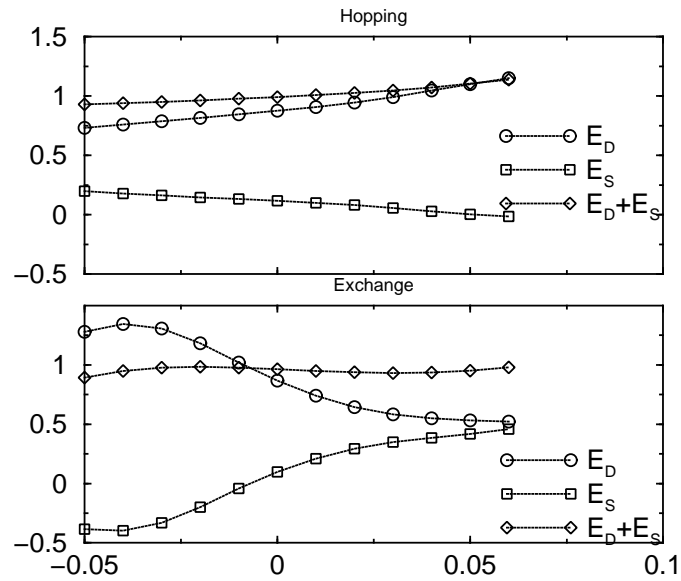


Figure 4.9: The influence of strain ($\varepsilon > 0$ means stretched) on the diffusion and Schwoebel barrier: Their sum is essentially a constant. The upper graph refers to ordinary hopping diffusion as envisaged in our model. The lower graph “exchange” represents a process where the exchange with a substrate atom is involved (Schindler, 1999). Data by courtesy of A. Schindler.

would be even more pronounced in the one dimensional case, where the corresponding factor $c^{\gamma-1}$ has the lower exponent $-3/4$.

While the data in fig. 4.9 suggest essentially the same probability for both diffusion mechanisms because of an identical energy barrier, experiments (Kellog, 1991) reveal only exchange diffusion to take place in the considered system. This discrepancy, discussed in (Schindler, 1999), is not our concern. Instead, we can argue that for exchange diffusion compressive strain enhances layer-by-layer growth, despite the decrease of the diffusion constant, and tensile strain just acts oppositely. This does not only apply for Pt/Pt(100) but for most of the other systems investigated in (Schindler, 1999) as the trend is quite general. For ordinary hopping diffusion, the influence of strain is just the opposite.

4.6.2 Experimental access of the damping time

It is interesting to note the difference between one and two dimensions regarding the impact of the Schwoebel barrier. While in $d = 1$, there is the crossover (4.10) which means that for large enough D/F , kinetic roughening will always dominate in the end, the curve for $l_s = 0$ in two dimensions almost immediately exceeds the plot bounds in fig. 4.7 on page 86. Here, the Schwoebel barrier moves the damping time into experimentally sensible regions. A moderate barrier of 0.1 eV at $T = 350$ K amounts according to eq. (4.2) to $l_s \approx 27$ which yields a damping time below a hundred monolayers, even for higher D/F . Under this conditions, the relation $t_d \propto F^{-0.57}$ for fixed D could be tested (tuning D by varying the temperature would change l_s as well).

Chapter 5

Mean Field Approach: Cohen's Model

In this chapter we investigate, in how far layer-by-layer growth and possibly its damping can be captured by a mean field model, where no individual adatoms and islands are traced.

A classical, most intuitive mean field model for growth of a high symmetry surface is the one proposed by Cohen et al. (Cohen et al., 1989). Surprisingly, up to now it lacked a detailed, quantitative investigation of its capabilities. In this chapter, we will make up for that to a certain extent.

The model's degrees of freedom are the relative coverages of the layers (numerated by k in the following), so that it does not incorporate any morphologic informations, but retains only the discreteness of the height variable. Together with the solid on solid condition the coverages θ_k obey

$$1 \geq \theta_k \geq \theta_{k+1} \geq 0.$$

If we neglect furthermore steps higher than one, then mass transport along the surface is only possible between adjacent layers, and the evolution of layer k is governed by

$$t_{\text{ML}} \dot{\theta}_k = (1 - \alpha_{k-1}) \cdot (\theta_{k-1} - \theta_k) + \alpha_k \cdot (\theta_k - \theta_{k+1}). \quad (5.1)$$

The coefficient α_k is defined as the fraction of the particle flux that “escapes” from the terrace^a $\theta_k - \theta_{k+1}$ to the lower one and thus contributes to the growth of layer k . This process is the origin of the second term. Correspondingly, the first term in eq. (5.1) describes the growth of layer k due to the material that did *not* escape from the terrace $\theta_{k-1} - \theta_k$ (cf. fig. 5.1).

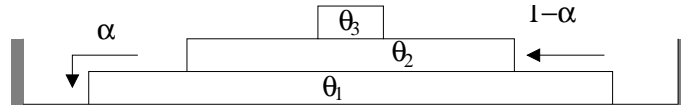


Figure 5.1: Interlayer transport in Cohen's model. The meaning of the abscissa is the relative coverage, the scenario shown is just one way to envisage such a configuration of coverages. The coefficients α control the final destination (upper/lower terrace) of the material impinging on the exposed surface.

The lowest terrace plays a special rôle, no material can escape from there:

$$\dot{\theta}_1 = 1 - \theta_1 + \alpha_1(\theta_1 - \theta_2) \quad \text{b} \quad (5.2)$$

^aSince there is no morphology information, “terrace” is meant in a generalized sense, it is the exposed coverage of layer k .

This is consistent with eq. (5.1) if we define

$$\theta_0 \equiv 1 \quad , \quad \alpha_0 \equiv 0 .$$

To prevent a “layer overflow”, we have the additional constraint

$$\theta_k = 1 \quad \Rightarrow \quad \dot{\theta}_k = 0 ,$$

which translates for the coefficients α_k to

$$\alpha_k(\theta_k = 1) = 0 . \tag{5.3}$$

Since the surface width is of primary interest in this model, the evaluation of \bar{h} and \bar{h}^2 has to be considered:

$$\bar{h} = \sum_{k=1}^{\infty} k(\theta_k - \theta_{k+1}) = \sum_{k=1}^{\infty} \theta_k \tag{5.4}$$

$$\bar{h}^2 = \sum_{k=1}^{\infty} k^2(\theta_k - \theta_{k+1}) = 2 \sum_{k=1}^{\infty} k\theta_k - \bar{h} \tag{5.5}$$

$$\Rightarrow w^2 = 2 \sum_{k=1}^{\infty} k\theta_k - \bar{h}(\bar{h} + 1) \tag{5.6}$$

If, at later times, the first $k_0 - 1$ layers are filled, they clearly do not contribute to the width (as can be seen also from eq. (5.6)), so that they can be dropped by renumbering the system $k \rightarrow k - k_0 + 1$ (i.e. $k_0 \rightarrow 1$) such that layer 1 is never completed.

In (Cohen et al., 1989) some suggestions concerning the form of the coefficients α_k were given. In the following, we will give a thorough treatment of the simplest case: a constant.

5.1 Constant coefficients

If we set all coefficients α_k equal to a constant α independent of the dynamic variables θ_k , then eq. (5.3) is not fulfilled. This can be cured by either multiplying α_k with $\Theta(1 - \theta_k)$ or by renumbering the system ($k \rightarrow k - 1$) each time the bottom layer is completed (i.e. $\theta_1 = 1$) as mentioned above.

^bFrom here on, we use natural units again.

Since $\alpha < 1/2$ favours the growth of the upper layer while $\alpha > 1/2$ favours the lower one, these cases can be seen to mimic Schwoebel barriers (cf. previous chapter) and island edge decoration respectively (Markov, 1994; Kandel, 1997). Therefore, we can already guess a qualitatively differing behaviour, separated by the unbiased $\alpha = 1/2$.

5.1.1 Poisson Growth: $\alpha = 0$

The simplest case is the complete inhibition of interlayer transport, i.e. $\alpha_k \equiv 0$ where (5.1) is reduced to

$$\begin{aligned}\dot{\theta}_k &= \theta_{k-1} - \theta_k \\ \theta_0 &\equiv 1,\end{aligned}$$

which can be solved recursively, yielding

$$\theta_n = 1 - \exp(-t) \sum_{k=0}^{n-1} \frac{t^k}{k!} .$$

The exposed coverage, defined as

$$\epsilon_k \equiv \theta_{k-1} - \theta_k ,$$

even takes on a simpler form, namely that of a Poisson distribution with parameter t (Gardiner, 1985) (hence the name of the growth mode):

$$\epsilon_n = \exp(-t) \frac{t^n}{n!} \tag{5.7}$$

This is convenient, since the squared surface with

$$\begin{aligned}w^2 &= \sum_{n=0}^{\infty} (n - \bar{h})^2 \epsilon_n \\ \bar{h} &= \sum_{n=0}^{\infty} n \epsilon_n\end{aligned}$$

is just the second central moment, known to be (cf. section 2.6)

$$w^2(t) = t$$

For large n the distribution (5.7) can be approximated by a Gaussian around $t = n$:

$$\epsilon_n \approx (2\pi n)^{-1/2} \exp\left(-\frac{(t-n)^2}{2n}\right) ,$$

which illustrates very well the constant velocity ($= 1$ with our unit of time) and the diffusive broadening of the active zone.

5.1.2 Anticipated numerical results

To get some hints for the analytical approach, let's first have a look at numerical solutions to the problem. fig. 5.2 shows, as already expected, a qualitative difference for values of α below and above $1/2$: In the former case, the behavior is Poisson-like $w^2 \propto t$, albeit with a slope smaller than unity that decreases further with growing α ; in the latter case an oscillatory stationary state – corresponding to layer-by-layer growth – is reached. There, the oscillation amplitude grows with larger α while its mean drops.

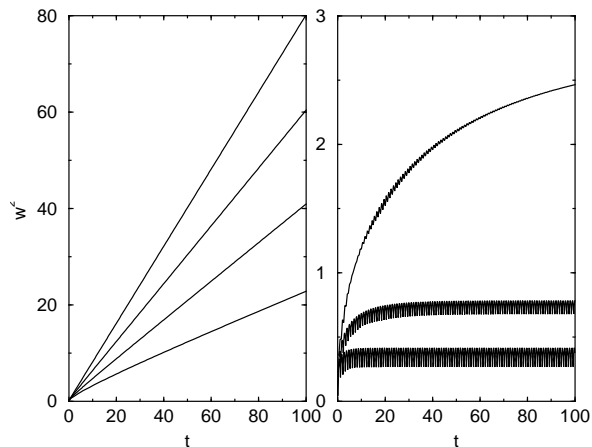


Figure 5.2: Temporal development of the surface width for values below $\alpha = 1/2$ (left graph: 0.1, 0.2, 0.3, and 0.4 from top to bottom) and above (right graph: 0.6, 0.7, and 0.8 from top to bottom). The steady state for $\alpha = 0.6$ is not reached yet, instead an algebraic transient can be seen.

5.1.3 Continuum approach

For the case of an ever growing width where an arbitrary large number of layers may contributed to the width, a continuum approach is expected to be of help. We replace the layer number n by the dimensionless variable h and define the corresponding smooth function

$$\theta(h = n, t) = \theta_n(t) . \quad (5.8)$$

Inserting the Taylor expansion of $\theta(h, t)$ in $\Delta h = 1$ into eq. (5.1) yields a differential equation (of infinite order in principle) for $\theta(h, t)$:

$$\begin{aligned} \partial_t \theta &= - \sum_{k=0}^{\infty} \frac{1}{(2k+1)!} \partial_h^{2k+1} \theta(h, t) \\ &+ (1 - 2\alpha) \sum_{k=1}^{\infty} \frac{1}{(2k)!} \partial_h^{2k} \theta(h, t) \end{aligned} \quad (5.9)$$

A promising ansatz is a scaling form

$$\theta(h, t) = \Phi((h - t) \cdot b(t) + y_0) , \quad (5.10)$$

where the shape function $\Phi(y)$ is time independent while a possible broadening of the profile is described by a diminishing $b(t) > 0$. The rôle of the shift y_0 finally is to assure mass conservation, as will be shown below.

The main task now is to determine the shape function $\Phi(y)$, but some of its properties can already be stated:

(5.11a) $y = 0$ is chosen to separate the completed from the uncompleted layers, i.e. $\Phi(y \leq 0) = 1$ and $0 < \Phi(y > 0) < 1$, the corresponding height is $h_0 \equiv t - y_0/b(t)$

(5.11b) $\Phi(y)$ shall be continuous

(5.11c) the SOS condition requires $\Phi'(y) \leq 0$

(5.11d) $\Phi(y \rightarrow \infty)$ must vanish fast enough to provide the existence of the corresponding improper intergal; accordingly its derivatives must vanish at plus infinity, too

For a functional form like eq. (5.10), mass conservation is involved in the following way:

$$\begin{aligned} t &\stackrel{!}{=} \int_0^\infty \theta(h, t) dh \\ &= h_0 + \frac{1}{b} \int_0^\infty \Phi(y) dy \\ &= t + \frac{M_0[\Phi] - y_0}{b} \end{aligned}$$

where

$$M_k[\Phi] \equiv \int_0^\infty y^k \Phi(y) dy. \quad (5.12)$$

Though this shows that y_0 must be chosen as being just the area below $\Phi(y > 0)$, i.e.

$$y_0 = M_0[\Phi], \quad (5.13)$$

it is not a trivial equation, since $\Phi(y)$ itself may depend on y_0 again.

The calculation of the width w^2 given by a continuum form (5.10) can be generalized quite readily from eq. (5.6):

$$\begin{aligned} \overline{h^2} &= \int_0^\infty -\partial_h \theta(h, t) h^2 dh \\ &= h_0^2 + 2 \int_{h_0}^\infty \theta(h, t) h dh \\ &= \left(t - \frac{M_0[\Phi]}{b} \right)^2 + \frac{2}{b^2} (M_1[\Phi] - M_0^2[\Phi]) + \frac{2tM_0[\Phi]}{b} \\ &= \frac{2M_1[\Phi] - M_0^2[\Phi]}{b^2} + t^2 \end{aligned} \quad (5.14)$$

$$\Rightarrow w^2 = \overline{h^2} - t^2 = \frac{2M_1[\Phi] - M_0^2[\Phi]}{b^2} \quad (5.15)$$

As had to be expected, the dynamics of $w(t)$ is fully determined by that of $b(t)$.

But first we have to check to what extent the ansatz (5.10) solves eq. (5.9). Insertion yields

$$(y - y_0) \Phi'(y) \frac{db}{dt} = - \sum_{k=1}^{\infty} \frac{b^{2k+2}}{(2k+1)!} \Phi^{(2k+1)}(y) + (1 - 2\alpha) \sum_{k=1}^{\infty} \frac{b^{2k+1}}{(2k)!} \Phi^{(2k)}(y) \quad (5.16)$$

where

$$y \equiv (h - t) \cdot b + y_0, \quad (5.17)$$

which reveals that the differential equation can only be satisfied if a function $b(t)$ can be found whose explicit presence cancels out in eq. (5.16). This is impossible to achieve exactly, but for a $b(t)$ approaching zero, only the dominant term on the right hand side must be kept, so that at least an asymptotic solution can be obtained.

This solution we will call $\tilde{\Phi}(y)$ and the requirement (5.11a) will be enforced by defining

$$\Phi(y) \equiv \min\{\tilde{\Phi}(y), 1\}.$$

which in turn imposes the conditions $\tilde{\Phi}(0) = 1$ and $\tilde{\Phi}(y < 0) \geq 1$, but allows for continuous derivatives.

5.1.4 The case $\alpha = 1/2$

First, we will investigate the borderline $\alpha = 1/2$ (cf. fig. 5.2 on page 95). Here, all even derivatives in eq. (5.16) vanish and the dominant term on the right hand side is $b^4 \Phi'''(y)$, so that the choice

$$b(t) = (2/t)^{1/3} \quad (5.18)$$

reduces eq. (5.16) asymptotically to

$$(y - y_0) \Phi'(y) = \Phi'''(y). \quad (5.19)$$

Regarding Φ' as the unknown function, the solutions of this ODE are well known to be the Airy functions $\text{Ai}(y)$ and $\text{Bi}(y)$ (cf. appendix E and (Abramowitz and Stegun, 1965)) and their linear combinations. Since $\text{Bi}(y)$

is unbounded for large arguments, it is ruled out by the condition (5.11d), and we are left with $\text{Ai}(y)$. More precisely, due to the explicit appearance of y_0 in eq. (5.19), it has to be evaluated at $y - y_0$:

$$\Phi'(y) = c \text{Ai}(y - y_0)$$

The factor c and the integration constant involved when obtaining $\Phi(y)$ are fixed by the requirements (5.11), resulting in

$$\tilde{\Phi}(y) = \frac{\text{Ai}'(y - y_0)}{\text{Ai}'(-y_0)},$$

where $\text{Ai}'(y)$ is the primitive of $\text{Ai}(y)$ as defined by eq. (E.3).

From eq. (5.13) we find y_0 to be the solution to

$$y_0 = \frac{M_0[\text{Ai}'(y - y_0)]}{\text{Ai}'(-y_0)} = -\frac{\text{Ai}''(-y_0)}{\text{Ai}'(-y_0)} = y_0 + \frac{\text{Ai}'(-y_0)}{\text{Ai}'(-y_0)},$$

where we have used definition (E.3) for $\text{Ai}''(y)$ and its property (E.5).

Hence, the condition for y_0 is that its negative has to denote a local extremal value of the Airy function $\text{Ai}(y)$. A look at fig. E.1 on page 172 tells that this can only be the rightmost maximum, otherwise $\tilde{\Phi}(y)$ would oscillate and with this it would exceed unity, both in contrast to the constraints (5.11c) and (5.11a) respectively. In tabulations (Abramowitz and Stegun, 1965) the value can be found to be $y_0 = 1.018792972$.

Moreover, this special value of y_0 does not only assure mass conservation, but it serves for another consistency, namely the different ODE of the bottom layer, which we did not take into account from eq. (5.9) on. There, the 2nd order spatial discretization of the lowest order term coincides (to no surprise) with the $\alpha = 1/2$ -form of eq. (5.1)

$$\dot{\theta}_k = \frac{\theta_{k-1} - \theta_{k+1}}{2},$$

and matches eq. (5.2) for $k = 1$ only if

$$\frac{\theta_0}{2} + \frac{\theta_1}{2} = 1 \tag{5.20}$$

holds true, where θ_0 is an unity exceeding fictive coverage.

According to property (5.11a), the bottom layer is found at $y = 0$ or

$$h_0(t) = t - y_0 (t/2)^{1/3} ,$$

and as we, when coming back to the discrete set θ_k , refine eq. (5.8) by renumbering the system ($k \rightarrow k - 1$) every time the bottom layer θ_1 reaches unity. Thus, we identify ^c

$$\theta_k(t) = \theta(h_0 + k - 1 + 1/2, t) = \tilde{\Phi} \left((k - 1/2) (2/t)^{1/3} \right) ,$$

and eq. (5.20) translates into

$$\begin{aligned} & \tilde{\Phi} \left(-(2/t)^{1/3}/2 \right) + \tilde{\Phi} \left((2/t)^{1/3}/2 \right) = 2 \\ \Leftrightarrow & \tilde{\Phi} \left(-(2/t)^{1/3}/2 \right) - \tilde{\Phi}(0) = \tilde{\Phi}(0) - \tilde{\Phi} \left((2/t)^{1/3}/2 \right) . \end{aligned}$$

This suggest a linear behavior of $\tilde{\Phi}$ around $y = 0$, which is precisely fulfilled because of the vanishing second derivative there:

$$\tilde{\Phi}''(y)|_{y=0} = \frac{\text{Ai}'(-y_0)}{\text{'Ai}(-y_0)} = 0$$

Now, with the fully determined shape function Φ and the time dependence $b(t)$, the evolution of the width w^2 can be calculated as shown in eq. (5.15). Integrating by parts, we find

$$\begin{aligned} M_1[\text{'Ai}(y - y_0)] &= \text{''''Ai}(-y_0) \\ \Rightarrow 2M_1[\Phi] - M_0^2[\Phi] &= -\frac{\text{Ai}(-y_0)}{\text{'Ai}(-y_0)} , \end{aligned}$$

where we have used the definition of $\text{''''Ai}(y)$ and its property according to the equations (E.3) and (E.6) respectively, together with $M_0[\Phi] = y_0$ and the vanishing of $\text{Ai}'(-y_0)$.

Thus, inserting the numerical values $\text{Ai}(-y_0) = 0.53565666$ and $\text{'Ai}(-y_0) = -0.8090733$, into

$$w^2(t) = -\frac{\text{Ai}(-y_0)}{\text{'Ai}(-y_0)} b^{-2}(t)$$

^cThe somewhat arbitrary offset $+1/2$ reflects the fact that the correct value changes from one down to zero during the lifetime of the bottom layer.

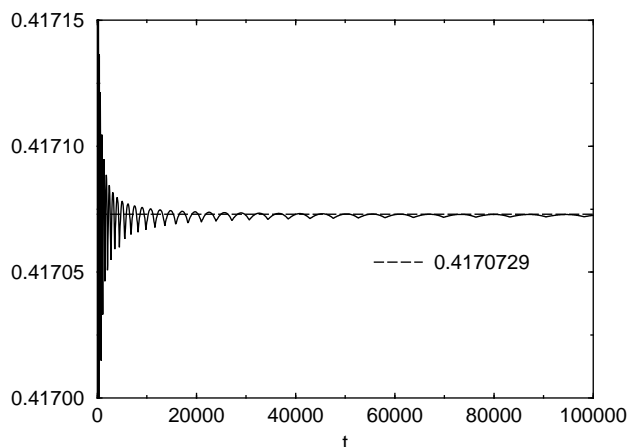


Figure 5.3: Numerical confirmation of $w^2 \propto t^{2/3}$ for $\alpha = 1/2$; at later times, the influence of the discrete height vanishes. (The oscillation's decreasing frequency is just a stroboscopic effect.)

we end up with

$$w^2 = 0.4170729 t^{2/3} .$$

In fig. 5.3, a comparison to the results of a numerical solution of the discrete model displays the confirmation of this amplitude of w^2 up to an additional offset. The latter can be assigned to small deviations at the bottom layer, where the influence of the vertical lattice cannot be cured completely by the consideration of eq. (5.20).

5.1.5 The case $\alpha < 1/2$

For a parameter $\alpha \neq 1/2$, the leading term in eq. (5.16) is the one containing $b^3 \Phi''(y)$, where the choice

$$b = \frac{t^{-\frac{1}{2}}}{\sqrt{2 - 4\alpha}} , \tag{5.21}$$

leads to the asymptotic ODE

$$-2(y - y_0)\Phi'(y) = \Phi''(y) .$$

This differential equation for $\Phi'(y)$ differs from eq. (5.19) only by a different sign and a lower derivative on the right hand side. Its solution is a shifted Gaussian

$$\tilde{\Phi}'(y) = c \exp(-(y - y_0)^2) ,$$

where again the requirements (5.11) lead to a unique solution

$$\tilde{\Phi}(y) = \frac{\operatorname{erfc}(y - y_0)}{\operatorname{erfc}(-y_0)},$$

which involves the complementary error function

$$1 - \operatorname{erfc}(y) \equiv \operatorname{erf}(y) \equiv \frac{2}{\sqrt{\pi}} \int_{-\infty}^y \exp(-x^2) dx.$$

As in the previous case, to determine y_0 , we have to evaluate $M_0[\Phi]$:

$$\begin{aligned} M_0[\operatorname{erfc}(y - y_0)] &= y_0 \operatorname{erfc}(-y_0) + \frac{\exp(-y_0^2)}{\sqrt{\pi}} \\ \Rightarrow y_0 &\stackrel{!}{=} y_0 + \frac{\exp(-y_0^2)}{\sqrt{\pi} \operatorname{erfc}(-y_0)} \end{aligned}$$

Obviously this equation has no finite solution, taking the limit $y_0 \rightarrow \infty$ is the best that can be done. But the meaning of an infinite y_0 is a bottom layer at minus infinity, or in other words: No layer is ever filled completely.

Now here, we have to remind ourselves to the solution's merely asymptotic validity. When α is close to one half, for early times the term $(1 - 2\alpha)b^3\Phi''(y)$ in eq. (5.16) will be small compared to $b^4\Phi'''(y)$ and the evolution proceeds like for $\alpha = 1/2$ with $b(t)$ given by eq. (5.18). This behavior gradually changes when the two terms become comparable, i.e. after a crossover time

$$t_{\dagger} \sim (1 - 2\alpha)^{-3}. \quad (5.22)$$

Around that time, there will be a last filled layer, i.e. h_0 becomes actually "pinned" and in this sense $\bar{h} - h_0$ indeed approaches infinity asymptotically.

For calculating the width's amplitude, an y_0 going to infinity is not a problem, since the difference in eq. (5.15) evaluates to

$$2M_1[\Phi] - M_0^2[\Phi] = \frac{3}{2} - \left(1 + y_0 \frac{\exp(-y_0^2)}{\sqrt{\pi} \operatorname{erfc}(-y_0)}\right)^2,$$

and thus approaches the value 1/2.

Given that, the result is a width growing like

$$w^2(t) = (1 - 2\alpha)t,$$

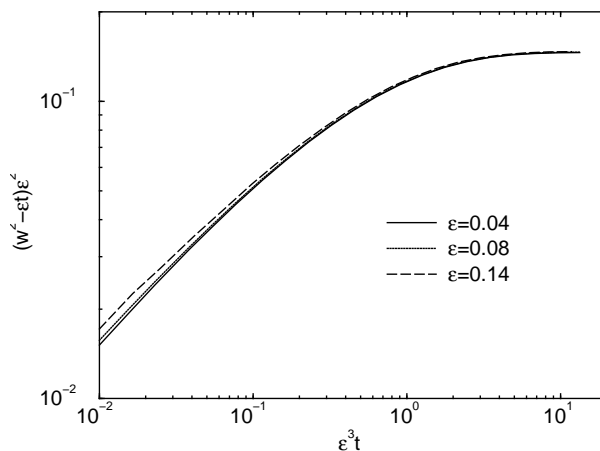


Figure 5.4: Data collapse showing the transient superimposed on the Poisson-like growth for $\alpha < 1/2$. The parameter $\epsilon = |1 - 2\alpha|$ measures the distance to the “critical point” $\alpha = 1/2$.

but once more we have to be careful about the transient regime. Though our solution

$$\theta(h, t) = \frac{1}{2} \operatorname{erfc} \left(\frac{h - t}{\sqrt{2t}\sqrt{1 - 2\alpha}} \right)$$

corresponds to the right initial condition of $\theta(h, 0) = \Theta(-h)$, it does not describe the behavior at these early times correctly. Instead, due to the prominent $w^2 \propto t^{2/3}$, the width gets ahead by a value of

$$w_0^2 \sim t_+^{2/3} \sim (1 - 2\alpha)^{-2}.$$

Exactly this behavior of the numerical solution is shown in fig. 5.4, where after subtracting the Poisson-like contribution, a corresponding data collapse could be obtained.

5.1.6 The case $\alpha > 1/2$

The choice $\sqrt{2 - 4\alpha}$ in eq. (5.21) was crucial, since trying $\sqrt{4\alpha - 2}$ would lead to

$$2(y - y_0)\Phi'(y) = \Phi''(y),$$

whose unbounded solutions fail to fit the conditions (5.11).

Yet another possibility to get rid of t appearing in eq. (5.16) is the assumption of a saturating b . Unfortunately such a constant b is incapable of promoting only one relevant term on the right hand side, i.e. we have to deal with *all* derivatives. But then we can come back to the original equation as well. As in the other cases, a prefactor of b can be chosen deliberately, which is compensated by the calculation of $\Phi(y)$. Hence, here we are free to set $b = 1$ resulting in

$$\begin{aligned} \partial_t \theta(h, t) &= (1 - \alpha) \theta(h - 1, t) \\ &\quad + (2\alpha - 1) \theta(h, t) \\ &\quad - \alpha \theta(h + 1, t) \\ \Rightarrow -\Phi'(y) &= (1 - \alpha) \Phi(y - 1) + (2\alpha - 1) \Phi(y) - \alpha \Phi(y + 1) \end{aligned}$$

A solution consistent with the conditions (5.11) is a decaying exponential

$$\tilde{\Phi}(y) = \exp(-cy) , \quad (5.23)$$

whereupon we get a transcendent equation for the parameter c :

$$c = (1 - \alpha) \exp(c) + 2\alpha - 1 - \alpha \exp(-c) \quad (5.24)$$

This equation has positive solutions $c(\alpha)$ only for $\alpha > 1/2$ as shown in fig. 5.5 on the following page. For $\alpha \rightarrow 1$, it diverges logarithmically^d, while for $\alpha \gtrsim 1/2$, the solution can be expanded in powers of $\varepsilon \equiv |1 - 2\alpha|$:

$$c = 3\varepsilon + \frac{9}{10}\varepsilon^3 + \frac{729}{1400}\varepsilon^5 + O(\varepsilon^7)$$

A major difference to the cases $\alpha \leq 1/2$ is the non-vanishing $b(t)$, which means we do not have an arbitrary high “density of layers under the curve $\Phi(y)$ ” and replacing sums by integrals is not exact.

Consequently, to determine y_0 , eq. (5.12) must be replaced by

$$\begin{aligned} t &\stackrel{!}{=} \sum_{h=1}^{\infty} \theta(h, t) \\ &= [t - y_0] + \sum_{h=[t-y_0]+1}^{\infty} \Phi(h - t + y_0) \\ \Leftrightarrow \tau + y_0 &= \frac{\exp(c\tau)}{\exp(c) - 1} , \end{aligned}$$

^dMore precisely, it diverges as $-W_{-1}(\alpha - 1)$, where W_{-1} is a branch of the *Lambert W function* (Corless et al., 1996)

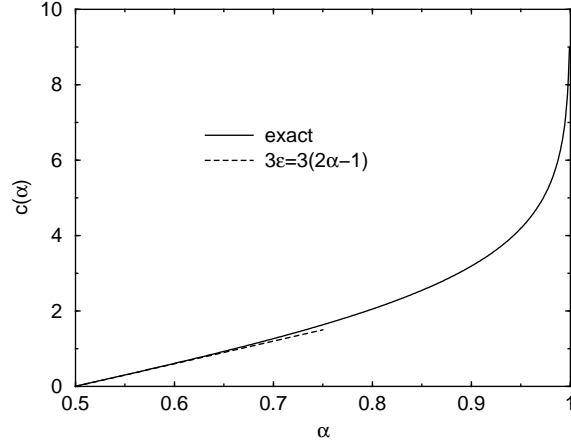


Figure 5.5: The solution to the transcendental equation (5.24) shows a linear behavior at the left boundary and a weak divergence on the right.

where $\tau \equiv t - y_0 - \lfloor t - y_0 \rfloor$ is the time since the most recent completion of a layer. It expresses the solution's periodicity with frequency unity.

Obviously, there is no exact solution y_0 for all $\tau \in [0 \dots 1]$, which means a mismatch between the increase in time and the increase in average height, it vanishes only asymptotically for $c \rightarrow 0$ where $y_0 = 1/c$ holds true.

Another flaw emerges upon calculating the surface width (5.6), namely

$$w^2 = \frac{\exp(c\tau) (\exp(c) - \exp(c\tau) + 1)}{(\exp(c) - 1)^2}, \quad (5.25)$$

which has identical minimal values at the time of layer completion (i.e. $\tau = 0$ and $\tau = 1$) and takes on its maximum at

$$\tau_{\max} = \frac{\ln(\exp(c) + 1) - \ln 2}{c}.$$

However, evaluating eq. (5.25) at these values, we find the oscillation's amplitude to be

$$w^2(\tau_{\max}) - w^2(\tau = 0) = \frac{1}{4},$$

i.e. a value independent of c which is in clear contrast to the numerical results shown in fig. 5.2 on page 95 and fig. 5.7 on page 107.

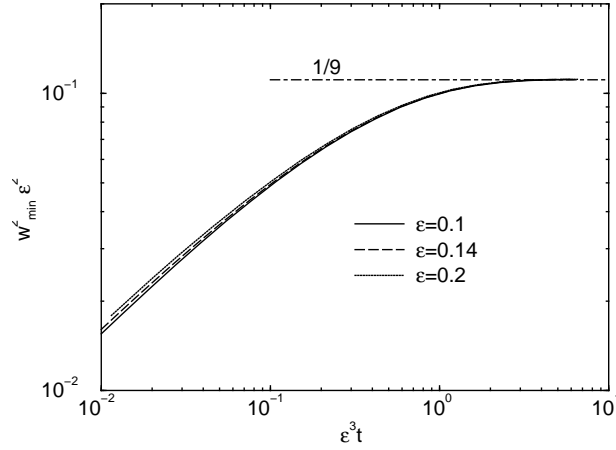


Figure 5.6: The scaling plot confirms the divergence of the stationary oscillation's minimum as $1/\varepsilon^2$ as well as that of the time to reach stationarity as $1/\varepsilon^3$ (with $\varepsilon = |1 - 2\alpha|$).

But at least, eq. (5.25) is correct to leading order, since it yields a minimal value for $\tau = 0$ of

$$\frac{\exp(c)}{(\exp(c) - 1)^2} = c^{-2} - \frac{1}{12} + O(c^2) = \frac{\varepsilon^{-2}}{9} - \frac{3}{20} + O(\varepsilon^2),$$

which is confirmed numerically in fig. 5.6 as well as the scaling of the crossover time again according to eq. (5.22). The latter fact was to be expected, since here applies the same argument as in the case $\alpha < 1/2$.

The shortcomings described above are obviously due to the fact that we neglected again the influence of the bottom layer completely. This we will cure in the following “to first order”. That means, we pretend that the different differential equation for the bottom only affects this layer itself while the higher ones still follow eq. (5.23). More precisely, an amplitude A for the exponential must be allowed, it is no longer fixed to unity. We also absorb the shift y_0 into this amplitude.

That means, after renumbering the system to let number one be the bottom layer also in the asymptotic regime, we have to solve the ODE

$$\frac{d\theta_1}{dt} = (\alpha - 1)\theta_1 - \alpha A \exp(-c \cdot (2 - \tau)) + 1,$$

together with the boundary conditions

$$\theta_1(\tau=0) = \theta_2(\tau=1) = A \exp(-c) \quad (5.26)$$

$$\theta_1(\tau=1) = 1. \quad (5.27)$$

The solution reads

$$\begin{aligned} \theta_1(\tau) = & \frac{1 - \exp(-(1 - \alpha)\tau)}{1 - \alpha} + A \exp(-(1 - \alpha)\tau - c) \\ & + \frac{A\alpha \exp(-2c)}{c + 1 - \alpha} (\exp(-(1 - \alpha)\tau) - \exp(c\tau)) , \end{aligned}$$

wherein A is fixed by the condition (5.27).

Supplied with $\theta_1(\tau)$ as above and $\theta_{h \geq 2} = A \exp(-c(h - \tau))$ the calculation of the width $w^2(\tau)$ is straightforward, but ends up in a rather lengthy expression, which we suppress here. Its leading order is of course again $\varepsilon^{-2}/9$ while its amplitude decreases roughly linear as plotted in fig. 5.7, albeit it does not vanish for $\alpha \rightarrow 1/2$. However, the actual value

$$w_{\alpha=1/2}^2(\tau_{\max}) - w_{\alpha=1/2}^2(0) = 0.0236465258$$

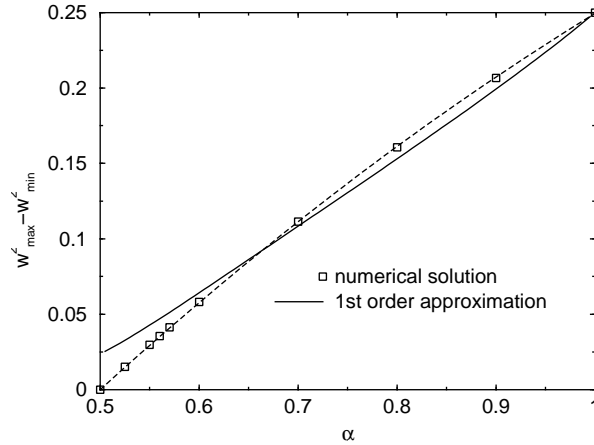


Figure 5.7: The stationary oscillation's amplitude vanishes linearly for $\alpha \rightarrow 1/2$. The dashed line is just a fit to guide the eye for better comparison to the 1st order approximation. A constant $1/4$ would correspond to the zeroth order approximation.

in this approximation is already about ten times smaller than the zeroth order result $1/4$ of eq. (5.25). Moreover the whole amplitude as a function of α agrees rather well with the numerically obtained data. In principle, this improvement could be extended systematically by solving the coupled system for $\theta_1(t)$ and $\theta_2(t)$, assuming the exponential solution to hold true from layer 3 onward and so on. However, the solution's complexity would exceed all bounds without getting any further insight.

5.1.7 Summary

Let's summarize the behavior of $w(t)$ in the vicinity of $\alpha = 1/2$, where $\varepsilon = |1 - 2\alpha|$ is small:

α	$w^2(t)$	profile ^e shape
$\lesssim 1/2$	$\varepsilon^{-2} W_{<}(\varepsilon^3 t) + \varepsilon t$	erfc –like
$= 1/2$	$0.4170729 t^{2/3}$	'Ai –like
$\gtrsim 1/2$	$\varepsilon^{-2} W_{>}(\varepsilon^3 t) + \varepsilon \omega(t)$	exponential decay

The function $\omega(t)$, describing the oscillations, has a fixed amplitude (≈ 0.3 as read off from fig. 5.7 on the page before) and frequency unity; the scaling functions $W_{\leq}(x)$ finally approach a constant for large values x and exhibit a power law $x^{2/3}$ for small ones.

5.2 Step functions

The non-trivial scaling exponent $\beta = 1/3$ for a constant $\alpha = 1/2$ is a promising basis for extensions of this model, especially since distributing the incoming particles equally among two concerned “steps” corresponds exactly to the one-dimensional case in the absence of Schwoebel barriers, for which the exponent according to the cKPZ equation coincides. The missing feature to achieve damped layer-by-layer growth seems to be the low coverage regime for each layer, where there are no nucleations on top of it yet. The suggesting generalization of the coefficients α is therefore

$$\alpha_k = 1 - \Theta(\theta_k - \theta_{\text{crit}})/2, \quad (5.29)$$

^eof incomplete layers, i.e. $\Phi(y > 0)$

where the critical coverage θ_{crit} depicts the onset of new nucleations, i.e. $\theta_n \leq \theta_{\text{crit}} \Rightarrow \theta_{k>n} = 0$. (Even without this nucleation argument, the pathological property of the model to produce an infinite number of layers with an arbitrary small coverage calls for a reintroduction of a lateral lattice constant which would take on the rôle of θ_{crit} .)

Unfortunately, this extension does not lead to the desired result as can be seen even without a detailed analytical treatment: The ODE for $\alpha = 1/2$,

$$\dot{\theta}_k = \frac{\theta_{k-1} - \theta_{k+1}}{2},$$

allows also for the homogeneous solution

$$\dot{\theta}_k = c$$

with some constant $c < 1$, i.e. a linear profile having a slope c .

In section 5.1.4, the boundary conditions prohibited such a homogeneous cascade, but now, in the presence of a “cut-off” at a layer k with $\theta_k \leq \theta_{\text{crit}}$, an essentially constant inflow to the cascade is possible: During its growth from zero to θ_{crit} the top terrace provides an average inflow of the order of θ_{crit} itself, i.e. we expect

$$c \sim \theta_{\text{crit}}. \quad (5.30)$$

Hence, with a linear profile as the (periodic) stationary regime, the number n of active layers is given by $nc = 1$, or, expressed as the saturated surface width and using relation (5.30):

$$w_\infty^2 \propto n^2 = \frac{1}{c^2} \sim \frac{1}{\theta_{\text{crit}}^2}$$

This behavior is verified in fig. 5.8 on the following page in the asymptotic sense $\theta_{\text{crit}} \rightarrow 0$, it also shows the transient time to reach this saturation value being $\propto \theta_{\text{crit}}^{-3}$. The latter was to be expected as it is the time of the unperturbed system^f, possessing a $\beta = 1/3$, to reach a fixed value $\propto \theta_{\text{crit}}^{-3}$.

If we now regard θ_{crit} as a lateral lattice constant, like mentioned above, then obviously the system size of $\theta = 1$ corresponds to $L = 1/\theta_{\text{crit}}$ lattice constants and hence the saturation time for w^2 scales like L^3 . It is tempting to interpret this as a dynamical exponent of $z = 3$, but because of the lack of a meaningful lateral correlation length this is merely a view of analogy.

^fThe perturbation can be regarded as a “cut-off” in the tail of $'\text{Ai}(y)$.

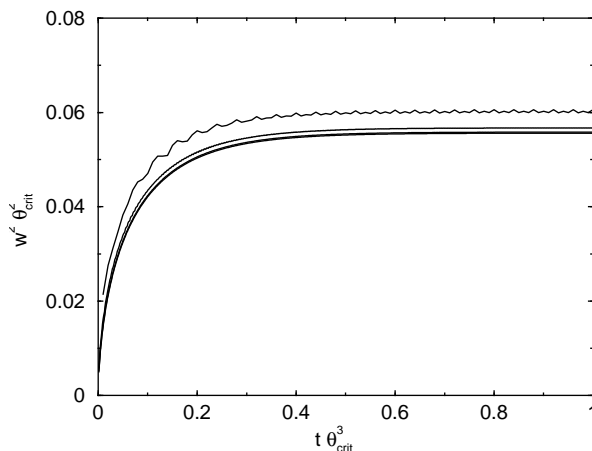


Figure 5.8: The saturation value $w_{\infty}^2 \propto \theta_{\text{crit}}^{-2}$ reached within a time $\propto \theta_{\text{crit}}^{-3}$. The coverage θ_{crit} ($= 1/5, 1/10, 1/20, 1/40$ from top to bottom) is the coverage where the interlayer transport happens no longer unhindered but is reduced to 50% according to eq. (5.29).

In other words: Unfortunately, the ever lasting $w \propto t^{1/3}$ in the previous section was merely caused by the model’s peculiarity of growing arbitrarily low covered layers on top of each other. When introducing some more realistic features, we are bound to a finite asymptotic width (unless we introduce an “uphill” $\alpha < 1/2$, which causes Poisson-like growth). The reason for this failure to mimic kinetic roughening and its damping effect on layer-by-layer growth lies in the mean field model’s inherent absence of noise, whose importance we have already seen in section 3.1.2.

For the scenario of unstable growth, the model can be of better use, though. Here a drastic step

$$\alpha_k = 1 - \Theta(\theta_k - \theta_{\text{crit}}),$$

represents the idealization of an infinite Schwoebel barrier, active only from a certain “island size” θ_{crit} onward. This should be a basic model for the “wedding cakes” with a flat top (Kallabis, 1997; Krug et al., 2000).

Chapter 6

Debunching

6.1 Inverted behavior

When investigating the relation between the growth parameter D/F and the lifetime of layer-by-layer growth in the chapters 3 and 4, we found that a higher D/F improves smooth growth, as is the intuitive expectation and as it was found in STM investigations (Stroscio et al., 1993) (albeit not exploited quantitatively). The situation of an opposite behavior occurred upon evaluating data of an experiment with Fe/Fe(001) on Cr(001) where systematic measurements concerning the number of RHEED-oscillations have been performed (Theis-Bröhl et al., 1998). Indeed, a powerlaw could be found, but the number of oscillations increased with growing deposition rate while they decreased with growing temperature. An attempt to explain this finding qualitatively has already been made in (Theis-Bröhl et al., 1998); here will have a closer, more quantitative inspection.

The underlying idea is the situation of a surface undergone a *step bunching instability*. In this instability, an effect opposite to the step-flow stabilizing Schwoebel barrier discussed in section 4.2 is operative: Larger terraces grow while smaller ones shrink further. Possible physical origins of this instability are inverse Schwoebel barriers, impurities (van der Eerden and Müller-Krumbhaar, 1986), strain (Asaro and Tiller, 1972; Grinfeld, 1986; Duport et al., 1995a; Duport et al., 1995b) or a direct influence of the DC current along the surface (originally used to control the sample's temperature) (Latyshev et al., 1989; Latyshev et al., 1998). Moreover, the resulting structure – often called *macro steps* – can have developed due to equilibration in the case the vicinal surface is not thermodynamically stable.

6.2 An idealized step bunch

We consider the idealized situation of the evolution of an infinitely high step bunch, where the cause for the bunching is no longer present. Under normal growth the bunch will dissolve and finally “flood” the terrace next to it where layer-by-layer growth took place before as sketched in fig. 6.1 on the next page. That is true even in the absence of the step-flow favoring Schwoebel barriers: In two dimensions the steps fluctuate and thus establish an entropic repulsion (Gruber and Mullins, 1967; Pimpinelli and Villain, 1999), but also in one dimension they cannot interpenetrate each other and are subjected to single-file diffusion (Levitt, 1973).

Along the lines of chapters 3 and 4, we are interested in the transient, the “unfurling” of the bunch, while for an already established step train, the dynamics are well studied (e.g. (Misbah and Pierre-Louis, 1996; Pimpinelli and Villain, 1999)).

In the simplest, one-dimensional picture (which applies to $d > 1$ as well, provided translational invariance along the steps), the lowest terrace gathers a number of particles of order Fl_D per unit time from the left (assuming the macro step’s orientation according to fig. 6.1); hence its velocity v is of the order Fal_D and the time needed to span a macro terrace of length L would

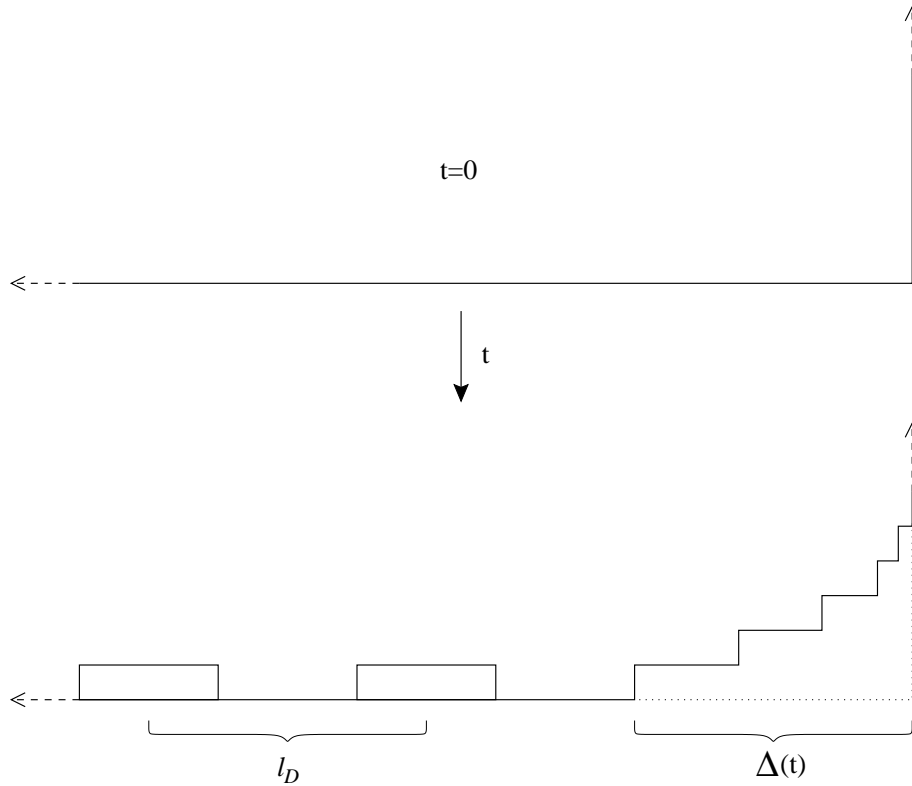


Figure 6.1: Debunching of a macro step. From the initial configuration of an infinitely high step, the lowest terraces unfurl in a telescope-like manner. When the bunch spans the whole macro terrace, no layer-by-layer growth is visible anymore.

be

$$\frac{t}{t_{\text{ML}}} = \frac{L}{vt_{\text{ML}}} \sim \frac{L}{l_D}. \quad (6.1)$$

This is quite promising, since indeed the extinction time of any oscillations *decreases* with growing l_D , even if in this case the damping is not due to the macro terrace becoming rough (like in chapters 3 and 4) but by providing a smaller and smaller contribution to e.g. the signal of the kinematic intensity.

Unfortunately, in this simple picture two features are overlooked: First, the steps advance by receiving material also from the right unless there are strong Schwoebel barriers present. Second and more important, upon completing a layer on the macro terrace, the existence of the bunch's lowest terrace ceases and the next higher terrace takes over.

6.2.1 Deterministic modeling

Let's first have a look at the consequences in a deterministic, simplified model. A flight of steps with positions x_k is terminated by an island, as sketched in fig. 6.2. Expressed in natural units, the dynamics of a step,

$$-\partial_t x_k = \underbrace{\frac{x_k - x_{k-1}}{2}}_{\text{lower terrace}} + \underbrace{\frac{x_{k+1} - x_k}{2}}_{\text{upper terrace}} = \frac{x_{k+1} - x_{k-1}}{2},$$

coincides with the case $\alpha = 1/2$ in section 5.1.4. This is not by chance, since the step bunch is nothing but a right aligned version of the stack in fig. 5.1 on page 92 (the negative sign here indicates the steps' movement to the left).

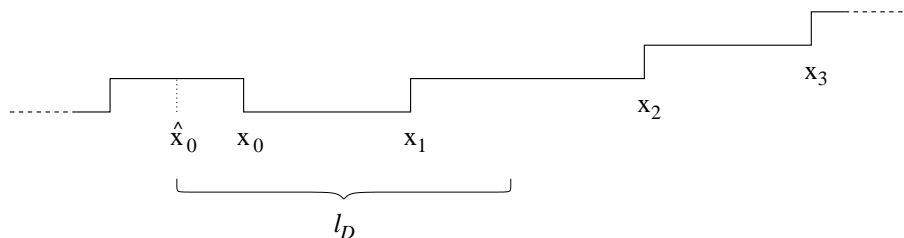


Figure 6.2: In the deterministic model, a nucleation event happens as soon as the gap between x_0 and x_1 closes. The nucleation's location is at \hat{x}_0 , that is at a distance l_D from the current x_2 (which then becomes the new x_1).

The boundary condition – here the growth of the terminating island – is slightly different, though:

$$\partial_t x_0 = \frac{x_1 - x_0}{2} + x_0 - \hat{x}_0 = \frac{x_1 + x_0}{2} - \hat{x}_0$$

Apart from the different sign, $\theta_0 \equiv 1$ in eq. (5.2) is replaced by \hat{x}_0 , the position of the island's nucleation. This is not fixed but (by virtue of our deterministic model) the nucleation is always located at a distance l_D in front of x_2 just when x_0 and x_1 become equal. At this time of the gap closing, the nucleation provides the new x_0 while the steps in the bunch are renumbered (x_k becoming the new x_{k-1}).

fig. 6.3 shows the temporal evolution of $x_1(t)$ from the initial condition $x_k(t = 0) = -l_D \delta_{k,0}$ within this model. Its sawtooth shape reflects the periodical vanishing of the lowest layer upon confluence with the island. The upper envelope grows according to a powerlaw $t^{0.42}$ showing that already the two ingredients mentioned above are enough to produce a nontrivial exponent. Unfortunately it does not agree with the following results.

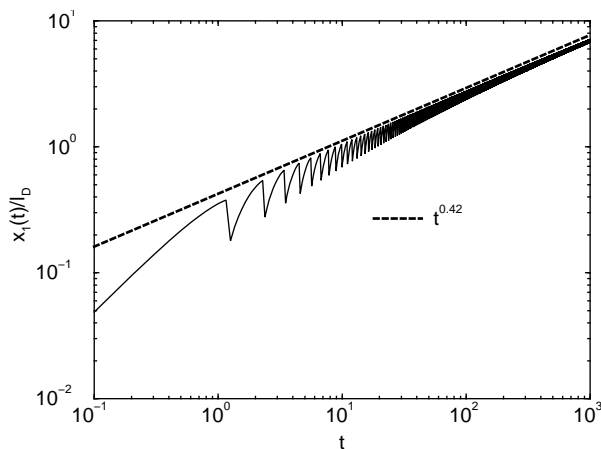


Figure 6.3: The time evolution of x_1 (being identical to the bunch width Δ) in the deterministic model, numerically solved. The oscillation is due to the recurring annihilation of island edge x_0 and step bunch front x_1 (cf. fig. 6.2 on the page before). The upper envelope obeys a powerlaw.

6.2.2 Numerical results in one dimension

Simulations of a one-dimensional system of size $L = 1600$ were performed for $D/F = 10^4 \dots 10^8$. The corresponding data in fig. 6.4 show a $t^{1/3}$ -progression of the bunch width Δ , which was measured by descending the step bunch until the encounter with an upward step. The validity of this method is proven in fig. 6.5 on the next page, where additionally the shape of the resulting bunch $x(h)$ is found to be exponential. Moreover, fig. 6.4 confirms the proportionality $\Delta \propto l_D$ by means of a data collapse.

Hence, we conclude for the damping time due to step debunching in one dimension:

$$\frac{t_{\text{db}}}{t_{\text{ML}}} \sim \left(\frac{L}{l_D}\right)^3 \propto \left(\frac{D}{F}\right)^{-3\gamma}$$

In other words, the decrease of the damping time with growing D/F is even more drastic than according to the simple picture leading to formula (6.1).

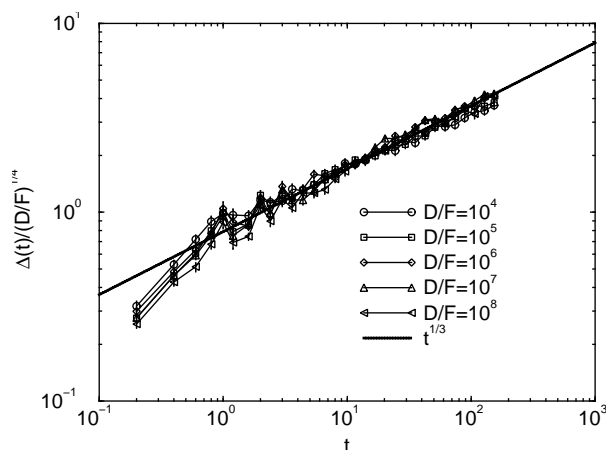


Figure 6.4: Temporal evolution of the step bunch's width in $d = 1$. The rescaling of the ordinate verifies $\Delta \propto l_D$.

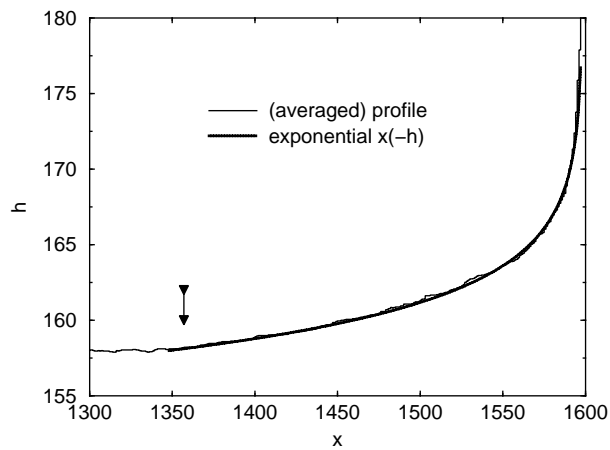


Figure 6.5: The step bunch after the deposition of 160 mono-layers, averaged over 200 simulation runs. The arrow marks the end of the step according to the measurements shown in fig. 6.4 on the preceding page. The fit to the profile reveals an exponential decrease of the steps' distance to the right border with height.

6.2.3 Numerical results in two dimensions

In chapter 3 and 4, we experienced the two dimensional system to behave substantially different compared to the case $d = 1$, which is true for the dissolving step bunch as well. Not only is in fig. 6.6 the width of the bunch found to follow the powerlaw $\Delta \propto t^{1/4}$, which is even slower than the one-dimensional dynamics. Also, as the rescaling of the ordinate demonstrates, the bunch's inherent length scale is proportional to $(D/F)^{1/4}$ again, which in two dimensions rules out l_D and brings in l_0 (cf. eq. (2.5)); this situation resembles the observation made in section 3.6.

Therefore, the time for spanning a macro terrace of length L , inferred from fig. 6.6, is

$$\frac{t_{\text{db}}}{t_{\text{ML}}} \sim \left(\frac{L}{l_0}\right)^4 \propto \frac{F}{D}, \quad (6.2)$$

in two dimensions.

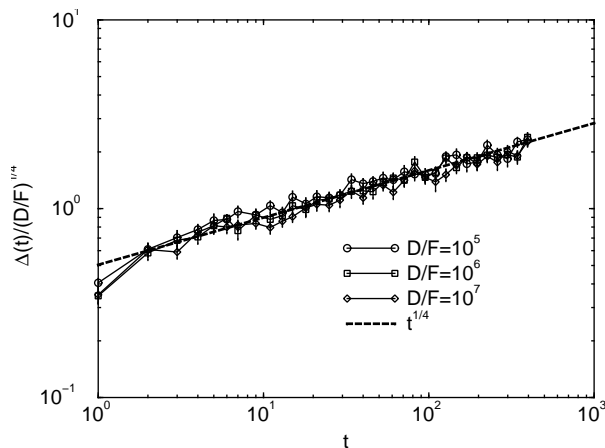


Figure 6.6: The width of the bunch in $d = 2$, rescaled by $l_0 \propto (D/F)^{1/4}$. Δ was measured as the width of the nucleation-free zone, which is justified in fig. 6.7 on the next page.

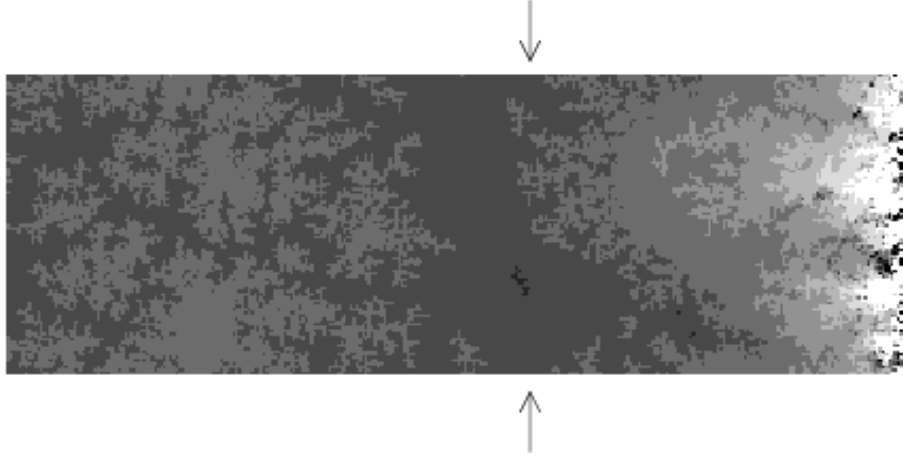


Figure 6.7: Surface configuration with the bunch at the right boundary after the deposition of 400 mono-layers for $D/F = 10^7$. Eight different height levels are displayed (black $\hat{=}$ lowest, white $\hat{=}$ highest). Height values below or above these levels are clipped black and white respectively. The arrows indicate the position according to fig. 6.6 on the preceding page (Δ measured from the right); the region to the right is the nucleation-free zone.

6.3 Discussion

From the equations (6.2) and (2.2) it follows that

$$\ln(t_{\text{db}}/t_{\text{ML}}) = c - \frac{E_D}{k_B T},$$

where the offset c contains the deposition rate F . If we identify $t_{\text{db}}/t_{\text{ML}}$ with the number of observable oscillations n , then the experimental result from (Theis-Bröhl et al., 1998)

$$\ln(n) \approx \text{const} - \frac{970 \text{ K}}{T} \quad (6.3)$$

(for fixed F) can be used to determine E_D . This yields

$$k_B 970 \text{ K} \approx 0.084 \text{ eV}$$

which is clearly too low for the activation barrier for Fe/Fe(100), which was found experimentally to be $E_D \approx 0.45 \text{ eV}$ (Stroscio et al., 1993). In fact, this

value agrees much better with the naive picture (6.1), which corresponds to

$$\ln(t_{\text{db}}/t_{\text{ML}}) = c' - \frac{\gamma E_D}{k_B T},$$

whereupon the interpretation of result (6.3) changes into $0.084 \text{ eV} = \gamma E_D$ or

$$E_D = \frac{0.084 \text{ eV}}{\gamma} \approx 0.5 \text{ eV}.$$

Regarding this discrepancy, we have to keep in mind the rather artificial boundary conditions of our model. In a real situation, the bunch of finite height also receives material from the upper macro terrace and possibly even directly from the beam (as the velocity of all impinging particles assumed to be exactly parallel to the macro step is a strong idealization as well). This is a feature hardly to accommodate within the SOS-model, since there the vertical diffusion constant is infinity and island formation “at the wall” is prohibited.

Finally, the lack of edge diffusion leads to an extremely ramified height configuration in the very vicinity of the step as can be seen from the many isolated black sites in fig. 6.7 on the page before. Here, the turning away from the too simplified picture of irreversible accretion upon gaining one lateral bond seems to be indispensable.

Chapter 7

Toy Models

7.1 Common features

In this chapter, we will deviate from the lines of the previous ones to a certain extent and consider several one-dimensional growth models that do not all relate to molecular beam epitaxy. Instead their common feature is the degree of simplicity in the growth rules (“toy models”), in fact they do not even include a tunable parameter at all. To investigate their behavior with respect to layer-by-layer growth, we have to introduce a parameter m which controls the strength of the shot noise, a technique described now.

7.1.1 Coarse graining and noise reduction

A result from chapter 3, namely the existence of a characteristic distance \tilde{l} , below which terraces remain flat, means that the shot noise is effectively averaged out over areas smaller than \tilde{l}^d . The small scale diffusive dynamics responsible for this averaging is not necessarily interesting in the context of kinetic roughening. Without specifying it any further one may try to model the growth kinetics directly on larger scales. The coarse grained modelling of growth processes (see section 2.5.4 and (Wolf, 1995)) as such an approach is a special refinement of the more general technique called noise reduction (Szép et al., 1985; Tang, 1985).

In noise reduced growth models the lattice consists of cells which can contain up to m particles and correspond in the picture of coarse graining to a volume $\ell^d \times a_{\perp}$. The fast kinetics (of whatever origin for each model), which guarantees that in a partially filled cell all particles are arranged within a single atomic layer, is not specified and thus not implemented explicitly. The growth rules of the model only determine the transfer of a mobile particle from one cell to an adjacent one. In the simple cases considered in this chapter these rules only depend on whether a cell is full or still can receive particles, but not on the degree to which a partially filled cell is occupied.

The technical realisation is done by installing a counter in each cell to register the arrival of a particle. Only when m of them are collected, that cell is treated as occupied, which has consequences on its neighbourhood depending on the model’s rules. As shown later the strength of the shot noise will decrease as m^{-1} using this technique. This explains why it is called noise reduction.

7.2 Simulated models

7.2.1 Eden growth

The Eden model, already introduced in 1958 (Eden, 1958) to describe growth of cell colonies, exists in three different variants (Jullien and Botet, 1985). Though in all three cases the growth of a cluster takes place by occupying a perimeter site (that is an empty site next to an occupied one) chosen at random, the particular choice differs:

- A All free perimeter sites have the same probability to be chosen. The chosen site is then occupied.
- B All “bonds” connecting a free perimeter site to the cluster have the same probability to be chosen. The site belonging to the chosen bond is occupied.
- C All cluster sites which have neighbouring free perimeter sites have equal probability to be chosen. Among the free neighbours of the chosen cluster site, the one to be occupied is again chosen with equal probability. This version will not be discussed in this article.

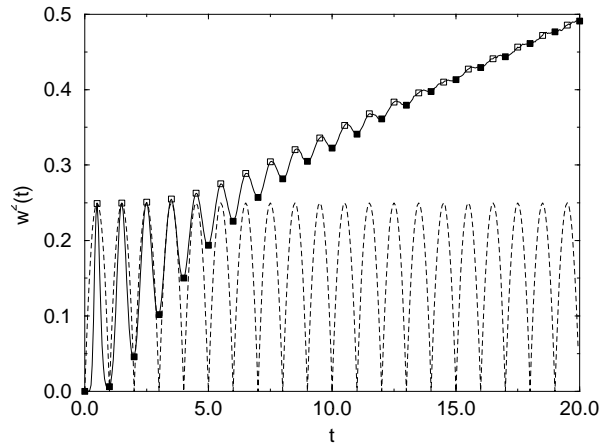


Figure 7.1: Oscillations of the surface width w^2 for the Eden model (version A) with a noise reduction parameter $m = 32$. Filled symbols emphasize integer times (in monolayers), open symbols half-integer times. The dashed line shows perfect layer-by-layer growth: The oscillations persist.

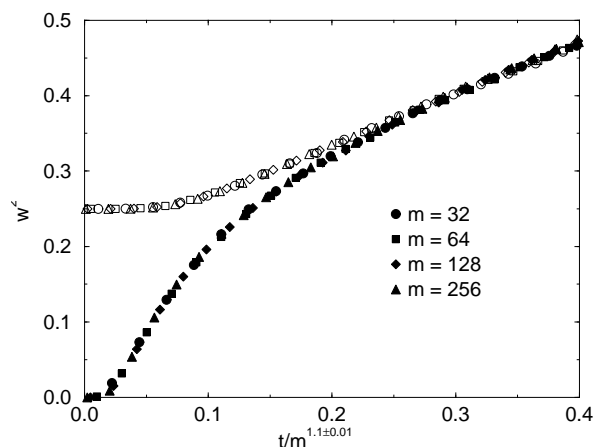


Figure 7.2: Data collapse with four different noise reduction parameters showing the damping time of the Eden model (version A). Filled symbols correspond to integer times, open symbols to half-integer times. For the uncertainty ± 0.01 cf. table 7.1.

In 1987, Kertész and Wolf (Kertész and Wolf, 1988) applied the noise reduction technique to version A and C and found that it improves the scaling behaviour and caused layer-by-layer growth. For the latter they found a linear relationship between the damping time \tilde{t} and the noise reduction parameter m : $\tilde{t} \propto m$.

In the simulations of version A and B presented here, a power law dependence $\tilde{t} \propto m^\mu$ is confirmed. The exponents were extracted by calculating $\mu(m) \equiv \log_2 \tilde{t}(m) - \log_2 \tilde{t}(m/2)$. The result for version A is $\mu(m) = 1.1 + \epsilon_A(m)$, where the small deviations ϵ are given in table 7.1 on the following page. The corresponding data collapse is shown in fig. 7.2. To point out the sensitivity of such a data collapse, a plot with $\mu = 1.0$ is shown in fig. 7.3 on the following page. Similarly we obtain for version B $\mu(m) = 1.6 + \epsilon_B(m)$ (cf. fig. 7.4 on page 126).

An interesting fact is that version B exhibits a different damping exponent ($\mu = 1.6 \pm 0.02$ as shown in fig. 7.4 on page 126) than version A and C though their asymptotic scaling behaviour is described by the same roughness exponent ζ and dynamic exponent z as version B, namely those of the KPZ universality class (Jullien and Botet, 1985; Zabolitzky and Stauffer, 1986). This rules out the universal validity of a scaling relation between the damping

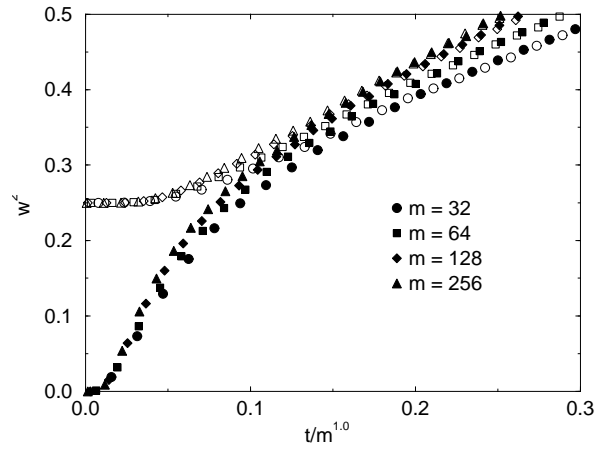


Figure 7.3: A linear rescaling shows that the damping exponent for version A is not simply $\mu = 1$.

exponent and the scaling exponents, as for example the relation

$$\mu = \frac{z}{2\zeta},$$

first found for the noise reduced *single step model* (Tang, 1993).

In other words, details which do not influence the universality class may influence the scaling of the damping time with m .

m	ϵ_A	ϵ_B
16		0.008
32		0.013
64	0.00625	-0.008
128	0.00502	
256	-0.00104	

Table 7.1: The corrections to the exponent μ for the Eden models.

7.2.2 Models related to MBE

As discussed in section 2.3, one of the basic assumptions for ideal MBE is the lack of desorption of particles back into the vacuum, as well as the absence of

holes and overhangs, the “solid on solid” (SOS) restriction. The additional feature of surface diffusion, reduces in the case of the toy models described below to a relaxation step just after the deposition which gives rise to the common name *limited mobility model*.

Edwards-Wilkinson model

In this lattice model suggested by Family (Family, 1986) particles are deposited one by one at randomly chosen sites and move to the lowest nearest neighbour site. As already said in section 2.6.3, possible microscopic reasons for this downward motion in the context of molecular beam epitaxy are funnelling, kick-out at terrace edges (Evans, 1991; Vvedensky et al., 1993), and the influence of surfactants (see section 7.4).

Fig. 7.5 on the next page shows the growth oscillations of the noise reduced EW model. The rescaling of time gives a damping exponent of $\mu = 2.05 \pm 0.05$.

Wolf-Villain model

In this model (Wolf and Villain, 1990), particles do not move to the lowest nearest neighbour site but to the one with the largest number of bonds (see

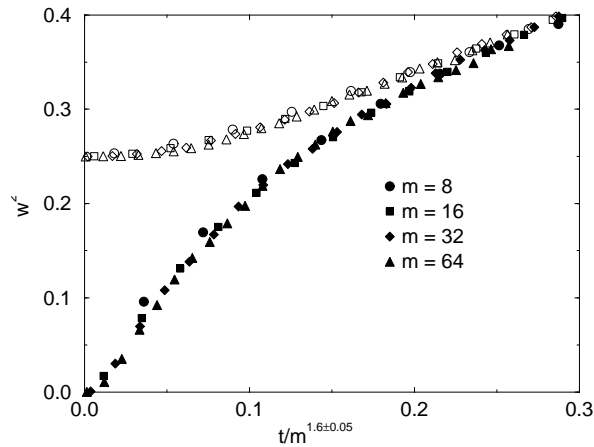


Figure 7.4: Data collapse with four different noise reduction parameters showing the damping time of the Eden model (version B). Filled symbols correspond to integer times, open symbols to half-integer times. For the uncertainty ± 0.02 cf. table 7.1.

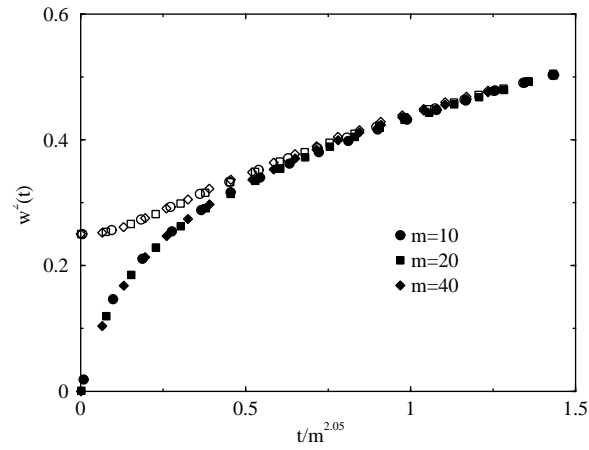


Figure 7.5: Data collapse with three different noise reduction parameters showing the damping time of the EW model (random deposition with surface relaxation). Filled symbols correspond to integer times, open symbols to half-integer times.

fig. 7.8 on page 130). The question of the universality class for the WV model has been debated for quite a long time, until after several strong hints

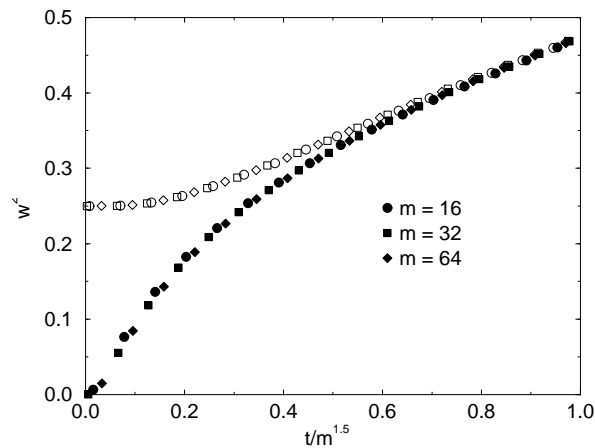


Figure 7.6: Data collapse with three different noise reduction parameters showing the damping time of the WV model. Filled symbols correspond to integer times, open symbols to half-integer times (in units of the mono-layer time).

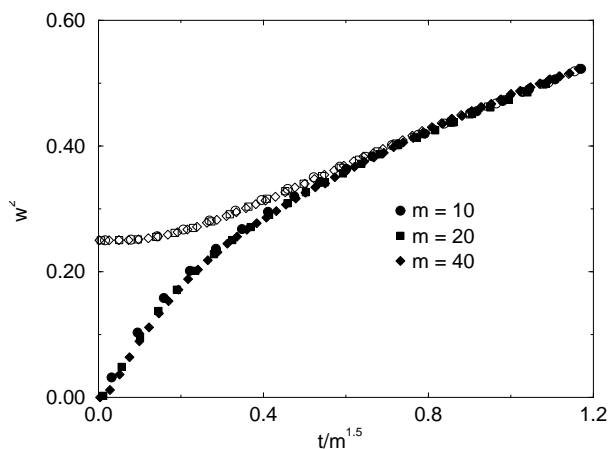


Figure 7.7: Data collapse with three different noise reduction parameters showing the damping time of the “1+”-model of Das Sarma and Tamborena. Filled symbols correspond to integer times, open symbols to half-integer times.

(Krug et al., 1993; Park et al., 1994; Šmilauer and Kotrla, 1994; Kotrla and Šmilauer, 1996; Krug, 1997) and finally explicit observation by means of this very noise reduction scheme (Punyindu and Sarma, 1998) the decision in favor of the EW class was settled. But since its downhill current is very weak, the corresponding scaling exponents really become visible only asymptotically.

Concerning its transient behavior, fig. 7.6 on the page before shows its damping exponent to be $\mu = 1.5 \pm 0.05$.

“1+”-model

This model (Sarma and Tamborena, 1991) is very similar to the WV model with surface dimension $d = 1$. However, sites offering 3 or 2 bonds are not distinguished, see fig. 7.8 on page 130. Though the diffusion rules differ only slightly from the WV rules, the “1+”-model behaves differently, especially regarding the surface current and step-height distribution (cf. (Krug, 1994; Sarma and Punyindu, 1997; Krug, 1997)), and only the usage of the noise reduction technique revealed its belonging to the cKPZ class (Punyindu and Sarma, 1998). Nevertheless, the damping exponent is the same as for the WV model ($\mu = 1.5 \pm 0.05$), as shown in fig. 7.7. This is in a way a situation

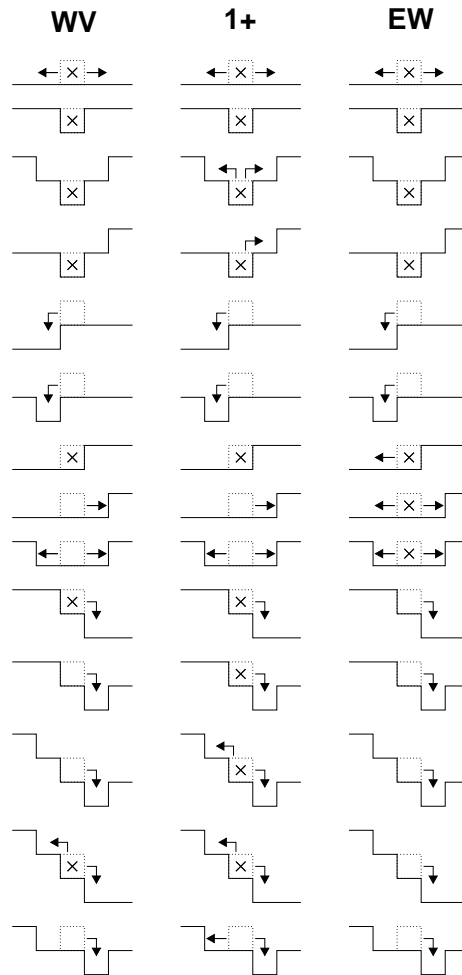


Figure 7.8: The most important situations, showing the differences in the rules for the WV, “1+” (see page 126) and EW model, respectively. The “x” denotes the particle remaining at its location of deposition. Whenever there are two or three possibilities one of them is chosen with probability 1/2 or 1/3 respectively. It should be noted that in all three models the rules were slightly modified: In a tie situation involving the deposition site, a random choice is made among the best, whereas in the original models the deposition site was taken.

opposite to the one of the Eden models where the universality class was identical while the damping exponents were not. This points out once more that these two properties can be quite independent of each other.

7.3 Analytical results

The simulations show that not only the envelopes of the damped oscillations but also the later time evolution scales with the same characteristic time \tilde{t} . Hence, the power law dependence of the number of oscillations on the noise reduction parameter m can be investigated by a dimensional analysis of the m -dependent parameters of the continuum equation which governs the surface kinetics in the onset of kinetic roughening regime, when the oscillations are no longer observable. This of course requires that a continuum description for the regime of early times is known.

First we have to consider the strength of the noise η , which represents the fluctuations of the deposition rate around its average value F and which is the usual shot noise (2.33). The other sources of randomness in the toy models we simulated are related to tie-situations in the microscopic kinetics, and are neglected in the continuum descriptions.

As we learned in section 2.6.1, the noise strength \mathcal{F} is related to the deposition rate F , even if the latter is removed from the growth by a transformation to the comoving frame ($h \rightarrow h - a_{\perp}t/t_{\text{ML}}$).

Without noise reduction, we have according to eq. (2.30)

$$\mathcal{F} = F \Omega^2 ,$$

but when noise reduction is applied, this is no longer true; instead we get an m -dependence of \mathcal{F} (Kertész and Wolf, 1988)

$$\mathcal{F} \propto 1/m . \tag{7.1}$$

The reason is that during the deposition of t mono-layers each cell receives $mt \pm \sqrt{mt}$ particles which corresponds to height fluctuations of $a_{\perp} \sqrt{mt}/m$. From the integration of η like eq. (2.32) we know that this should be $\sqrt{\mathcal{F}t/a^d}$, which proves eq. (7.1).

From now on we only discuss special cases of the KPZ-equation (2.52) to treat the Eden models and the EW model (special case $\lambda = 0$), i.e. we have to deal with the parameters $\nu(m)$, $\lambda(m)$ and $\mathcal{F}(m)$. To handle the WV model and the “1+” model, we would need a continuum description for intermediate times (larger but not much larger than \tilde{t}), the asymptotic ones (Punyindu and Sarma, 1998) are of no help, unfortunately.

It is clear that for random deposition, i.e. in the absence of correlations between neighbouring cells, layer-by-layer growth is still possible, because of the strong correlations within a cell: All m particles inside a cell are

accommodated within the same layer, before the next layer can start (Bren-
del, 1994). The oscillations end when the typical height fluctuations equals
about one lattice constant, i.e. $\mathcal{F}\tilde{t}/a^d \approx a_\perp$. Thus, for random deposition,
one obtains (Wolf and Kertész, 1989)

$$\tilde{t} \propto m. \quad (7.2)$$

7.3.1 Dimensional arguments

Let us reformulate this argument in a slightly different way, which will turn
out to be useful in more general situations: Let \tilde{t} be the time when the typical
height fluctuations \tilde{h} have reached the size of the vertical lattice constant a_\perp .
At this time \tilde{t} the layer coherence will be maintained up to the characteristic
length \tilde{l} , which in the case of random deposition is the lateral lattice constant
 a , but as we know from chapter 3, it can be bigger if communication between
cells is allowed. Just as there in eq. (3.16), we have

$$\mathcal{F} \sim \frac{\tilde{l}^d}{\tilde{t}} a_\perp^2, \quad (7.3)$$

Using (7.1) and solving for \tilde{t} , one obtains (7.2).

Now let us look at the EW-model. Here, correlations can spread among
neighbouring cells. The only new parameter entering the continuum descrip-
tion is ν . The corresponding dimensional argument yields

$$\nu \sim \frac{\tilde{l}^2}{\tilde{t}}. \quad (7.4)$$

Solving (7.3) and (7.4) for \tilde{t} and \tilde{l} for $d = 1$ gives

$$\tilde{t} \sim \frac{\nu}{\mathcal{F}^2} a_\perp^4, \quad \tilde{l} \sim \frac{\nu}{\mathcal{F}} a_\perp^2. \quad (7.5)$$

In section 7.3.3 we shall show that in the EW-model ν is m -independent
for not too small m . Together with (7.1) and (7.5) this implies

$$\tilde{t} \propto m^2, \quad \tilde{l} \propto m,$$

in very good agreement with our simulation results for \tilde{t} .

Now let us turn to the Eden model: For the “full” KPZ equation (i.e.
 $\lambda \neq 0$) we have to take the renormalisation of the coefficients ν and \mathcal{F} into

account; λ is not renormalised (Kardar et al., 1986). Fortunately, in $d = 1$ (Nattermann and Tang, 1992), the combination \mathcal{F}/ν is also not renormalised, which enables us to do the dimensional analysis in the same way as above. This leads to

$$\frac{\mathcal{F}}{\nu} \sim \frac{a_{\perp}^2}{\tilde{l}}, \quad \lambda \sim \frac{\tilde{l}^2}{a_{\perp} \tilde{t}}$$

or

$$\tilde{t} \sim \frac{\nu^2}{\mathcal{F}^2 \lambda} a_{\perp}^3, \quad \tilde{l} \sim \frac{\nu}{\mathcal{F}} a_{\perp}^2.$$

While (7.1) still holds true, we do not know the m -dependence of ν and λ in the Eden model. Assuming the power laws

$$\nu \propto m^{e_{\nu}}, \quad \lambda \propto m^{e_{\lambda}}$$

we arrive at

$$\tilde{t} \propto m^{2e_{\nu}-e_{\lambda}+2}, \quad \tilde{l} \propto m^{e_{\nu}+1}. \quad (7.6)$$

As we learned in section 2.6.2, the invariance of the KPZ equation under the tilt transformation allows for the explicit measurement of the parameter λ : The excess velocity of an inclined surafe depends on the tilt as

$$v(|\nabla h|) - v(0) = \frac{\lambda}{4} |\nabla h|^2$$

Then a variation of m allows for the determination of the exponent e_{λ} . Fig. 7.9 on the following page shows that λ varies in deed as a function of m according to a power law. Using $e_{\nu} = \mu/2 + e_{\lambda}/2 - 1$ (cf. eq. (7.6)) and the numerical results for μ , also e_{ν} can be predicted. The results are shown in table 7.2. In the next section (7.3.2), we will have another estimate for e_{ν} .

For version A, the signs of the exponents e_{λ} and e_{ν} can be understood in the following way: Consider a regular surface with a global tilt s , i.e. due to the discreteness a step train of terrace size $\ell = a_{\perp}/|s|$. If all steps are at least

version	e_{λ}	e_{ν}
A	-0.72±0.01	-0.81±0.01
B	0.42±0.01	0.01±0.015

Table 7.2: The exponents e_{λ} and e_{ν} for the Eden models.

two lattice constants apart (i.e. $\ell \geq 2a$), there are three types of growth sites: The lower site next to a step is called kink site and the upper one edge site; all the others are terrace sites. Now we apply the growth according to the Eden rules in the noise free limit (i.e. $m \rightarrow \infty$). In the absence of noise, no steps higher than two lattice constants, no overhangs and no holes can emerge. Thus, in version A each site has the same local growth velocity. Therefore $\partial_t h(x, t)$ does not depend on the slope s . In fact it is totally independent of the surface configuration and (2.52) reduces to the trivial equation

$$\partial_t h = \frac{a_{\perp}}{t_{\text{ML}}},$$

i.e. $\nu = \lambda = \mathcal{F} = 0$, in accordance with negative exponents e_{ν} and e_{λ} .

In version B, according to the rules, the kink sites have twice the local growth velocity as edge and terrace sites, and hence they provide an excess velocity which is proportional to their density $|s|/a_{\perp}$, so that (2.52) becomes

$$\partial_t h = \frac{a_{\perp}}{t_{\text{ML}}} + \frac{a}{t_{\text{ML}}} |\nabla h|.$$

For large but finite m the cusp in $a/t_{\text{ML}}|\nabla h|$ will be rounded and can be approximated by a parabolic part $\lambda(\nabla h)^2 + a^2/(4t_{\text{ML}}^2\lambda)$ for $|\nabla h| \leq a/(2t_{\text{ML}}\lambda)$.

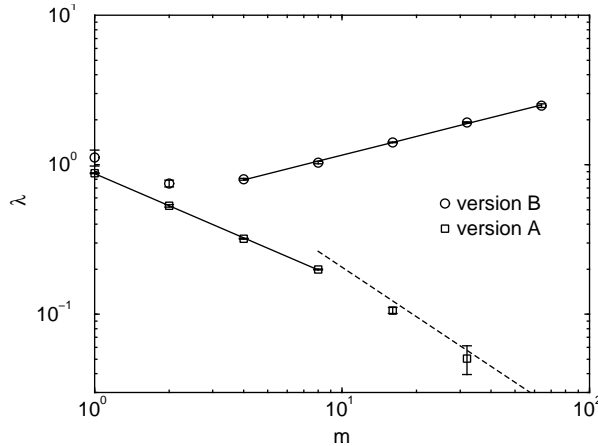


Figure 7.9: The measured λ in the case of the Eden model as a function of m in a log-log plot. The slopes of the regression lines (solid) are -0.72 ± 0.01 (version A) and 0.42 ± 0.01 (version B). The dashed line corresponds to an exponent of -1.1 (cf. section 7.3.2).

Thus, the cusp for $m \rightarrow \infty$ can be seen as the limit $\lambda \rightarrow \infty$ and so we have $\nu = \lambda^{-1} = \mathcal{F} = 0$ in agreement with a positive e_λ , while for $e_\nu \simeq 0$ the situation is unclear.

7.3.2 Scaling

It is instructive to point out again the role of the quantities \tilde{t} and \tilde{l} introduced in 7.3.1. There we used dimensional arguments to find out the only way in which the parameters \mathcal{F} , ν and λ can enter the proposed time and length.

Now let us take the exact solution of the EW equation in one dimension (Nattermann and Tang, 1992)

$$w^2(t, L) = \frac{\mathcal{F}}{\nu} L f\left(\frac{\nu t}{L^2}\right), \quad (7.7)$$

where L is the linear dimension of the system, and the scaling function $f(x)$ behaves like \sqrt{x} for $x \ll 1$ and approaches a constant for larger values.

Using the relations (7.3) and (7.4) with their numerical prefactors set to 1, and reinserting the EW scaling exponents $z = 2$, $\zeta = 1/2$ into (7.7), this can be written as

$$\frac{w^2(t, L)}{a_\perp^2} = (L/\tilde{l})^{2\zeta} \cdot f\left(\frac{t/\tilde{t}}{(L/\tilde{l})^z}\right). \quad (7.8)$$

This is not a new result, of course, but a more detailed version of the well known and widely used general scaling expression, first given in (Family and Vicsek, 1985). Detailed, because it takes into account the dimensions of height, length and time via a_\perp , \tilde{l} and \tilde{t} respectively. Apart from dimensional consistency it reminds of the fact that the validity of power laws describing the scaling behaviour is always limited from below by a cutoff value, which serves then as the natural unit. This does not play a role as long as it is fixed (e.g. the lattice constant) but in this situation the units turn out to be just \tilde{l} and \tilde{t} and thus depend on the parameters (\mathcal{F} , ν) and therefore on m .

Moreover it was not by chance that \tilde{l} appeared in (7.8) instead of e.g. the lattice constant a . If a power law would already apply on scales comparable to a , there should be a change in behaviour when eventually the scale of \tilde{l} is reached (which is larger than a). This statement is a general one; the natural unit appearing in a power law (i.e. its lower cutoff) is the largest of all characteristic scales with the correct dimension.

Hence, with the general scaling function $f(x)$ (which varies like $x^{2\zeta/z}$ for small x), eq. (7.8) is not restricted to the EW equation, and it can be used to predict the saturation behaviour of w^2 :

The saturation time is reached when the argument of the scaling function is of order one, i.e.

$$t_{\text{sat}} \sim L^z \tilde{t}^{-z} \tilde{t},$$

and inserting the power laws

$$\tilde{t} \propto m^\mu, \quad \tilde{l} \propto m^\kappa$$

yields

$$t_{\text{sat}} \propto m^{\mu-z\kappa} L^z. \quad (7.9)$$

For times longer than t_{sat} the width saturates as

$$w_\infty^2 \propto \tilde{l}^{-2\zeta} L^{2\zeta} \propto m^{-2\kappa\zeta} L^{2\zeta}. \quad (7.10)$$

Two special cases arise from the equations (7.9) and (7.10):

1. $\kappa = 0 \Rightarrow$ The saturation time varies like the damping time (i.e. $t_{\text{sat}} \propto m^\mu$), while the saturation width is independent of m .
2. $\kappa = \mu/z \Rightarrow$ The saturation time does not depend on m , while the saturation width w_∞^2 varies like $m^{-2\mu\zeta/z}$, as $w^2(t)$ does for all times $t > \tilde{t}$.

In (Kertész and Wolf, 1988) it was found that for version A of the Eden model the scaled saturation width w_∞^2/L approached a constant value of about 0.052 in a $1/m$ fashion. Thus, for large m version A could be a candidate for case one (i.e. $\kappa = 0$). With this, we obtain $e_\nu = -1$ from eq. (7.6), and that in turn predicts $e_\lambda = -\mu = -1.1$, which deviates rather strongly from the values of table 7.2. But it should be pointed out that the value $e_\lambda = -0.72$ therein was obtained by evaluating $\lambda(m)$ for rather small values of m . In the last two points ($m = 16, m = 32$), there is an indication for a crossover to a lower exponent. The expected value of -1.1 is shown as a dashed line in fig. 7.9 on page 133. This crossover will be discussed later in section 7.4.1.

A better agreement is obtained in the case of version B. For this model, it was found in (Devillard and Stanley, 1988) (and also in our own simulations) that the saturation time is not influenced by the noise reduction, and thus

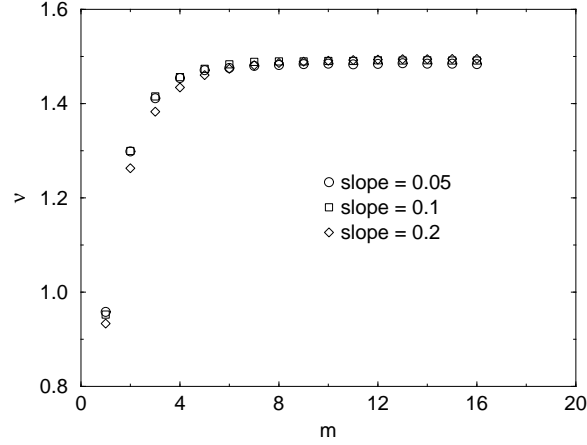


Figure 7.10: The dependence of the surface current on the noise reduction parameter m for three different global tilts in the EW model. Normalising the negative current with the tilt leads directly to the coefficient ν , cf. eq. (7.11). This coefficient is independent of m for larger values of m . The limiting value $\nu = 1.5$ (in natural units) is explained in the text.

we are in class two (i.e. $\kappa = \mu/z$). Using the exact value $z = 3/2$ and our result $\mu = 1.6$ (cf. table 7.1), the result of eq. (7.6) is $e_\nu = 0.067$, which is well in the range of that in Tab. 7.2.

Another model in class two is the EW model. This means with $z = 2$ and $\mu \simeq 2$ that $\kappa = 1$ should hold true, which fits well to the result $e_\nu = 0$ of the next section.

7.3.3 Surface current in the EW model

For the EW equation, the m -dependence of the occurring surface current \vec{j} arises from the influence of m on ν since

$$\vec{j} = -\nu \nabla h. \quad (7.11)$$

This identity results when bringing eq. (2.52) into the form of (2.48), which is only possible for $\lambda = 0$.

Actually the m -dependence of ν is weak and vanishes for larger m as shown in fig. 7.10 on the following page. The limiting value of $\nu = 1.5$ (in natural units) for $m \rightarrow \infty$ (i.e. no noise) can be explained as follows:

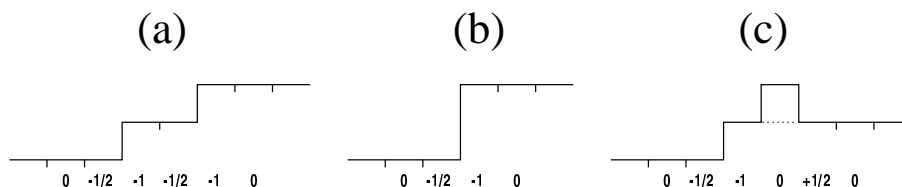


Figure 7.11: Surface currents for the EW model. The numbers denote the contribution of each site to the average current (in natural units). The case a) is the typical one where each step contributes $-3/2$, resulting in a downhill current being $3/2$ times the step density. The scenarios b) and c) show how a double step or a decoration reduce the contribution to $-3/4$ and -1 respectively; such configurations are suppressed in the presence of noise reduction.

If we consider again a regular surface with a positive global tilt s , the contribution to the average current is -1 for the edge sites, $-1/2$ for the kink sites (cf. fig. 7.11 on the next page and fig. 7.8 on page 130 lines 5 and 7, respectively), and zero for the terrace sites. Since we have s steps per unit length this results in a current of $j_\infty = -3/2s$, which, when compared to equation (7.11), reveals the limiting value for ν . For lower noise reduction we get deviations from the perfect steps during growth. Their effect is a reduction of the current (cf. fig. 7.11 on the next page).

7.4 Discussion

7.4.1 Description by continuum equations

For version A and B of the Eden model and for the EW model we were able to relate the m dependence of the damping time to the m dependence of the coefficients of the corresponding continuum equations. This was done by identifying the damping time \tilde{t} and the associated layer coherence length \tilde{l} with the characteristic time and length scales appearing in the scaling law which follows from the continuum equations. This identification was indirectly confirmed by measuring the corresponding m dependencies explicitly.

Whereas the damping time exponent could be explained in this way for the EW model and version B of the Eden model, version A of the Eden model turned out to be more subtle, because the coefficient λ of the corresponding KPZ equation has no simple power law dependence on m (cf.

fig. 7.9 on page 133). In this context an important property of the Eden models should be brought back into mind: the intrinsic width (Zabolitzky and Stauffer, 1986; Kertész and Wolf, 1988). This additional contribution to the surface width has a different behaviour than the long wavelength fluctuations described by eq. (2.52) and thus leads to strong corrections to scaling laws like eq. (7.8). Since the intrinsic width influences the growth velocity v via the perimeter density (Hirsch and Wolf, 1986), direct measurements of $v(\nabla h)$ exhibit just an effective λ . Only under a sufficient suppression of the intrinsic width by means of the noise reduction (Kertész and Wolf, 1988), the “real” behaviour (i.e. the one described by eq. (2.52)) is revealed. The same effect (yet weaker) can be seen for version B in fig. 7.9 on page 133: The first three data points indicate a crossover from a negative exponent to the correct one. Apparently the effect of the intrinsic width on the measured λ is more pronounced in the case of version A, for which a stronger correction to scaling is already known (Jullien and Botet, 1985; Kertész and Wolf, 1988). Unfortunately the desired range of larger m is difficult to access, since there the tilt dependence of the velocity gets smaller than the error bars.

7.4.2 Microscopic considerations

Because of the lack of a suitable continuum description for the early time behaviour of the WV and the “1+” model (for the asymptotic regime cf. (Šmilauer and Kotrla, 1994; Kotrla and Šmilauer, 1996; Punyindu and Sarma, 1998)), their value $\mu = 1.5$ will not be analyzed further here. But still a comparison of these models with the EW model gives insight into microscopic mechanisms which have a bearing on real molecular beam epitaxy.

This is because it seems – regarding the microscopic rules – at first sight unclear why the EW model and WV model should behave differently for early times. Since for an atom located at an edge site, the kink site has a lower height and at the same time a higher coordination, the atom will hop down in both cases (cf. fig. 7.8 on page 130, lines 5 and 6; this argumentation only holds true for $d = 1$).

The small but crucial difference arises when the atom is deposited directly at the kink site or at the terrace site next to it: After relaxation it will be found at the kink site with a probability of $p = 1$ for WV rules but only with $p = 5/12$ for EW rules (cf. fig. 7.8 on page 130, lines 7 and 8). This results in a larger island density for the EW model (i.e. in smaller islands at a fixed coverage) which increases the chance for a deposited atom to relax into the

incomplete layer.

The fact that small islands are good for layer-by-layer growth (here manifested by $\mu = 2$ for EW being larger than $\mu = 1.5$ for WV) is not merely specific to the toy models considered here, where atoms can only escape islands when they are deposited on an edge site and the effect only becomes visible by using the noise reduction technique. Indeed in experiments layer-by-layer growth can be promoted by artificially increasing the density of islands (e.g. by sputtering, cf. (Rosenfeld et al., 1993)).

Moreover the difference between EW rules and WV rules can be regarded as an example for the inverse Schwoebel effect (Markov, 1994), by which surfactants can improve layer-by-layer growth: If the surfactant atoms preferentially attach to the kink sites they may suppress the accretion of adatoms at a step from the *lower* terrace, but still may give way for adatoms coming down from the *upper* terrace. Thus the surfactant would make a WV-type growth more EW-like. As explained above this would increase the island density and hence improve layer-by-layer growth.

Chapter 8

Conclusion

Let us summarize what we learned in total from our major findings and what remains to be clarified.

A remarkable result from chapter 3 is the substantially different behavior of the two-dimensional surface compared to the one-dimensional one. While the latter shows excellent agreement with the theory, the former rules out two common assumptions. First, the diffusion length l_D is *not* the only relevant lateral scale, instead l_0 – being larger than l_D for $i^* = 1$ – appears as the crucial length for the reaction of the adatom diffusion field on the surface tilt $|\nabla h|$. In (Schroeder and Wolf, 1995) it was already argued that this larger scale should be more susceptible to finite size effects than l_D . In fact, the tilt-induced steps *are* boundaries which in a way isolate the terraces from each other and hence impose a finite size of $a_\perp/|\nabla h|$ in the direction of the tilt. Now we can wonder why this l_0 does not show up in the one-dimensional case^a. As the explanation we can invoke the same as the one for the second contradiction to common belief: The non-vanishing of the of first derivative of $\rho(|\nabla h| = 0)$, the quasi-stationary adatom density at zero tilt (see section 3.6). Namely, since communication over the distance l_0 can be mediated only by the diffusing adatoms, it cannot be effective for $d = 1$ since there the sinks with a typical distance of l_D absorb every adatom for sure. In higher dimensions however, adatoms may circumvent the islands. To further clarify this subtle interplay of length scales, simulations extending to $i^* > 1$ (where $l_D \geq l_0$ for $d = 2$, cf. equations (2.5) and (3.10)) are desirable, of course. Further decisive data could be obtained from simulations in $d = 3$, since this is the critical dimension according to eq. (3.31) as well as to eq. (3.35) in contrast to eq. (3.19), which predicts $d = 4$ as the dimensionality where the lifetime of layer-by-layer growth tends to infinity. Secondly, since a parabolic shape of $\rho(|\nabla h|)$ around $|\nabla h|$ could be definitely not confirmed, the common motivation of the cKPZ-nonlinearity $\nabla^2(\nabla h)^2$ has lost its basis for the ideal MBE model studied here^b. Therefore the quest for a new continuum equation compatible with eq. (3.33) should be a future task of high priority.

The breakdown of the simple, $d=1$ -inspired picture of island-edges and tilt-induced steps becomes apparent in chapter 4 as well. Also here, the naive theory (leading to equations (4.7) and (4.9)) provides a quantitatively correct description only for the one-dimensional case. Also here, simulations

^aWe did not prove this directly but infer it from the applicability of the theory in $d = 1$.

^bFor a weak effect of the lattice, the nonlinearity is produced in a renormalization group approach (Rost and Krug, 1997b).

with $i^* > 1$ would be helpful, namely to separate the contributions of l_D and l_0 to the damping time (cf. equations (4.11) and (4.12)). Nevertheless, we were able to use the numerical findings for illuminating the ambiguous situation of covarying diffusion length l_D and Schwoebel length l_s . The resulting prediction about the positive/negative influence of strain on layer-by-layer growth can well be verified experimentally. The same applies to the powerlaw-dependence of the damping time on the flux F .

From chapter 5 as well as from section 3.1.2 we learned about the importance of shot-noise as a mechanism to counteract layer-by-layer growth. This should be kept in mind when simulation methods more sophisticated than the “brute force” KMC technique are going to be employed, like e.g. the *level-set method* (Gyure et al., 1998), which generically lacks shot-noise. Such alternative approaches are especially appealing when diffusion along island rims is to be included, since the corresponding KMC simulations are considerably more time consuming than the ones presented here. But we see that unless dominant mechanisms like Schwoebel barriers (in $d = 2$) are present, special care has to be taken to include the effect of shot-noise.

While the comparison of the simulations of the “melting” step-bunch in chapter 6 to the experimental data did not lead to a truly satisfactory confirmation of the scenario, the step-bunch’s inherent length scale – l_D for $d = 1$ as opposed to l_0 for $d = 2$ – is in excellent agreement with the results concerning the different length scales in chapter 3.

Chapter 7 finally taught us that the behavior during the ceasing of layer-by-layer growth may be quite independent from the universality class of the underlying model: The Eden models A and B both belong to the KPZ class, but the latter shows a weaker damping. WV model and “1+”-model coincide perfectly with respect to their layer-by-layer growth but are in different classes (EW and cKPZ, respectively). This revalues models’ characterization according to universality classes for practical purposes.

Bibliography

- Abramowitz, M. and Stegun, I. (1965). *Handbook of mathematical functions*. Dover, New York.
- Ala-Nissila, T. (1998). Comment on "Upper critical dimension of the Kardar-Parisi-Zhang equation". *Phys. Rev. Lett.*, 80:887.
- Ala-Nissila, T., Hjelt, T., Kosterlitz, J., and Venalainen, O. (1993). Scaling exponents for kinetic roughening in higher dimensions. *J. Stat. Phys.*, 72:207.
- Amar, J. and Family, F. (1992). Universality in surface growth: scaling functions and amplitude ratios. *Phys. Rev. E*, 45:5378.
- Amar, J. and Family, F. (1996a). Effects of crystalline microstructure on epitaxial growth. *Phys. Rev. B*, 54:14742.
- Amar, J. and Family, F. (1996b). Kinetics of submonolayer and multilayer epitaxial growth. *Thin Solid Films*, 272:208.
- Amar, J. and Family, F. (1998). Mound formation, coarsening and instabilities in epitaxial growth. *Surface Review & Letters*, 5:851.
- Amar, J., Family, F., and Lam, P.-M. (1994). Dynamic scaling of the island-size distribution and percolation in a model of submonolayer molecular-beam epitaxy. *Phys. Rev. B*, 50:8781.
- Amar, J., Lam, P.-M., and Family, F. (1993). Groove instabilities in surface growth with diffusion. *Phys. Rev. E*, 47:3242.
- Arthur, J. (1968). *J. Appl. Phys.*, 39:4032.

- Asaro, R. and Tiller, W. (1972). Interface morphology development during stress corrosion cracking. I. Via surface diffusion. *Metallurgical Transactions A-Physical Metallurgy & Materials Science*, 3:1789.
- Ashcroft, N., Mermin, N., and Mermin, D. (1976). *Solid State Physics*. Harcourt College Publishers, Philadelphia.
- Bales, G. and Chrzan, D. (1994). Dynamics of irreversible island growth during submonolayer epitaxy. *Phys. Rev. B*, 50:6057.
- Bales, G. and Zangwill, A. (1990). Morphological instability of a terrace edge during step-flow growth. *Phys. Rev. B*, 41:5500.
- Barabasi, A.-L. and Stanley, H. (1995). *Fractal Concepts in Surface Growth*. Cambridge Univ Press, Cambridge.
- Bartelt, M. and Evans, J. (1993). Crossover from anisotropic-to-isotropic diffusion-mediated island growth on surfaces. *Europhys. Lett.*, 21:99.
- Bell, E. (1934). Exponential polynomials. *Ann. Math.*, 35:258.
- Blue, J., Beichl, I., and Sullivan, F. (1995). Faster Monte Carlo simulations. *Phys. Rev. E*, 51:R867.
- Bortz, A., Lebowitz, J., and Kalos, M. (1975). A new algorithm for Monte Carlo simulation of ising spin systems. *J. Comp. Phys.*, 17:10.
- Braun, W. (1996). *Reflection High-Energy Electron Diffraction Studies of Semiconductor Interfaces During Molecular Beam Epitaxy Growth*. Dissertation, Humboldt-Universität zu Berlin.
- Brendel, L. (1994). Fluktuationsschwächung in Wachstumsmodellen für Molekularstrahlepitaxie. Master's thesis, Gerhard-Mercator-Universität-GH Duisburg, Germany.
- Bromann, K., Brune, H., Roder, H., and Kern, K. (1995). Interlayer mass transport in homoepitaxial and heteroepitaxial metal growth. *Phys. Rev. Lett.*, 75:677.
- Burton, W., Cabrera, N., and Frank, F. (1951). The growth of crystals and the equilibrium structure of their surfaces. *Phil. Trans. Roy. Soc. (Lond.) A*, 243:299.

- Cho, A. and Arthur, J. (1975). Molecular beam epitaxy. *Progress in Solid State Chemistry*, 10:157.
- Chrisey, D. and Hubler, G., editors (1994). *Pulsed Laser Deposition of Thin Films*, New York. John Wiley & Sons.
- Clarke, S., Wilby, M., and Vvedensky, D. (1991). Theory of homoepitaxy on si(001). i. kinetics during growth. *Surf. Sci.*, 255:91.
- Cohen, P., Petrich, G., Pukite, P., Whaley, G., and Arrott, A. (1989). Birth-death models of epitaxy. diffraction oscillations from low index surfaces. *Surf. Sci.*, 216:222.
- Corless, R., Gonnet, G., Hare, D., Jeffrey, D., and Knuth, D. (1996). On the Lambert W function. *Advances in Computational Mathematics*, 5:329.
- Devillard, P. and Stanley, H. (1988). Evolution of interfaces for a model interpolating between diffusion-limited aggregation and the Eden model. *Phys. Rev. A*, 38:6451.
- Duport, C., Nozieres, P., and Villain, J. (1995a). New instability in molecular beam epitaxy. *Phys. Rev. Lett.*, 74:134.
- Duport, C., Politi, P., and Villain, J. (1995b). Growth instabilities induced by elasticity in a vicinal surface. *J. Phys. I France*, 5:1317.
- Eden, M. (1958). In Yockey, H., editor, *Symposium on Information Theory in Biology*, New York. Pergamon Press.
- Edwards, S. and Wilkinson, D. (1982). The surface statistics of a granular aggregate. *Proc. R. Soc. London A*, 381:17.
- Ehrlich, G. and Hudda, F. (1966). Atomic view of surface diffusion: tungsten on tungsten. *J. Chem. Phys.*, 44:1039.
- Ernst, H.-J., Fabre, F., Folkerts, R., and Lapujoulade, J. (1994). Observation of a growth instability during low temperature molecular beam epitaxy. *Phys. Rev. Lett.*, 72:112.
- Evans, J. (1991). Factors mediating smoothness in epitaxial thin-film growth. *Phys. Rev. B*, 43:3897.

- Family, F. (1986). Scaling of rough surfaces: Effects of surface diffusion. *J. Phys. A: Math. Gen.*, 19:L441.
- Family, F. and Vicsek, T. (1985). Scaling of the active zone in the Eden process on percolation networks and the ballistic deposition model. *J. Phys. A: Math. Gen.*, 18:L75.
- Family, F. and Vicsek, T., editors (1991). *Dynamics of Fractal Surfaces*, Singapore. World Scientific.
- Forster, D., Nelson, D., and Stephen, M. (1977). Large-distance and long-time properties of a randomly stirred fluid. *Phys. Rev. A*, 16:732.
- Frey, E. and Tauber, U. (1994). Two-loop renormalization-group analysis of the Burgers-Kardar-Parisi-Zhang equation. *Phys. Rev. E*, 50:1024.
- Fu, T., Wu, H., and Tsong, T. (1998). Energetics of surface atomic processes near a lattice step. *Phys. Rev. B*, 58:2340.
- Gardiner, C. (1985). *Handbook of Stochastic Methods*. Springer, Berlin.
- Golubović, L. and Bruinsma, R. (1991). Surface diffusion and fluctuations of growing interfaces. *Phys. Rev. Lett.*, 66:321.
- Grinfeld, M. (1986). Instability of the separation boundary between a non-hydrostatically stressed elastic body and a melt. *Doklady Akademii Nauk SSSR*, 290:1358.
- Gruber, E. and Mullins, W. (1967). *J. Phys. Chem. Solids*, 28:875.
- Gyure, M., Ratsch, C., Merriman, B., Caffisch, R., Osher, S., Zinck, J., and Vvedensky, D. (1998). Level-set methods for the simulation of epitaxial phenomena. *Phys. Rev. E*, 58:R6927.
- Halpin-Healy, T. and Zhang, Y. (1995). Kinetic roughening phenomena, stochastic growth, directed polymers and all that. Aspects of multidisciplinary statistical mechanics. *Physics Reports*, 254:215.
- Harris, J., Joyce, B., and Dobson, P. (1981). Oscillations in the surface structure of Sn-doped GaAs during growth by MBE. *Surf. Sci.*, 103:L90.

- Henye, F. and Seshadri, V. (1982). On the number of distinct sites visited in 2d lattices. *J. Chem. Phys.*, 76:5530.
- Herman, M. and Sitter, H. (1989). *Molecular Beam Epitaxy*. Springer, Berlin.
- Hinnemann, B. (2000). Layer-by-layer growth with pulsed laser deposition. Master's thesis, Gerhard-Mercator-Universität-GH Duisburg, Germany.
- Hirsch, R. and Wolf, D. (1986). Anisotropy and scaling of Eden clusters in two and three dimensions. *J. Phys. A: Math. Gen.*, 19:L251.
- Janssen, H. (1997). On critical exponents and the renormalization of the coupling constant in growth models with surface diffusion. *Phys. Rev. Lett.*, 78:1082.
- Jenniches, H., Shen, J., Mohan, C., Manoharan, S. S., Barthel, J., Ohresser, P., Klaua, M., and Kirschner, J. (1999). Structure and magnetism of pulsed-laser-deposited ultrathin films of Fe on Cu(100). *Phys. Rev. B*, 59:1196.
- Jensen, P., Larralde, H., and Pimpinelli, A. (1997). Effect of monomer evaporation on a simple model of submonolayer growth. *Phys. Rev. B*, 55:2556.
- Johnson, M., Orme, C., Hunt, A., Graff, D., Sudijono, J., Sander, L., and Orr, B. (1994). Stable and unstable growth in molecular beam epitaxy. *Phys. Rev. Lett.*, 72:116.
- Jullien, R. and Botet, R. (1985). Surface thickness in the Eden model. *Phys. Rev. Lett.*, 54:2055.
- Kallabis, H. (1997). *Theoretical Aspects of Crystal Growth*. Dissertation, Gerhard-Mercator-Universität Duisburg, Germany.
- Kallabis, H., Brendel, L., Krug, J., and Wolf, D. (1997). Damping of oscillations in layer-by-layer growth. *Int. J. Mod. Phys. B*, 11:3621.
- Kallabis, H., Krapivsky, P., and Wolf, D. (1998). Island distance in one-dimensional epitaxial growth. *European Physical Journal B*, 5:801.
- Kandel, D. (1997). Initial stages of thin film growth in the presence of island-edge barriers. *Phys. Rev. Lett.*, 78:499.

- Kardar, M., Parisi, G., and Zhang, Y. (1986). Dynamic scaling of growing interfaces. *Phys. Rev. Lett.*, 56:889.
- Kellog, G. (1991). Temperature dependence of surface self-diffusion on Pt(001). *Surf. Sci.*, 246:31.
- Kertész, J. and Wolf, D. (1988). Noise reduction in Eden models: II. Surface structure and intrinsic width. *J. Phys. A: Math. Gen.*, 21:747.
- Kodiyalam, S., Khor, K., and Sarma, S. D. (1996). Calculated schwoebel barriers on Si(111) steps using an empirical potential. *Phys. Rev. B*, 53:9913.
- Kotrla, M. and Šmilauer, P. (1996). Nonuniversality in models of epitaxial growth. *Phys. Rev. B*, 53:13777.
- Krug, J. (1989). Classification of some deposition and growth processes. *J. Phys. A: Math. Gen.*, 22:L769.
- Krug, J. (1994). Turbulent interfaces. *Phys. Rev. Lett.*, 72:2907.
- Krug, J. (1997). Origins of scale invariance in growth processes. *Advances in Physics*, 46:139.
- Krug, J., Dobbs, H., and Majaniemi, S. (1995). Adatom mobility for the solid-on-solid model. *Zeitschrift für Physik B-Condensed Matter*, 97:281.
- Krug, J., Plischke, M., and Siegert, M. (1993). Surface diffusion currents and the universality classes of growth. *Phys. Rev. Lett.*, 70:3271.
- Krug, J., Politi, P., and Michely, T. (2000). Island nucleation in the presence of step-edge barriers: Theory and applications. *Phys. Rev. B*, 61:14037.
- Krug, J. and Spohn, H. (1991). Kinetic roughening of growing surfaces. In Godrèche, C., editor, *Solids far from equilibrium*, Cambridge. Cambridge University Press.
- Kunkel, R., Poelsema, B., Verheij, L., and Comsa, G. (1990). Reentrant layer-by-layer growth during molecular-beam epitaxy of metal-on-metal substrates. *Phys. Rev. Lett.*, 65:733.

- Kuwabara, G. and Kono, K. (1987). Restitution coefficient in a collision between two spheres. *Japanese Journal of Applied Physics Part 1*, 26:1230.
- Kyuno, K. and Ehrlich, G. (1997). Step-edge barriers: truths and kinetic consequences. *Surf. Sci.*, 383:L766.
- Kyuno, K. and Ehrlich, G. (1998). Step-edge barriers on Pt(111): an atomistic view. *Phys. Rev. Lett.*, 81:5592.
- Lai, Z.-W. and Sarma, S. D. (1991). Kinetic growth with surface relaxation: Continuum versus atomistic models. *Phys. Rev. Lett.*, 66:2848.
- Langevin, P. (1908). Sur la théorie du mouvement brownien. *Comptes rendus*, 146:530.
- Lässig, M. and Kinzelbach, H. (1997). Upper critical dimension of the Kardar-Parisi-Zhang equation. *Phys. Rev. Lett.*, 78:903.
- Latyshev, A., Aseev, A., Krasilnikov, A., and Stenin, S. (1989). Transformations on clean Si(111) stepped surface during sublimation. *Surf. Sci.*, 213:157.
- Latyshev, A., Minoda, H., Tanishiro, Y., and Yagi, K. (1998). Electromigration and gold-induced step bunching on the Si(111) surface. *Surf. Sci.*, 401:22.
- Lee, H.-W. and Doochul, K. (1997). Universal macroscopic background formation in surface super-roughening. *Phys. Rev. E*, 56:R2347.
- Levitt, D. (1973). Dynamics of a single-file pore: non-Fickian behavior. *Phys. Rev. A*, 8:3050.
- Lopez, J., Rodriguez, M., and Cuerno, R. (1997). Superroughening versus intrinsic anomalous scaling of surfaces. *Phys. Rev. E*, 56:3993.
- Maca, F., Kotrla, M., and Trushin, O. (2000). Energy barriers for diffusion on stepped Rh(111) surfaces. *Surf. Sci.*, 454–456:579.
- Maksym, P. (1988). Fast Monte Carlo simulation of MBE growth. *Semiconductor Science & Technology*, 3:594.

- Mandelbrot, B. (1983). *The Fractal Geometry of Nature*. Springer, New York.
- Markov, I. (1994). Kinetics of surfactant-mediated epitaxial growth. *Phys. Rev. B*, 50:11271.
- Meakin, P. (1993). The growth of rough surfaces and interfaces. *Physics Reports*, 235:189.
- Medina, E., Hwa, T., Kardar, M., and Zhang, Y. (1989). Burgers equation with correlated noise: Renormalization-group analysis and applications to directed polymers and interface growth. *Phys. Rev. A*, 39:3053.
- Misbah, C. and Pierre-Louis, O. (1996). Pulses and disorder in a continuum version of step-bunching dynamics. *Phys. Rev. E*, 53:R4318.
- Moore, M., Blum, T., Doherty, J., Marsili, M., Bouchaud, J.-P., and Claudin, P. (1995). Glassy solutions of the Kardar-Parisi-Zhang equation. *Phys. Rev. Lett.*, 74:4257.
- Moser, K. and Wolf, D. (1992). In Jullien, R., Kertész, J., Meakin, P., and Wolf, D., editors, *Surface Disordering: Growth, Roughening, and Phase Transitions*, page 21, Commack. Nova Science.
- Mullins, W. (1963). Solid surface morphologies governed by capillarity. In Gjostein, N. and Robertson, W., editors, *Metal Surfaces: Structure, Energetics and Kinetics*, Metals Park. American Society of Metals.
- Myers-Beaghton, A. and Vvedensky, D. (1991). Generalized Burton-Cabrera-Frank theory for growth and equilibration on stepped surfaces. *Phys. Rev. E*, 44:2457.
- Nattermann, T. and Tang, L.-H. (1992). Kinetic surface roughening. I. the Kardar-Parisi-Zhang equation in the weak-coupling regime. *Phys. Rev. A*, 45:7156.
- Nostrand, J. V., Chey, S., Hasan, M.-A., Cahill, D., and Greene, J. (1995). Surface morphology during multilayer epitaxial growth of Ge(001). *Phys. Rev. Lett.*, 74:1127.

- Ohresser, P., Shen, J., Barthel, J., Zheng, M., Mohan, C., Klaua, M., and Kirschner, J. (1999). Growth, structure, and magnetism of fcc Fe ultra-thin films on Cu(111) by pulsed laser deposition. *Phys. Rev. B*, 59:3696.
- Pang, N.-N. and Tzeng, W.-J. (2000a). Discerning influences of orientational instability on anomalously roughened interfaces. *Phys. Rev. E*, 61:3212.
- Pang, N.-N. and Tzeng, W.-J. (2000b). Interfaces with superroughness. *Phys. Rev. E*, 61:3559.
- Park, K., Kahng, B., and Kim, S. (1994). Surface dynamics of the Wolf-Villain model for epitaxial growth in 1+1 dimensions. *Physica A*, 210:146.
- Pimpinelli, A. and Villain, J. (1999). *Physics of Crystal Growth (Collection Alea-Saclay, 4)*. Cambridge University Press.
- Pimpinelli, A., Villain, J., and Wolf, D. (1992). Surface diffusion and island density (comment with reply). *Phys. Rev. Lett.*, 69:985.
- Plischke, M. (1999). private communication.
- Politi, P. (1997). Different regimes in the Ehrlich-Schwoebel instability. *J. Phys. I France*, 7:797.
- Politi, P. (1998). Kink dynamics in a one-dimensional growing surface. *Phys. Rev. E*, 58:281.
- Politi, P. and Villain, J. (1996). Ehrlich-Schwoebel instability in molecular-beam epitaxy: a minimal model. *Phys. Rev. B*, 54:5114.
- Punyindu, P. and Sarma, S. D. (1998). Noise reduction and universality in limited-mobility models of nonequilibrium growth. *Phys. Rev. E*, 57:R4863.
- Rosenfeld, G., Servaty, R., Teichert, C., Poelsema, B., and Comsa, G. (1993). Layer-by-layer growth of Ag on Ag(111) induced by enhanced nucleation: A model study for surfactant-mediated growth. *Phys. Rev. Lett.*, 71:895.
- Rost, M. and Krug, J. (1997a). Coarsening of surface structures in unstable epitaxial growth. *Phys. Rev. E*, 55:3952.

- Rost, M. and Krug, J. (1997b). Damping of growth oscillations in molecular beam epitaxy: a renormalization group approach. *J. Phys. I France*, 7:1627.
- Rost, M. and Spohn, H. (1994). Renormalization of the driven sine-Gordon equation in 2+1 dimensions. *Phys. Rev. E*, 49:3709.
- Rost, M., Šmilauer, P., and Krug, J. (1996). Unstable epitaxy on vicinal surfaces. *Surf. Sci.*, 369:393.
- Sarma, S. D., Ghaisas, S., and Kim, J. (1994). Kinetic super-roughening and anomalous dynamic scaling in nonequilibrium growth models. *Phys. Rev. E*, 49:122.
- Sarma, S. D. and Punyindu, P. (1997). Dynamic scaling in a (2+1)-dimensional limited mobility model of epitaxial growth. *Phys. Rev. E*, 55:5361.
- Sarma, S. D. and Tamborena, P. (1991). A new universality class for kinetic growth: One-dimensional molecular-beam epitaxy. *Phys. Rev. Lett.*, 66:325.
- Schindler, A. (1999). *Theoretical aspects of growth on one and two dimensional strained crystal surfaces*. Dissertation, Gerhard-Mercator-Universität Duisburg, Germany.
- Schroeder, M., Siegert, M., Wolf, D., Shore, J., and Plischke, M. (1993). Scaling of growing surfaces with large local slopes. *Europhys. Lett.*, 24:563.
- Schroeder, M. and Wolf, D. (1995). Magic islands and submonolayer scaling in molecular beam epitaxy. *Phys. Rev. Lett.*, 74:2062.
- Schwoebel, R. (1968). Step motion on crystal surfaces II. *J. Appl. Phys.*, 40:614.
- Schwoebel, R. and Shipsey, E. (1966). Step motion on crystal surfaces. *J. Appl. Phys.*, 37:3682.
- Siegert, M. (1998). Coarsening dynamics of crystalline thin films. *Phys. Rev. Lett.*, 81:5481.

- Siegert, M. and Plischke, M. (1994). Slope selection and coarsening in molecular beam epitaxy. *Phys. Rev. Lett.*, 73:1517.
- Siegert, M. and Plischke, M. (1996). Formation of pyramids and mounds in molecular beam epitaxy. *Phys. Rev. E*, 53:307.
- Somfai, E., Wolf, D., and Kertesz, J. (1996). Correlated island nucleation in layer-by-layer growth. *J. Phys. I France*, 6:393.
- Spohn, H. (1993). Interface motion in models with stochastic dynamics. *J. Stat. Phys.*, 71:1081.
- Stoyanov, S. and Kashchiev, D. (1981). Thin film nucleation and growth theories: a confrontation with experiment. In Kaldis, E., editor, *Current Topics in Material Science*, volume 7, page 69, Amsterdam. North-Holland.
- Stroscio, J., Pierce, D., and Dragoset, R. (1993). Homoepitaxial growth of iron and a real space view of reflection-high-energy-electron diffraction. *Phys. Rev. Lett.*, 70:3615.
- Stroscio, J., Pierce, D., Stiles, M., Zangwill, A., and Sander, L. (1995). Coarsening of unstable surface features during Fe(001) homoepitaxy. *Phys. Rev. Lett.*, 75:4246.
- Stumpf, R. and Scheffler, M. (1994). Theory of self-diffusion at and growth of Al(111). *Phys. Rev. Lett.*, 72:254.
- Stumpf, R. and Scheffler, M. (1996). Ab initio calculations of energies and self-diffusion on flat and stepped surfaces of al and their implications on crystal growth. *Phys. Rev. B*, 53:4958.
- Sun, T., Guo, H., and Grant, M. (1989). Dynamics of driven interfaces with a conservation law. *Phys. Rev. A*, 40:6763.
- Sun, T. and Plischke, M. (1994). Field-theory renormalization approach to the Kardar-Parisi-Zhang equation. *Phys. Rev. E*, 49:5046.
- Szép, J., Cserti, J., and Kertész, J. (1985). Monte Carlo approach to dendritic growth. *J. Phys. A: Math. Gen.*, 18:L413.

- Tang, C. (1985). Diffusion-limited aggregation and the Saffman-Taylor problem. *Phys. Rev. A*, 31:1977.
- Tang, L., Šmilauer, P., and Vvedensky, D. (1998). Noise-assisted mound coarsening in epitaxial growth. *European Physical Journal B*, 2:409.
- Tang, L.-H. (1993). Island formation in submonolayer epitaxy. *J. Phys. I France*, 3:935.
- Tang, L.-H. and Nattermann, T. (1991). Kinetic roughening in molecular-beam epitaxy. *Phys. Rev. Lett.*, 66:2899.
- Theis-Bröhl, K., Zoller, I., Bödeker, P., Schmitte, T., Zabel, H., Brendel, L., Belzer, M., and Wolf, D. (1998). Temperature- and rate-dependent RHEED oscillation studies of epitaxial Fe(001) on Cr(001). *Phys. Rev. B*, 57:4747.
- Thürmer, K., Koch, R., Weber, M., and Rieder, K. (1995). Dynamic evolution of pyramid structures during growth of epitaxial Fe(001) films. *Phys. Rev. Lett.*, 75:1767.
- Trushin, O., Kotrla, M., and Maca, F. (1997). Energy barriers on stepped Ir/Ir(111) surfaces: a molecular statics calculation. *Surf. Sci.*, 389:55.
- Tsao, J. (1993). *Materials Fundamentals of Molecular Beam Epitaxy*. Academic Press, San Diego.
- van der Eerden, J. and Müller-Krumbhaar, H. (1986). Dynamic coarsening of crystal surfaces by formation of macrosteps. *Phys. Rev. Lett.*, 57:2431.
- Venables, J., Spiller, G., and Hanbucken, M. (1984). Nucleation and growth of thin films. *Reports on Progress in Physics*, 47:399.
- Villain, J. (1991). Continuum models of crystal growth from atomic beams with and without desorption. *J. Phys. I*, 1:19.
- Villain, J. (1992). Terrace sizes in molecular beam epitaxy. *J. Phys. I France*, 2:2107.
- Villain, J., Pimpinelli, A., and Wolf, D. (1992). Layer by layer growth in molecular beam epitaxy. *Comments Cond. Mat. Phys.*, 16:1.

- Voigtlander, B. and Zinner, A. (1993). Simultaneous molecular beam epitaxy growth and scanning tunneling microscopy imaging during Ge/Si epitaxy. *App. Phys. Lett.*, 63:3055.
- Šmilauer, P. and Harris, S. (1995). Determination of step-edge barriers to interlayer transport from surface morphology during the initial stages of homoepitaxial growth. *Phys. Rev. B*, 51:14798.
- Šmilauer, P. and Kotrla, M. (1994). Crossover effects in the wolf-villain model of epitaxial growth in 1+1 and 2+1 dimensions. *Phys. Rev. B*, 49:5769.
- Šmilauer, P., Rost, M., and Krug, J. (1999). Fast coarsening in unstable epitaxy with desorption. *Phys. Rev. E*, 59:R6263.
- Šmilauer, P. and Vvedensky, D. (1995). Coarsening and slope evolution during unstable epitaxial growth. *Phys. Rev. B*, 52:14263.
- Vvedensky, D., Zangwill, A., Luse, C., and Wilby, M. (1993). Stochastic equations of motion for epitaxial growth. *Phys. Rev. E*, 48:852.
- Witten, T. and Sander, L. (1983). Diffusion-limited aggregation. *Phys. Rev. B*, 27:5686.
- Wolf, D. (1995). Computer simulation of molecular beam epitaxy. In Droz, M., McKane, A., Vannimenus, J., and Wolf, D., editors, *Scale Invariance, Interfaces, and Non-Equilibrium Dynamics*, page 215, New York. Plenum Press.
- Wolf, D. (1997). Adatom diffusion and epitaxial growth. In Kim, D., Park, H., and Kahng, B., editors, *Dynamics of Fluctuating Interfaces and Related Phenomena*, page 173, Singapore. World Scientific.
- Wolf, D. and Kertész, J. (1989). Growth: Noise reduction and universality. *Phys. Rev. Lett.*, 63:1191.
- Wolf, D. and Villain, J. (1990). Growth with surface diffusion. *Europhys. Lett.*, 13:389.
- Yu, B. and Scheffler, M. (1997). Ab initio study of step formation and self-diffusion on Ag(100). *Phys. Rev. B*, 55:13916.

- Zabolitzky, J. and Stauffer, D. (1986). Simulation of large Eden clusters. *Phys. Rev. A*, 34:1523.
- Zangwill, A. (1988). *Physics at surfaces*. Cambridge University Press, Cambridge.
- Zhang, Q.-M., Roland, C., Boguslawski, P., and Bernholc, J. (1995). Ab initio studies of the diffusion barriers at single-height Si(100) steps. *Phys. Rev. Lett.*, 75:101.
- Zinsmeister, G. (1968). Theory of thin film condensation. Part B: solution of the simplified condensation equation. *Thin Solid Films*, 2:497.
- Zinsmeister, G. (1969). Theory of thin film condensation. III. Aggregate size distribution in island films. *Thin Solid Films*, 4:363.
- Zinsmeister, G. (1971). Theory of thin film condensation. IV. Influence of a variable collision factor. *Thin Solid Films*, 7:51.

*

Appendix A

Natural units

A few words about “setting a quantity to unity” are in order, since for many experimentalists (let alone non-physicists) it seems to imply a loss of information. Indeed, the expression is rather sloppy and misleading. What is really meant is “using the quantity as a unit” and then employing only dimensionless variables. An example is expedient here; let’s consider the differential equation

$$m\partial_t^2 x + kx^{3/2} + \Gamma x^{1/2}\partial_t x = 0, \quad (\text{A.1})$$

where m and x may denote a particle’s mass and position respectively while k and Γ are further parameters to the system^a, whose dimensions can be read off eq. (A.1) to be

$$[k] = \frac{\text{M}}{\text{L}^{1/2}\text{T}^2} \quad \text{and} \quad [\Gamma] = \frac{\text{M}}{\text{L}^{1/2}\text{T}}.$$

Natural units for mass, time and length are therefore m , Γ/k and $k^2 m^2/\Gamma^4$ respectively. With these, every dimensionful quantity will be explicitly decomposed into the numerical value times the (natural) unit like

$$x = x' \frac{k^2 m^2}{\Gamma^4}$$

for length and

$$t = t' \frac{\Gamma}{k}$$

for time.

Inserting theses products into eq. (A.1) causes all three parameters to cancel out and we are left with a differential equation in terms of the numerical values (the primed quantities in our example):

$$\partial_{t'}^2 x' + x'^{3/2} + x'^{1/2}\partial_{t'} x' = 0$$

Normally one would drop the primes now and, voilà, the parameters m , k and Γ are “set to unity”. The gain is the reduction of parameters (by at most the number of introduced natural units) and the consequent mathematical convenience. The price to pay is that each quantity calculated as a result or used as input is dimensionless as well and possibly has to be

^aThis differential equation arises in the context of modeling sphere collisions(Kuwabara and Kono, 1987) but that is of no importance to this example.

made dimensionful by means of multiplying it by the appropriate unit. For example, for a dimensionless energy E' that would be

$$E = E' \underbrace{m}_{\mathbf{M}} \underbrace{\left(\frac{k^2 m^2}{\Gamma^4}\right)^2}_{\mathbf{L}^2} \underbrace{\left(\frac{\Gamma}{k}\right)^{-2}}_{\mathbf{T}^{-2}} = E' \frac{m^5 k^6}{\Gamma^{10}} .$$

The “turning into unity” of m , k and Γ can be understood from a more general point of view than plugging into eq. (A.1) and doing some algebra: Trivially, a quantity being a product of powers of base units has the numerical value one in just these units (like a meter divided by a second is the velocity *one* meter per second). But natural units *are* products of powers of certain chosen parameters *and vice versa*. This implies necessarily

$$m' = k' = \Gamma' = 1 .$$

In molecular beam epitaxy, gravity and inertial effects do not play a rôle, hence the dimension \mathbf{M} does not occur. Instead, due to the broken symmetry between length scales parallel and normal to the particle beam, we can distinguish between the dimension \mathbf{H} for the height (the vertical lattice constant a_{\perp} is an example) and \mathbf{L} for the lateral length. That means we have still three physical dimensions at hand.

Now, if we set the lattice constants and the mono-layer time to one, we mean using a , a_{\perp} and $t_{\text{ML}} = 1/(F a^d)$ as units for quantities of dimension \mathbf{L} , \mathbf{H} and \mathbf{T} respectively. These are our natural units in MBE, where it is very plausible why the dimensionless flux F' must equal one: Since a lattice site has unit area a^d , we have *one* particle per site and unit time ($= t_{\text{ML}}$).

It should be noted that equations containing only numerical values of originally dimensionful quantities got a bad reputation since commonly they are employed (especially in fields like chemistry, biology or engineering) to be valid only for one specific, yet mostly not explicitly mentioned, system of units. But then these units are *not natural* in contrast to our example where it is indeed much more natural to relate a mass to something specific to the system under investigation rather than to something kept in a strongroom in Sèvres/France.

Appendix B

Order instead of haphazard

B.1 Kicking balls

In section 2.5.3 we discussed the following approach to randomize a list of references to lattice sites: The first reference to an adatom is exchanged with another element chosen at random. To make this process more graphic, we change the view in the following way: We regard the list as a one-dimensional, discrete “field”, whose sites may be either empty (reference to an atom with lateral bonds) or occupied by a “ball” (reference to an adatom).

To be more specific, we consider N balls on an array with L sites, where consecutively the rightmost one (its position is denoted by x_0) is kicked away and relands on a random site (cf. fig. B.1). If the latter is occupied by another ball, these two are exchanged, yielding the same state. (In principle, the balls are distinguishable, but their order is not important to our considerations.) Before proceeding to calculate the evolution of x_0 (equivalent to the width of the occupied zone), let’s introduce the abbreviations

$$q \equiv 1 - \frac{1}{N} \quad \text{and} \quad \rho \equiv \frac{N}{L} .$$

Elementary combinatorics tells us the probability to find the rightmost ball’s left neighbor at x_1 is given by

$$p(x_1) = \binom{x_1 - 1}{N - 2} / \binom{x_0 - 1}{N - 1} ,$$

which yields an average position x_1 of

$$\langle x_1 \rangle = \sum_{x_1=N-1}^{x_0-1} x_1 p(x_1) = x_0 \frac{N-1}{N} = x_0 q .$$

Kicking the ball at x_0 beyond the one at x_1 without performing an exchange (let’s call this a *success*) results in renumbering the positions, i.e. the

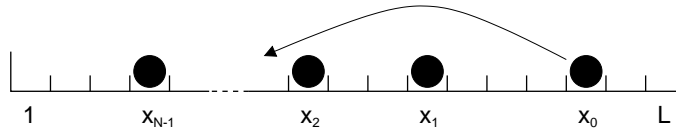


Figure B.1: The rightmost ball is kicked away, relanding on a random site; if this is an empty one to the left of its neighbor, we call it a *success*.

old x_1 becomes the new x_0 . Thus, with each success, x_0 decreases on average as

$$x_0 \rightarrow x_0 q ,$$

which amounts to

$$x_{0,k} = x_{0,0} q^k = x_{0,0} \exp(k \ln q) \quad (\text{B.1})$$

after k successes when starting with $x_{0,0}$.

Though we see that with each success x_0 approaches the field's left end exponentially fast, the probability for a success depends on the current x_0 , too, namely it is

$$\begin{aligned} p_{\text{succ}} &= \sum_{x_1=N-1}^{x_0-1} p(x_1) \underbrace{\frac{x_1 - 1 - (N - 2)}{L}}_{\text{clearance to the left of } x_1} \\ &= \frac{\langle x_1 \rangle - N + 1}{L} = \frac{x_0 - N}{L} q , \end{aligned}$$

which vanishes consequentially when all the balls are gathered at the array's left end (i.e. $x_0 = N$). The average number of kicks to get one success is just the reciprocal, i.e.

$$t(x_0) = \frac{1}{p_{\text{succ}}} = \frac{L}{x_0 - N} \frac{1}{q} , \quad (\text{B.2})$$

which we may as well call “time”, regarding a kick as the unit time.

Let's keep things simpler by choosing $x_{0,0} = L$, then the average number of successes k to reach the final state $x_{0,K} = N$ becomes, according to eq. (B.1),

$$q^K = \frac{x_{0,K}}{x_{0,0}} = \frac{N}{L} = \rho \quad \Leftrightarrow \quad K = \frac{\ln \rho}{\ln q} .$$

In the reasonable limit $L \gg N \gg 1$ (i.e. $1 - q \ll 1, \rho \ll 1$ and hence large K), we can estimate the total count of kicks necessary for a certain number of successes by summing up all times $t(x_{0,k'})$ according to the equations (B.2) and (B.1), a sum which can be approximated well (except near the pole at $k = K$) by the corresponding integral:

$$\begin{aligned} T(k) &\equiv \sum_{k'=0}^{k-1} t(x_{0,k'}) \approx \frac{1}{q} \int_0^k \frac{1}{q^{k'} - \rho} dk' \\ &= \frac{\ln(1 - \rho/q^k) - \ln(1 - \rho)}{\rho q \ln q} \end{aligned}$$

Inserting q^k from eq. (B.1) and inverting finally reveals the time evolution of x_0 :

$$\begin{aligned} x_0(T) &= \frac{N}{1 - (1 - \rho) \exp(T\rho q \ln q)} \\ &= \frac{N}{1 - (1 - N/L) \exp(-T/L + O(N^{-2}))} \end{aligned} \quad (\text{B.3})$$

B.2 Three regimes

The behavior of $x_0(T)$ according to eq. (B.3) depends on the considered time regime as discussed in the following. In fig. B.2 on the next page, these (three) regimes can be seen clearly in the simulation data obtained from one single run of the described kicking process.

Early times: $T \ll N \ll L$

Here, the exponential in the denominator of (B.3) can be expanded to yield

$$x_0(T) \approx \frac{L}{1 + T/N}, \quad (\text{B.4})$$

proceeding with the expansion of the denominator itself, we get

$$x_0(T) \approx L \left(1 - \frac{T}{N} \right).$$

This linear decrease is plausible: In the beginning, essential every try is a success and hence x_0 decays exponentially not only in k but in time as well. The large decay constant of $-1/\ln q \approx N$ in eq. (B.1) makes the exponential appear linearly in this considered regime.

Intermediate times: $N \ll T \ll L$

While the expansion leading to eq. (B.4) is still valid, the addend unity in the denominator can be neglected and we are left with an algebraic decay:

$$x_0(T) \approx \frac{LN}{T} \quad (\text{B.5})$$

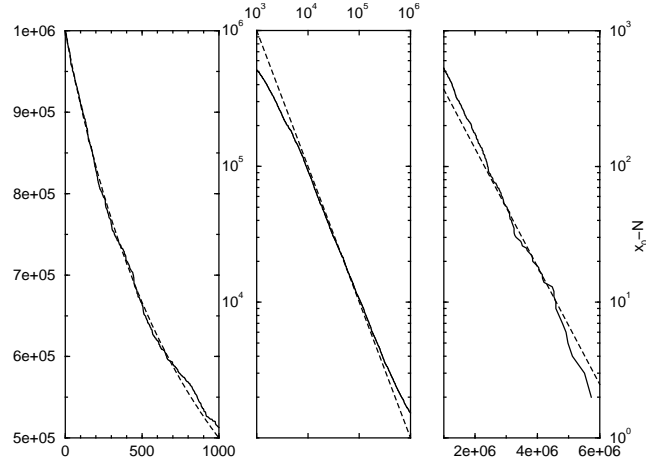


Figure B.2: Position of rightmost ball, x_0 , developing in time; $N = 1000$ balls in an array of length $L = 10^6$ were processed. The three plots show the regimes of early, intermediate and late times from left to right for one single run; the theoretical predictions (B.4), (B.5) and (B.6) respectively, are included as dashed lines.

Late times: $T \gg L$

In eq. (B.3) the exponential gets much smaller than unity and hence allows for an expansion of the denominator:

$$x_0(T) \approx N (1 + \exp(-T/L)) \quad (\text{B.6})$$

Inserting this asymptotical relation into eq. (B.2), we find with

$$t(T) \approx \frac{L}{N} \exp(T/L)$$

an exponentially increasing number of kicks striking the rightmost ball. This would be always the same ball, were it not for the possibility of an exchange. The corresponding probability does not depend on x_0 :

$$p_{\text{ex}} = \frac{N - 1}{L}$$

In the considered regime of late times, this probability is much larger than p_{succ} and consequently the same ball is kicked $1/p_{\text{ex}} \approx 1/\rho$ times on average, a scenario which could hardly be further from the desired random kicking.

Appendix C

Conserved dynamics

A intuitive explanation for the scaling relation

$$2\zeta + d = z$$

is given in the following along the lines of (Wolf and Villain, 1990).

If the system is subdivided into N areas of the same size ξ^d , the width can be decomposed into local and global contributions:

$$w^2 = \frac{1}{N} \sum_{j=1}^N w_j^2 + \frac{1}{N} \sum_{j=1}^N (\bar{h}_j - \bar{h})^2, \quad (\text{C.1})$$

where \bar{h}_j and w_j^2 are average height and surface width, respectively, within the area j . Since w_j^2 is the width inside an area of the size of the correlation length, it is fully developed and the first term in eq. (C.1) stagnates (excluding anomalous scaling). Thus, w^2 can grow any further only due to the second term, whose contributions due to the fluctuating flux can be calculated: During the time Δt the area receives

$$F\xi^d\Delta t \pm \sqrt{F\xi^d\Delta t}$$

particles corresponding to height fluctuations of

$$\delta h^2 = a_{\perp}^2 \left(\frac{a}{\xi}\right)^d F a^d \Delta t$$

between different areas of this size. This is just measured by the second term in eq. (C.1) which yields an increase of

$$w^2(t + \Delta t) = w^2(t) + a_{\perp}^2 \left(\frac{a}{\xi}\right)^d F a^d \Delta t,$$

or, expressed in natural units,

$$\frac{d}{dt} w^2 = \xi^{-d}.$$

A comparison with eq. (2.42), i.e.

$$w^2 \sim t^{2\beta},$$

leads to

$$2\beta - 1 = -\frac{d}{z} \quad \Leftrightarrow \quad 2\zeta = z - d.$$

Appendix D

Crossover times

To address the question of crossover times in section 3.3.4, we consider the following continuum equation:

$$\frac{\partial h}{\partial t} = \nu \nabla^2 h - K \nabla^4 h - \lambda \nabla^2 (\nabla h)^2 + \eta + \eta_c \quad (\text{D.1})$$

where η and η_c are random forces with zero mean and their second moment according to (2.33) and (2.37)

$$\begin{aligned} \langle \eta(\vec{x}, t) \eta(\vec{x}', t') \rangle &= \mathcal{F} \delta^d(\vec{x} - \vec{x}') \delta(t - t'), \\ \langle \eta_c(\vec{x}, t) \eta_c(\vec{x}', t') \rangle &= -\mathcal{F}_c \nabla^2 \delta^d(\vec{x} - \vec{x}') \delta(t - t'), \end{aligned}$$

describing the shot noise and the diffusion noise (Sun et al., 1989), respectively. Combining equations (2.35) and (3.22), we yield the well known expression

$$\mathcal{F}_c \sim \mathcal{F} l_D^2$$

for the correlator of the conserved noise (Tang and Nattermann, 1991). This implies that the conserved noise dominates the fluctuations only on distances shorter than the typical diffusion length l_D (Moser and Wolf, 1992). As we are dealing with larger length scales, the conserved noise may be neglected in the following.

The physical dimensions of the remaining parameters in (D.1) are

$$[\nu] = \text{L}^2 \text{T}^{-1} \quad [K] = \text{L}^4 \text{T}^{-1} \quad (\text{D.2})$$

$$[\lambda] = \text{L}^4 \text{T}^{-1} \text{H}^{-1} \quad [\mathcal{F}] = \text{L}^d \text{T}^{-1} \text{H}^2. \quad (\text{D.3})$$

Comparing those of ν and \mathcal{F} one gets

$$h_\nu(t) = (\mathcal{F}/\nu)^{d/4} (\mathcal{F}t)^{(2-d)/4}, \quad (\text{D.4})$$

comparing those of λ and \mathcal{F} one gets (Amar and Family, 1992)

$$h_\lambda(t) = (\mathcal{F}/\lambda)^{d/(8+d)} (\mathcal{F}t)^{(4-d)/(8+d)},$$

and finally comparing those of K and \mathcal{F} one gets

$$h_K(t) = (\mathcal{F}/K)^{d/8} (\mathcal{F}t)^{(4-d)/8}. \quad (\text{D.5})$$

The dimensional analysis of the linear equations, leading to (D.4) and (D.5), already gives the right scaling behaviour of h as function of t , due to the non-renormalisation of the parameters ν , K and \mathcal{F} (Krug, 1997).

Setting $h_\lambda(t_{\lambda\nu}) = h_\nu(t_{\lambda\nu})$ gives the crossover time $t_{\lambda\nu}$ in (3.27). In the same fashion, by setting $h_K(t_{K\lambda}) = h_\lambda(t_{K\lambda})$ one gets

$$\mathcal{F}t_{K\lambda} = \left(\frac{K}{\mathcal{F}}\right)^{(8+d)/(4-d)} \left(\frac{\mathcal{F}}{\lambda}\right)^{8/(4-d)} = a_\perp a^d \left(\frac{l}{a}\right)^{4d/(4-d)}$$

for the crossover time from K - to λ -dominated roughening. In the last equality eqns. (3.17) and (3.18) have been used. Then the crossover time agrees with the expression (3.28), consistent with the fact, that the K -term and the λ -term give the same result.

Finally, one can ask for the typical times, where h_K , h_λ or h_ν become of order one, i.e. the times which can be interpreted as the damping times, if only the corresponding term is present:

$$\mathcal{F}\tilde{t}_K = a_\perp^2 \left(\frac{K a_\perp^2}{\mathcal{F}}\right)^{d/(4-d)} \quad (\text{D.6})$$

$$\mathcal{F}\tilde{t}_\lambda = a_\perp^2 \left(\frac{\lambda a_\perp^3}{\mathcal{F}}\right)^{d/(4-d)} \quad (\text{D.7})$$

$$\mathcal{F}\tilde{t}_\nu = a_\perp^2 \left(\frac{\nu a_\perp^2}{\mathcal{F}}\right)^{d/(2-d)} . \quad (\text{D.8})$$

Appendix E

Airy Functions

The Airy functions $\text{Ai}(y)$ and $\text{Bi}(y)$ are two linear independent solutions of the ODE

$$\frac{d^2}{dy^2} f(y) = y f(y). \quad (\text{E.1})$$

Successive differentiation of eq. (E.1) leads to the relation

$$\frac{d^{k+2}}{dy^{k+2}} \text{Ai}(y) \equiv \text{Ai}^{(k+2)}(y) = y \text{Ai}^{(k)}(y) + k \text{Ai}^{(k-1)}(y), \quad (\text{E.2})$$

for $k \geq 0$, which also holds true for $\text{Bi}(y)$, of course.

Since only $\text{Ai}(y)$, whose graph is shown in fig. E.1 on the following page, vanishes for large arguments sufficiently rapid, namely in the asymptotic manner

$$\text{Ai}(y) \xrightarrow{y \rightarrow \infty} \frac{1}{2\sqrt{\pi}y^{1/4}} \exp\left(-\frac{2}{3}y^{3/2}\right),$$

we can define

$$'\text{Ai}(y) \equiv \text{Ai}^{(-1)} \equiv - \int_y^\infty \text{Ai}(x) dx, \quad (\text{E.3})$$

which vanishes similarly (Abramowitz and Stegun, 1965)

$$'\text{Ai}(y) \xrightarrow{y \rightarrow \infty} -\frac{1}{2\sqrt{\pi}y^{3/4}} \exp\left(-\frac{2}{3}y^{3/2}\right).$$

With this, we can extend eq. (E.2) to orders $k < 0$, namely by defining

$$\text{Ai}^{(k)}(y) \equiv - \int_y^\infty \text{Ai}^{(k+1)}(x) dx$$

and successively integrating by parts, we find

$$-k \text{Ai}^{(k-1)}(y) = y \text{Ai}^{(k)}(y) - \text{Ai}^{(k+2)}(y), \quad (\text{E.4})$$

which indeed has the same form as eq. (E.2).

Equipped with this relations, we are able to express all derivatives higher than $\text{Ai}'(y)$ in terms of $\text{Ai}(y)$ and $\text{Ai}'(y)$, while for all indefinite integrals higher than $'\text{Ai}(y)$ we need $'\text{Ai}(y)$, $\text{Ai}(y)$ and $\text{Ai}'(y)$. Unfortunately, $'\text{Ai}(y)$ itself cannot be reduced further, it corresponds to $k = 0$ in eq. (E.4).

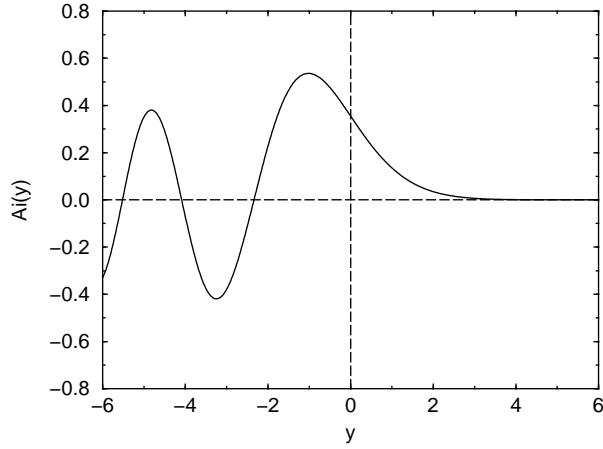


Figure E.1: The Airy function $\text{Ai}(y)$. On the positive axis, it vanishes asymptotically like $y^{-1/4} \exp(-\frac{2}{3}y^{3/2})$. The frequency of the oscillations on the negative axis increases like $\sqrt{-y}$ while their amplitude decays like $(-y)^{-1/4}$.

In section 5.1, mainly the cases $k = -1$ and $k = -2$ of eq. (E.4) are of interest:

$$y''\text{Ai}(y) = y' \text{Ai}(y) - \text{Ai}'(y) \quad (\text{E.5})$$

$$\begin{aligned} y'''\text{Ai}(y) &= \frac{y'' \text{Ai}(y) - \text{Ai}(y)}{2} \\ &= \frac{y^2 y' \text{Ai}(y) - \text{Ai}(y) - y \text{Ai}'(y)}{2} \end{aligned} \quad (\text{E.6})$$

Lebenslauf

Name: Lothar Brendel
10/1989 – 11/1994 Studium der Physik an der Gerhard-Mercator-Universität Duisburg
Abschluss: Diplom (Abschlussarbeit "Fluktuationsschwächung in
Wachstumsmodellen für Molekularstrahlepitaxie")
12/1994 – 12/1997 Promotionstudium am Höchstleistungsrechenzentrum des FZ Jülich
01/1998 – 05/2001 Weiterführung und Abschluss des Promotionstudiums an der
Gerhard-Mercator-Universität Duisburg

Selbstständigkeitserklärung

Hiermit erkläre ich, die vorliegende Arbeit selbstständig ohne fremde Hilfe verfasst zu haben, nur die angegebene Literatur und Hilfsmittel verwendet zu haben und wörtlich übernommene Ausführungen in der Arbeit explizit als solche ausgewiesen habe.

Lothar Brendel
30. März 2001